Characterization of Coarse Backfill Materials for Prevention of Corrosion of MSE Metallic Wall Reinforcement

Research Report 0-6359-1

TXDOT Project Number 0-6359

Performed in cooperation with the Texas Department of Transportation and the Federal Highway Administration

April 2013

Center for Transportation Infrastructure Systems
The University of Texas at El Paso
El Paso, TX 79968
(915) 747-6925
http://ctis.utep.edu

TECHNICAL REPORT STANDARD TITLE PAGE

1. Report No. FHWA/TX 11/0-6359-1	**2. Government Accession No.**	**3. Recipient's Catalog No.**
4. Title and Subtitle Characterization of Coarse Backfill Materials for Prevention of Corrosion of MSE Metallic Wall Reinforcement		**5. Report Date** October 2012 Revised April 2013
		6. Performing Organization Code
7. Author(s) David Borrok, Arturo Bronson and Soheil Nazarian		**8. Performing Organization Report No.** 0-6359-1
9. Performing Organization Name and Address Center for Transportation Infrastructure Systems The University of Texas at El Paso, El Paso, Texas 79968-0516		**10. Work Unit No. (TRAIS)**
		11. Contract or Grant No. Project No. 0-6359
12. Sponsoring Agency Name and Address Texas Department of Transportation Research and Technology Implementation Office 125 E. 11th St., Austin, TX 78701-2483		**13. Type of Report and Period Covered** Technical Report (Final) September 2008 – August 2012
		14. Sponsoring Agency Code

15. Supplementary Notes
Research Performed in Cooperation with the Texas Department of Transportation and Federal Highway Administration
Research Study Title: Characterization of Backfill Materials for Prevention of Corrosion of MSE Metallic Wall Reinforcement

16. Abstract
The service life of mechanically stabilized earth (MSE) walls depends on the rate of corrosion of the metallic reinforcements used in their construction. Assessment of corrosion potential requires the accurate evaluation of pH, resistivity, and ionic (e.g., sulfate and chloride) concentrations of aqueous solutions in contact with the surrounding aggregate. There is a tendency to utilize larger-size aggregates that contain only a small amount of fine material (passing No. 40 sieve) in the backfill. Evaluation of the electrochemical parameters of coarse aggregates is challenging because traditional methods utilize only fine-grained material. The effectiveness of traditional soil characterization techniques for use with coarse aggregates was evaluated by performing leaching experiments with coarse limestone and dolomite aggregates from six materials in Texas. Chemical differences were isolated from size-related kinetic leaching effects by comparing results from the same-sized material collected in the field versus material derived from the crushing of larger (≥ 3/8") aggregates in the laboratory. Testing demonstrated that the fines collected from the field were enriched in chemicals that when exposed to water decreased pH and resistivity and increased chloride or sulfate concentrations relative to the bulk rock. This phenomenon can bias traditional soil testing results and therefore the assessment of corrosion potential. In this report a more representative geochemical testing protocol is recommended. The rate of corrosion was primarily controlled by the chloride content developed from the geochemistry of the backfill and the rate was predicted from the measured conductivity, as well as a two-step corrosion model was determined for the MSE.

17. Key Words MSE Wall Reinforcement Corrosion Prevention Backfill Material Characterization	**18. Distribution Statement** No restrictions. This document is available to the public through the National Technical Information Service, 5285 Port Royal Road, Springfield, Virginia 22161, www.ntis.gov		
19. Security Classif. (of this report) Unclassified	**20. Security Classif. (of this page)** Unclassified	**21. No. of Pages: 137**	**22. Price**

DISCLAIMERS

The contents of this report reflect the view of the authors who are responsible for the facts and the accuracy of the data presented herein. The contents do not necessarily reflect the official views or policies of the Texas Department of Transportation or the Federal Highway Administration. This report does not constitute a standard, a specification or a regulation.

The material contained in this report is experimental in nature and is published for informational purposes only. Any discrepancies with official views or policies of the Texas Department of Transportation or the Federal Highway Administration should be discussed with the appropriate Austin Division prior to implementation of the procedures or results.

NOT INTENDED FOR CONSTRUCTION, BIDDING, OR PERMIT PURPOSES

David Borrok, PhD
Arturo Bronson, PhD
Sergio Rocha, BSEE
Soheil Nazarian, Ph.D., PE (66495)

Characterization of Coarse Backfill Materials for Prevention of Corrosion of MSE Metallic Wall Reinforcement

by

David Borrok, PhD
Arturo Bronson, PhD
Sergio Rocha, BSEE
and
Soheil Nazarian, PhD, PE

Conducted for
Texas Department of Transportation

Project Number 0-6359

Characterization of Backfill Materials for Prevention of Corrosion MSE of Metallic Wall Reinforcement

Research Report 0-6359-1

April 2013

Center for Transportation Infrastructure Systems
The University of Texas at El Paso
El Paso, TX 79968-0516

Acknowledgements

The authors would like to express their sincere appreciation to Mr. Marcus Galvan for his outstanding support and guidance on this project. The authors also thank the Project Management Committee of this project, consisting of Mike Arellano, Claudia Kern and Jimmy Si for their ever-present support.

We are grateful to a number of TxDOT district personnel for their support and cooperation with the interviews, material collection and field testing including:

- Austin District: Rodney Matthews
- Dallas District: Duke Hall
- Waco District: Jacob Bell (TxDOT) and James B. Toon (W.W. Webber)

We are also thankful to a number of graduate and undergraduate research assistances and CTIS staff that worked very hard to generate the information presented. These students include:

- Carlos Castillo, MSME
- Jose Garibay, MSCE
- Jesus Hinojos, MSME
- Adalberto Ordanez, BSCE
- Anita Thapalia, MSGS

Special gratitude goes to Dr. Ken Fishman for his support and helpful comments.

Abstract

The service life of mechanically stabilized earth (MSE) walls depends on the rate of corrosion of the metallic reinforcements used in their construction. Assessment of corrosion potential requires the accurate evaluation of pH, resistivity, and ionic (e.g., sulfate and chloride) concentrations of aqueous solutions in contact with the surrounding aggregate. There is a tendency to utilize larger-size aggregates that contain only a small amount of fine material (passing No. 40 sieve) in the backfill. Evaluation of the electrochemical parameters of coarse aggregates is challenging because traditional methods utilize only fine-grained material. The effectiveness of traditional soil characterization techniques for use with coarse aggregates was evaluated by performing leaching experiments with coarse limestone and dolomite aggregates from six materials in Texas. Chemical differences were isolated from size-related kinetic leaching effects by comparing results from the same-sized material collected in the field versus material derived from the crushing of larger (≥ 3/8") aggregates in the laboratory. Testing demonstrated that the fines collected from the field were enriched in chemicals that when exposed to water decreased pH and resistivity and increased chloride or sulfate concentrations relative to the bulk rock. This phenomenon can bias traditional soil testing results and therefore the assessment of corrosion potential. In this report a more representative geochemical testing protocol is recommended. The rate of corrosion was primarily controlled by the chloride content developed from the geochemistry of the backfill and the rate was predicted from the measured conductivity, as well as a two-step corrosion model was determined for the MSE.

Implementation Statement

The products of this study are proposed new procedures that can be implemented by TxDOT. Recommendations have been made in terms of improving the process of estimating the corrosion rates of MSE reinforcement strands. This study seems to be one of the first studies focused on coarse backfill materials in the US. However, the recommendations are based on a rigorous study of a limited number of coarse backfill.

The implementable products can consist of:

- Implementing the recommendations at a number of actual construction sites in Texas to fine-tune the specification
- Developing a database of electrochemical properties of the more common coarse backfill materials in Texas using the test protocols proposed
- Providing training-oriented presentations at annual construction conferences

During the course of this study, a number of other highway agencies contacted the research team for information about the proposed protocols and procedures. The possibility of establishing a national pooled-fund study is recommended.

Table of Contents

List of Figures

List of Tables

Chapter 1 - Introduction

Mechanically Stabilized Earth (MSE) walls are economical to construct and have the potential to exhibit good serviceability over long duration. To prevent premature corrosion and the resulting reduced service life of MSE walls, the corrosive potential of backfills has to be evaluated. A number of factors are associated with corrosion in soils. These include soil type, moisture content and the position of the water table. The corrosion potential of MSE wall backfill materials is typically characterized in terms of their resistivity, pH and chloride sulfate contents.

Several studies in Europe and in the US showed concern that with the current specifications, indicating that the rates of corrosion estimated in the laboratory from short-term tests are often exaggerated as compared to the results from field observations. Hence, the laboratory-estimated rates of corrosion are often conservative. Given this empirical evidence, current specifications for coarser backfill materials may exclude a number of sources of aggregate that can be successfully used.

The use of coarser backfill materials raises the question as to the proper method of measuring the electrochemical properties of these backfill materials and establishing the proper threshold values to ensure a 75-year or 100-year wall design life. More specific research is needed in how to measure and assess backfill characteristics and how they influence the corrosion and resulting service life of MSE wall systems. This document contains information about techniques that potentially assess the degradation of steel from a porous backfill more precisely, and about models that may predict the short-term and long-term corrosion of the MSE metallic earth reinforcements more accurately. To that end, the geotechnical, geochemical, electrochemical and metallurgical aspects of the corrosion of MSE metallic earth reinforcements are discussed in this document.

The main objectives of this study can be summarized in the following items:

- Evaluate current practices within Item 423 for coarse backfills
- Fully characterize and understand geochemistry of common coarse backfills
- Propose geochemical methods for more realistically estimating corrosion-potential of coarse backfills
- Study corrosion rate of typical metallic reinforcement for typical coarse backfill geochemistry and environmental conditions, and
- Partially validate laboratory results with field instrumentation

Organization of Report

The report consists of nine chapters. A review of literature focusing on the reinforcement corrosion process, a description of the different backfill materials, as well as their physical characteristics and the material testing methodology used by TxDOT are included in chapter 2. Chapter 3 focuses on the different backfill materials and metallic reinforcements that are used

throughout the duration of this project. Chapter 4 describes the laboratory test setup, specimen preparation, equipment and protocol used for monitoring the specimens with a summary of typical results acquired. Chapter 5 describes the corrosion studies of the reinforcement material. A detailed description of the coupon preparation is also included in that chapter. In Chapter 6, the geotechnical and corrosion results are summarized and interpreted. Chapter 7 covers the field-testing done for this project; it includes the site selection, description of the sensors used and the layout of those sensors at each site. Chapter 8 contains practical recommendations and summary and conclusions derived from the project.

Chapter 2 - Background

Corrosion of Embedded Reinforcement

Corrosion of embedded reinforcement is the deterioration or dissolution of steel, which usually caused by one of the following mechanisms:

- Electrochemical corrosion of carbon steel: Given a potential difference between two points that are electrically coupled, a current will flow from the anodic area through the electrolyte soil to the cathodic area and then through the metal to complete the circuit. The anodic area becomes corroded by the loss of metal ions to the electrolyte (Elias, 2000).
- Galvanic corrosion: When two dissimilar metals (e.g. zinc and steel) are electrically coupled in contact with electrolyte soil, the more positive metal becomes a cathode and the more negative one acts as an anode (Davis, 2000). The anodic metal (e.g., zinc) is then corroded first and provides 'cathodic protection' for the other metal (e.g., steel).
- Stray-Current corrosion: This is a special form of corrosion caused by externally induced electrical current and is basically independent of environmental factors (Davis, 2000).

Excluding stray-current effects, the corrosion rate of embedded reinforcing steel depends on the backfill and the reactivity of the reinforcement with the surrounding backfill material. In the next sections, the corrosion of carbon steel and galvanized steel is briefly reviewed, the modeling aspects of corrosion in general and carbon steel in particular are discussed, and the techniques used for evaluating corrosion are described.

The corrosion of carbon steel surfaces is aided by the knowledge of atmospheric corrosion and pitting corrosion of iron. The layers of rust formed on iron depend on the surrounding pH of the electrolyte to form mixtures of oxyhydroxides as reported by Misawa et al. (1971). For a pH of 12.5-13.5, α-FeOOH (goethite), Fe_3O_4 (magnetite) and γ-FeOOH (lepidocrocite) develop; for pH of 7.0-8.0, magnetite forms; for a pH of 6.0-6.5, higher contents of lepidocrocite form. Misawa et al. inferred that amorphous δ-FeOOH forms on mild steel with coarse grains of Fe_3O_4 embedded in a goethite-lepidocrocite mixture that cracks allowing water solution and O_2 to ingress and react with the iron surface. Significant temperature fluctuations may further cause more cracking because of the thermal expansion differences among the oxyhydroxide phases. Misawa et al. noted and Nishimura et al. (2000) confirmed that chlorides, which increase the acidity, stabilize the β-FeOOH phase. Eriksson and Johansson (1986) found goethite (α-FeOOH) and lepidocrocite (γ-FeOOH) among the steel corrosion products at low and high relative humidity in the presence of SO_2 and/or NO_2. Eriksson and Johansson concluded that at high humidity, the SO_2 might form ferrous sulfate, attracting water to the surface and thus accelerating corrosion with little contribution from NO_2. Of course, chloride also has an effect on the rust as determined by Nishimura et al. (2000). They reported that the β-FeOOH phase increases with increasing chloride content. Although their study was more directed toward

atmospheric corrosion, a similar behavior would develop on carbon steel embedded in soils depending on its moisture content.

For pitting corrosion, the initiation and growth of pits depend on several factors (Szklarska-Smialowska, 1986; and Knittel and Bronson, 1984) including the electrochemical potential, surface inhomogeneity (Arroyo et al., 1990), the chloride-sulfate solution (Chen et al., 1985), and the characteristics of the passive film. As noted above, iron develops an oxyhydroxide passive film decreasing the corrosion from an un-oxidized iron, but chloride ions would attack the oxide film causing pits to initiate on the surface, usually by forming an acidic solution adjacent to the surface. In addition to pit formation, the chloride solution may diffuse through a porous or cracked oxyhydroxide film and cause further dissolution, as per the following simplified reaction sequence (Jones, 1992).

$$FeOOH + Cl^- \rightarrow FeOCl + OH^- \quad (2.1)$$

$$FeOCl + H_2O \rightarrow Fe^{3+} + Cl^- + 2OH^- \quad (2.2)$$

A zinc coating on galvanized carbon steel protects it from long-term atmospheric corrosion because the zinc serves as a barrier against steel dissolution. If a defect in the coating develops, the zinc will continue to corrode and will protect the underlying steel substrate (Kaesche, 1985 and Jones, 1992). The Tsuru research group (El-Mahdy et al., 2000, Yadav et al., 2004 and 2005) has more recently categorized the corrosion of galvanized steel undergoing wet-dry conditions into three stages. In the first stage, the zinc experiences an accelerated corrosion forming white rust [ZnO and $ZnCl_2 \cdot 4Zn(OH)_2$]. During the second stage the dissolution as a result of the corrosion slows. At the end of the second stage, the steel is exposed to the electrolyte and subsequently red rust indicative of FeOOH appears and plateaus the corrosion rate on the surface.

A scanning electron micrograph of the zinc/steel interface shows distinctly three phases composed of a Zn layer, a Zn-Fe phase ($Zn_{13}Fe$ composition) and the Fe substrate (Yadav et al., 2004). The corrosion front decreases when the Zn-Fe phase is exposed at the start of the first stage. However, the Zn coating still serves as a sacrificial anode protecting the Fe substrate when the surface is covered with electrolyte. However, in the dry condition the Fe substrate is unprotected and corrodes if the electrolyte does not come in contact with the Zn layer. Within the third stage, the corrosion of the carbon steel stabilizes as a result of the FeOOH, which only becomes problematic if cracking of the oxide coating develops.

Corrosion Patterns and Modeling

The corrosion behavior of metallic earth reinforcements depends on the type of constituents within carbon steel and whether the steel is galvanized. In the case of galvanized steel, the thickness of the protective zinc, as well as its contact with moisture within the backfill, determines the extent of the corrosion process. In addition, the level of induced stress in the reinforcing bars may also affect the corrosion behavior of embedded steel, if the Zn coating degrades sufficiently to expose the carbon steel substrate. The maximum stress sustained by the MSE metallic reinforcements is considered very low for stress corrosion cracking. The stress needed for stress corrosion cracking may range from 10% to 70% of the yield strength (Fontana and Greene, 1986) depending on the initial state of the surface and the stress developed by the corrosion products, as well as the adjacent electrolyte. However, localized corrosion may still

initiate on surface heterogeneities (sulfide inclusions and grain boundaries), which for example, can first start as pitting corrosion and then progress to stress corrosion cracking. Hence, an understanding of the metallurgical aspects of corrosion would aid in understanding the short-term corrosion accelerated tests and subsequently linking them to the in-situ (or real-time) corrosion rates in the field.

The state of practice in modeling corrosion is to assume a simple log-linear relationship between the corrosion of metal and time (Elias 2000). As reflected in Figure 2.1, the corrosion rate is rather rapid in the short-term and rather gradual in the long-term. If the log-linear predictive model is developed based on short-term corrosion tests, the rate of corrosion of the strand will be overestimated. As such, a predictive model that would mathematically combine the corrosion rate for short-term and long-term exposure times seems necessary.

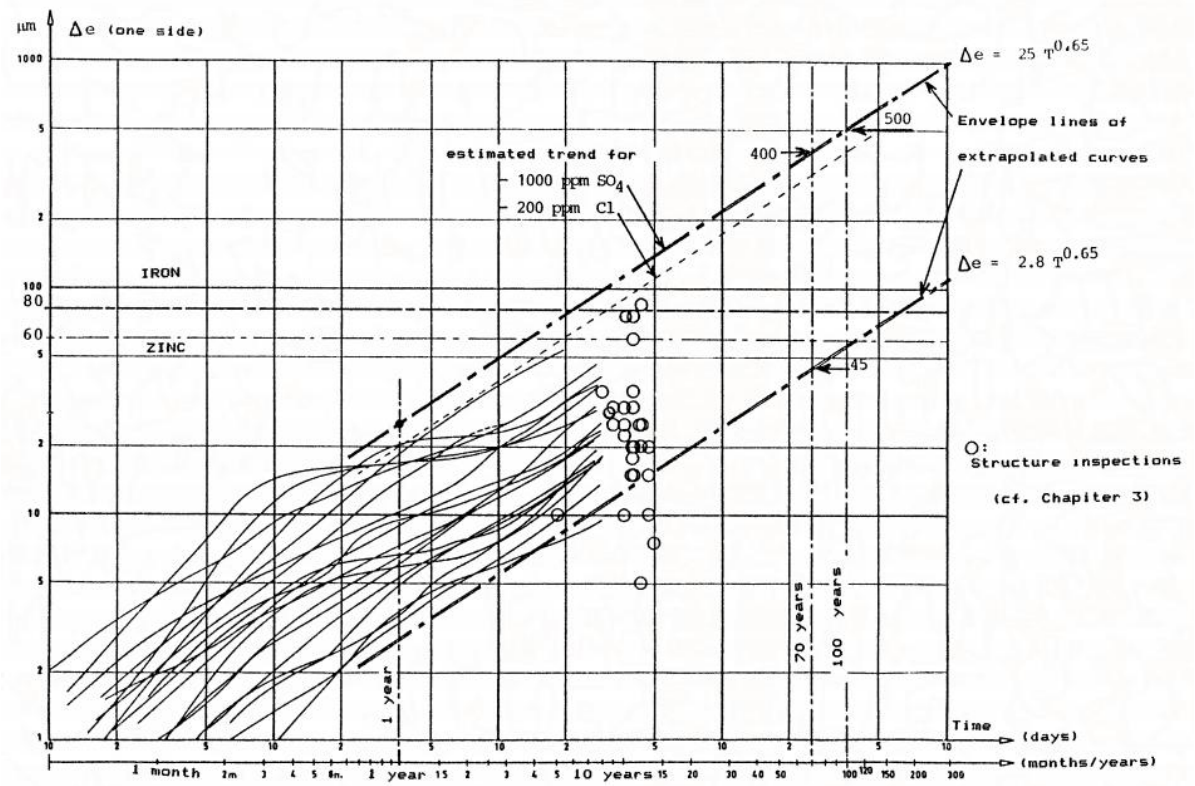

Figure 2.1 – Typical Rate of Corrosion with Time (Elias, 2000)

The modeling of corrosion behavior to predict future behavior can be categorized based on experimentation or based completely on thermodynamic, kinetic and fluid transport mechanisms. However, the computational-experimental technique currently provides a better statistical prediction of corrosion behavior than the latter category. The modeling of corrosion behavior has been developed for storage containers of nuclear wastes (Freon et al., 2008), corrosion of pipelines embedded in soils (e.g., Song and Sridhar, 2008) and even weathering steels for bridge components (e.g., Wang et al. 1996). For predicting corrosion behavior based on strictly fundamental concepts, the reader can start with Macdonald's research group development of the point-defect model (e.g., Ahn et al., 2005) or Kelly's research group recent computational effort to model atmospheric corrosion resulting from a thin film electrolyte on a stainless steel (Cui et al., 2005).

Wang et al. (1996) proposed that the weight loss measurements could be used to link the corrosion rate from accelerated laboratory tests to *in-situ* tests. Their prediction model mathematically combined the weight loss (W_{Corr}) for short-term (t_1) and long-term exposure times (t_2) as follows:

$$W_{Corr} = At_1^{B_1-B_2}t_2^{B_2} \tag{2.3}$$

This model has the added flexibility of being able to change the A, B_1 and B_2 parameters as a function of environmental factors (e.g., temperature, moisture and chloride) that can vary spatially and temporally throughout Texas.

Estimating Corrosion of Metallic Earth Reinforcement

The current method of estimating the corrosion rate of metallic earth reinforcements usually uses the potentio-dynamic technique as covered in Elias (2000). Although the potentio-dynamic, or sometimes referred as the polarization test (ASTM G5), has been established for determining the corrosion rate for metals (Knittel and Bronson, 1984) as well as the foundation for transient techniques (Odegard and Bronson, 1997), the test sometimes does not have sufficient accuracy for coated metals (e.g., galvanized carbon steel). Gladstone et al. (2006) found that the linear loss model estimates considerably less than the actual performance data. Halmen et al. (2008) reported that the corrosion of galvanized steel culverts embedded in engineered backfill material primarily consisting of Portland cement does not correlate with service life models (e.g., California 643 Method). Additional experimental techniques are needed to properly characterize not only the electrochemical reactions on the metal surface but also the fluid aiding the corrosion. The potentio-dynamic techniques are valuable in characterizing a dense, thin oxide layer on a metal, but electrochemical impedance spectroscopy (EIS) will also aid in analyzing the oxide film usually developed on a metal. The oxide film formed on galvanized carbon steel can be an iron oxide, which is either semi-conductive or insulating, or ZnO on the Zn layer. The fluid adhering onto the metal can also change the electrochemical reactivity by complicated synergistic effects such as solution conductivity, oxygen solubility from the gas phase, oxide porosity and chemical reaction at the solution/metal surface. Another electrochemical technique recently surfaced into usage has been a monitoring methodology (i.e., electrochemical noise), which characterizes the corrosion behavior in-situ. In addition, the technique monitors the corrosion passively or without imposing an electrical perturbation onto the surface but rather measures the potential and current created by the fluid/metal interface. In the following paragraphs, these techniques are briefly reviewed.

Electrochemical Impedance Spectroscopy (EIS)

Electrochemical impedance spectroscopy (EIS) is used to analyze corrosion mechanisms by assuming usually one or a series of resistance-capacitive equivalent circuits to simulate the charge transfer reactions, diffusive processes through solid or liquid phases, and ions through the electrolyte. Macdonald (1991) and Mansfeld and Lorenz (1991) have critically reviewed the technique and more recently Orazem and Tribollet (2008) thoroughly developed EIS with their monograph analyzing the experimental methods, equivalence of circuits and interpretative strategies. EIS was used in this study to determine primarily the polarization resistance, which was transformed to the corrosion rate, as well as the capacitive nature of the corrosion products (e.g., FeOOH layer) and the solution resistance of the thin film electrolyte. The EIS technique can also be used in the analysis of the electrochemical noise measuring the in-situ corrosion.

The value of the EIS technique is that another equivalent circuit can be devised to adjust to the corrosion behavior such as the contribution of the resistance of the pore solution, which can be varied in experimentation. Hence, through an adjustment of the equivalent circuit, experimental parameters can be incorporated into estimating more accurately the corrosion rate.

Although electrochemical tests, such as pH, resistivity, chloride content, sulfate content and organics content, are used to characterize corrosivity of the backfill, additional tests are suggested to monitor the corrosion of galvanized carbon steel with thin-film electrolyte tests coupled with separate EIS measurements. The EIS measurements can form the corrosion baseline for predicting the life of MSE walls, especially for short-term and long-term behavior. To better assess the corrosion of galvanized and uncoated carbon steel, they should be exposed to the backfill solutions, undergoing wet/dry cycles in which water will circulate into the pores of the backfill to immerse samples in backfill soil for 4 days followed by draining the pore water to simulate a dry backfill for 3 days. The sample can serve as a working electrode (WE) surrounded by a counter-electrode (CE) along with the reference electrode (RE), both placed an inch away from the WE surface.

Thin Electrolyte Layer Technique

A two-electrode electrochemical cell consisting of electrodes separated 1 to 3 mm as previously devised by Nishikata et al. (1996) can acquire the electrochemical impedance spectroscopy in the unstressed condition and to aid in the *in-situ* electrochemical technique. The thin electrolyte configuration would simulate the pore solution available within the soil after rainfall instead of immersing fully the electrodes. Although the thin electrolyte technique uses EIS, the configuration of a thin electrolyte simulates the effect of oxygen from the atmosphere and/or within the openings of a granulated soil. To control the electrolyte layer thickness, a 0.5 mm wall can surround the electrodes to study the wet/dry conditions. In addition, the following oxygen reduction is expected in an alkaline solution, which would quickly equilibrate with the metal.

$$O_2 + 2H_2O + 4e^- \rightarrow 4OH^- \tag{2.4}$$

Tsuru's research group (e.g., Nishikata et al., 1995) explained the thin electrolyte technique as well as the specific applicability to galvanized steel (i.e., Yadav et al., 2004). At active anodic sites, zinc dissolves as Zn^{2+} and diffuses into the corrosion products through its pores. The corrosion develops through three stages. In the third stage, the underlying Fe corrodes forming the red rust.

Electrochemical Noise

Electrochemical noise (or in-situ test) is a relatively new technique under development to determine the extent of corrosion by measuring the current and/or potential signals acquired from a passive monitoring system. Electrochemical noise (EN) is considered a passive measurement because no perturbation signals (e.g., sinusoidal potential waveform, potential pulse or current pulse) are used to determine the extent of corrosion and the technique will be used to monitor corrosion on site. Giriga et al. (2005) provided the details of the technique using potential and current monitoring methodologies to determine the extent of the corrosion although in most cases, EN is usually used to determine pitting corrosion. Al-Mazeedi and Cottis et al. 2004 used the EN parameters as indicator of corrosion type, using a three electrodes technique, where two

of the electrodes were working electrodes measuring the electrochemical current noise using a zero-resistance ammeter (ZRA, Al-Mazeedi and Cottis, 2004). The current transients are analyzed with the low frequency power spectral density (PSD) with the fast Fourier transform (FFT) and the maximum entropy method (MEM). The FFT produces noisy spectra, while the MEM produces smother spectra, though Bertocci et al. (1998) reported that erroneous spectra could be identified easier in the FFT than with the MEM method. Cottis (2001) has also reported a summary of the interpretative views concerning electrochemical noise for corrosion.

The electrochemical noise technique can be compared to the EIS, because EIS can measure the capacitance, as well as the coating's crack characteristic, which can infer early deterioration of the coating. The key to the EIS technique is in developing an equivalent circuit during the interpretive phase of analyzing the data (Mansfeld and Lorenz, 1991, Macdonald, 1991). Hence, all the techniques outlined above were used to determine the long-term corrosion of MSE metallic earth reinforcements, as well as to develop a monitoring system.

Geochemical Properties of Backfill

TxDOT defines the following three gradations for the permanent backfill:

- Type A backfill with maximum aggregate size of 3 in. (50-100% retained on the 1/2 in sieve and 85-100% retained on sieve # 40).
- Type B backfill with maximum aggregate size of 3 in. (40-100% retained on sieve # 40 and 85-100% retained on sieve # 200).
- Type D backfill, (85-100% greater than 3/8")

From a geological standpoint, Type A and D MSE backfill materials are best described as crushed "rock" or aggregate, and should not be considered a "soil". The best way to learn about the corrosive potential of coarse-grained backfill, "rock", is to evaluate it using a comprehensive geochemical framework. Therefore traditional "soil tests" may not provide an adequate framework for understanding the chemical relationships to metallic corrosion.

The geochemistry associated with waters in contact with MSE backfill materials depends on four factors (van der Sloot and Dijkstra, 2004):

1) Abundance of key minerals containing the element(s) of interest,
2) Solubility of the key mineral phases,
3) Kinetic of mineral dissolution,
4) Action of secondary processes like surface adsorption, oxidation, reduction, and mineral precipitation.

These factors are impacted by internal or external variables such as pH, surface area, temperature, microbial activity, and the duration and degree of water contact (van der Sloot et al., 1997). For example, pH controls mineral solubility and dissolution rates, and exerts a strong control over surface adsorption and precipitation reactions. Surface area directly impacts moisture retention and ion release rates. Although annual temperature fluctuation in backfills is small, regional temperature increase generally increases reaction rates and promotes chemical diffusion. Finally, some amount of moisture is necessary to facilitate the leaching process.

A host of interrelated geochemical parameters control the chemistry of waters in contact with MSE backfill materials. To achieve a complete understanding of how these factors impact the corrosion of metallic earth reinforcements, a suite of geochemical parameters, including, but not

limited to the following items should be considered (e.g., Doyle et al., 2003; Akpofure and Kehinde, 2006):

pH of Backfill Leachate

pH is the "master variable" in that it exerts a first-order control on the types, amounts, and forms of other ions in aqueous solution. pH controls pore water chemistry by its direct impact on the solubility of mineral phases (Buchholz and Landsberger, 1995). pH also impacts the distributions of these soluble components through surface adsorption and aqueous complexation reactions (van der Sloot and Dijkstra, 2004). Under low pH (i.e., acidic) conditions, the concentration of H^+ ions is elevated, which can increase corrosion of metallic objects by inhibiting the formation of oxide layers that act to pacify corrosion. Many oxide minerals, including Fe(III)-oxides are soluble (i.e., dissolve) under acidic pH conditions. Moreover because of the increased solubility, more ions are present in acidic solutions. Corrosion of metallic reinforcements is driven by the electric potential difference between two points in the metal. Hence, ions in the electrolyte solution help to bridge these electric potential differences. In other words, the more ions in the medium are present, the more electrically connected the anode and cathode regions of the metal will be. At elevated pH conditions OH^- ions are abundant, which can lead to similar electrochemical corrosion problems. Hence, TxDOT along with most other state DOT's have placed limitations on the pH of backfill materials used for MSE walls in that they can be neither too acidic nor too basic (generally not less than pH=5 or more than pH=10; see Table 2.1). The American Water Works Association (AWWA) soil corrosiveness scoring system suggests that materials with a pH less than 4 or greater than 8.5 are corrosive (ANSI/AWWA, 1999).

Table 2.1 – Electrochemical Specifications for Selection of MSE Backfills by other DOTs

Agency	pH	Resistivity (ohm-cm)	Chloride content (ppm)	Sulfate content (ppm)	Organics
AASHTO	5-10 (T-289)	≥ 3000 (T-288)	≤ 100 (T-291)	≤ 200 (T-290)	≤ 1% (T-267)
California DOT	5.5-10	>2000	≤ 250	≤ 500	NS
Kentucky DOT	5-10	≥ 3000	≤ 100	≤ 200	≤ 1%
North Carolina DOT	4.5-9.5	≥ 5000			≤ 0.1%
Iowa DOT	5-10	≥ 3000	≤ 100	≤ 200	≤ 1%
Kansas DOT	5-10	≥ 5000 ≤5000, ≥ 3000	-- ≤ 100	-- ≤ 200	≤ 1%
Nebraska DOT	5 – 10	> 3000 at saturation	< 100	< 200	NS
Oregon DOT		> 5000	NS*	NS	NS
Vermont DOT	5-10	≥ 3000	≤ 100	≤ 200	≤ 1%

**** NS = not specified***

Resistivity of Backfill Leachate

Resistivity is a measure of the impedance of electrical current. Hence, materials/solutions with high resistivity have low ion concentrations and do not efficiently transmit electrons. Materials with low resistivity have high ion concentrations and readily transmit electrons. Resistivity is related to pH in that acidic and basic pH conditions tend to promote higher ion concentrations in solution and thus lower the resistivity. Because corrosion rates are related to the ability of the

solution to transmit electrons, resistivity is considered an important indirect measure of the susceptibility of a system for corrosion (Doyle et al., 2003; Akpofure and Kehinde, 2006). TxDOT, along with most other state DOT's, has placed limitations on the electrical impedance of materials used for MSE walls in that the resistivity of the backfill must be greater than 3000 ohm-cm (see Table 2.1). The AWWA soil corrosiveness scoring system suggests that materials with a resistivity>2000 ohm-cm are non-corrosive (ANSI/AWWA, 1999). Note, however, that the resistivity of soil is partly dependent upon the measurement technique.

Chlorine and Sulfate Content of Backfill Leachate

In addition to being major anion components of pore water fluids in contact with rocks (i.e., a direct impact on resistivity), chlorine and sulfate can uniquely influence metallic corrosion. Chlorine catalyzes metallic corrosion mainly by breaking down the passive oxide layers that protect the metal surface (Broomfield, 1997; Bertolini et al., 2004). Sulfate can be reduced, most often via sulfate-reducing bacteria (SRB), generating large amounts of acid, which leads to pitting corrosion. For these reasons TxDOT, along with most other state DOT's, has placed limitations on the concentrations of soluble chlorine and sulfate in materials used for MSE walls. Chlorine and sulfate concentrations must be less than or equal to 100 mg/L and 200 mg/L, respectively (see Table 2.1).

Sulfide Content

Sulfide minerals like pyrite (FeS_2) are common as trace constituents in many rocks. Sulfide is the reduced form of sulfur, and when exposed to aerobic conditions can oxidize to produce sulfate (SO_4^{2}), which is coupled to acid generation (i.e., the release of H^+). For example, the oxidation of pyrite can occur via either the O_2 or Fe(III) reduction pathway, as described by the following reactions (e.g., Nordstrom and Southam, 1997; Rimstidt and Vaughan, 2003):

$$FeS_2 + 7/2O_2 + H_2O = Fe^{2+} + 2SO_4^{2-} + 2H^+ \quad (2.5)$$

$$FeS_2 + 14Fe^{3+} + 8H_2O = 15Fe^{2+} + 2SO_4^{2-} + 16H^+ \quad (2.6)$$

To maintain oxidative weathering via the Fe(III) pathway, Fe(II) must be oxidized to regenerate Fe(III) according to the following reaction:

$$Fe^{2+} + 1/4O_2 + H^+ = Fe^{3+} + 1/2H_2O \quad (2.7)$$

Sulfate and H^+ ions can impact corrosion rates (see discussions above). TxDOT does not specify requirements for the sulfide content of backfill materials for MSE walls. However, the AWWA soil corrosiveness scoring system suggests that materials with even a trace amount of sulfide may be corrosive (ANSI/AWWA, 1999).

Organic Content

The natural organic matter (NOM) found in rocks/soils is ultimately derived from the breakdown of plants, animals, and microbes. Other sources of organic material might include atmospheric deposits from smoke-stack emissions or organics included in sprays that are used to treat the soil/rock material. NOM is composed of various aliphatic and aromatic hydrocarbons as well as other organic molecules like fatty acids, carbohydrates, and lipids (Aiken, 1991). Organic macromolecules are often hydrophobic and can coat surfaces of rocks and metal. The organic content of backfill materials impacts metallic corrosion in three ways: 1) a carbon source is

necessary for the growth of microbial colonies which in turn can impact corrosion (see below), 2) dissolved organic matter can act as an electron transfer bridge to enhance redox reactions that occur during galvanic corrosion (Kappler et al., 2004), and 3) NOM strongly complexes cations, which increases the solubility of mineral phases and therefore the ion content of the electrolyte. For these reasons, TxDOT specifies that less than 1% of the backfill material can be organic material (see Table 2.1).

Buffering Capacity

Buffering capacity is a measure of the ability of a substance to hold its pH constant. For corrosion purposes, the buffering capacity of the pore water in contact with metals is the primary concern. For example, many siliceous rocks like sandstones and various igneous or metamorphic rocks do not have chemistries that allow them to effectively buffer pore water pH. Hence, the pH of the pore waters in these rocks will probably reflect the pH of the original fluids that contacted them (e.g., rain water, or storm water runoff). Conversely, carbonate rocks have a great deal of buffering capacity and can easily neutralize acidic solutions. In the case of carbonates the pore water pH will be a reflection of the chemistry of the rock.

Oxidation Reduction Potential (ORP)

ORP is a measure of the potential for oxidation or reduction in an aqueous fluid. This is a bulk electrochemical measurement where positive mV readings indicate the net ability of the solution to become reduced (i.e., accept electrons), while negative voltage readings indicate the net ability of the solution to become oxidized (i.e., to give up electrons). The magnitude of the mV readings is proportional to the redox activity of the solution. Hence, ORP is a reflection of the type and abundance of ions in solution. Because of galvanic corrosion occurs via electron transfer, ORP should have at least an indirect relationship to corrosion. The AWWA soil corrosiveness scoring system suggests that ORP values greater than +100 mV are non-corrosive (ANSI/AWWA, 1999). ORP is not a measurement currently utilized by TxDOT.

Microbial Impacts

Microbes can impact metallic corrosion in many different ways from the localized generation of organic acids to the metabolic production of H_2S, which can add to acidification and catalyze the penetration of hydrogen into steels (Little and Lee, 2007). The production of H_2S is a hallmark of sulfur-reducing bacteria (SRB), which are widely considered the worst offenders for increasing metallic corrosion. SRB are strict anaerobes that utilize organic carbon as the electron donor when reducing SO_4^{-2} to S^{-2}. Hence, the presence and activity levels of SRB are directly tied to the availability of organic carbon and SO_4^{-2} (see descriptions above). The oxidation of carbon associated with SRB can lead to a buildup of CO_2, which will also contribute to acidic pore water solutions. Other bacterial metabolic pathways can similarly impact corrosion. For example, Fe(III)-reducing bacteria can dissolve the passivating oxide-layers that frequently develop on metal surfaces (Little and Lee, 2007). Biofilms comprised of many different species, capable of many different metabolic pathways, are extremely effective in corroding metallic surfaces (Beech, 2004). TxDOT does not have requirements regarding the identities of microbes or their quantities. However, the regulation of sulfate and organic carbon in backfill materials for MSE walls would tend to limit the impact of microbes.

Surface Area

The size of the rock fraction has a tremendous impact on the kinetics of leaching. Smaller particle sizes have more surface area per volume, which leads to accelerated leaching rates. Hence, the smaller particles are likely to exert a stronger control on the overall chemistry of pore waters than the larger particles when equilibrium has not been reached with the backfill material. Disequilibrium would be the most common situation when water percolates through unsaturated MSE backfill material. Whereas, in saturated systems the pore water is likely to have adequate time to reach equilibrium with all sizes of the rock fragments. If the smaller rock particles are of a different chemical composition than the larger particles, the enhanced impact of the smaller material grades on pore water chemistry could lead to surprising results that would be unpredicted by many leach tests or by thermodynamic modeling (i.e., modeling based on chemical equilibrium) testing. Therefore, the grade (gradation) of the backfill materials used for construction of MSE walls is critical to understanding the pore water chemistry. This "size problem" is also critical to selecting the proper baseline leaching test method and evaluating the results from these studies (see discussion below).

Types of Leaching Tests

Considering the complexity of interrelated geochemical parameters that can impact corrosion, great care must be taken in choosing methods for evaluating/quantifying these parameters. Leaching tests are used to determine the chemistries (e.g., pH, resistivity, ion content, etc.) of waters flushed through and/or otherwise in contact with backfill and building materials. Leaching tests determine the likely concentrations of soluble constituents that may be corrosive (Kosson et al., 1996; Johnson et al., 1996; Marguí et al., 2004). All leaching tests have the interaction of the solid material of interest (soils, rocks, dust, construction materials, etc.) with water in common. However, the details (e.g., how much material, how much water, what sizes, what types of water, time of contact, etc.) vary widely among different leach test procedures. Table 2.2 summarizes the most frequently used U.S. and European leaching tests, as well as those currently used by TxDOT. A leach test should be chosen based on the following characteristics:

1. It should serve the purpose for which it is intended whether it be for regulatory compliance or to evaluate the geochemical properties that impact metallic corrosion.
2. It should be the most economical solution.
3. It should be reliable and repeatable.
4. It should be easily accomplished in the shortest effective time period.
5. It should be flexible and adaptable enough to work using a variety of materials and material sizes.

Currently, TxDOT specifications for MSE backfill require the measurement of soil resistivity, pH, and chloride and sulfate concentrations via several specialized leaching tests. Methods Tex-128-E and Tex-620-J, are used for quantifying the pH, resistivity, and chloride and sulfate contents, respectively, for each selected backfill materials. These tests are very specific regarding requirements for backfill material size, liquid-solid ratio, and leaching time (see Table 2.2).

Table 2.2 - Summary of Leaching Methods

Method	Agency	Original Purpose	Ratio (L:S)	Duration of mixing	Procedure	Measurements	Reference or Method
Method 1312 Synthetic Precipitation Leaching Procedure (SPLP). Also adopted by ASTM	USEPA (1986; 1994)	Potential for leaching metals into ground and surface waters	20 : 1	18 hrs	All material <1 cm. Extracting fluid consists of slightly acidified de-ionized water to achieve appropriate pH (4.2 to 5) to simulate natural precipitation. 100 g of mine waste material and 2000g of extraction fluids mixed on rotary agitator for 18 hrs slurry at 30 rpm.	pH, Conductivity, Temperature (all measured in-situ). Sample filtered using 0.7 µm glass fiber filter and measure for metal and anion concentrations.	EPA SW-846 ASTM D6234-98 (2007)
EPA 1311 Toxicity Characteristic Leaching Procedure (TCLP)	USEPA (1992; 1996)	Evaluation of metal mobility in landfill environments	20 : 1	18 hrs	Used for both solids and liquid wastes Extraction fluid used is a function of alkalinity of the solid phase of waste Buffered acetic acid (pH 2.88 or 4.93, depending on the buffering capacity of waste).	Extraction fluid is separated from solid phase filtered sample through 0.6 to 0.8 µm glass fiber filter Measure extraction fluid for metal concentrations.	EPA SW-846
USGS Field Leach Test (FLT)	USGS 2000	Evaluation of potential metal release from mine wastes.	20 : 1	5 min	50 g of sample added to 1L of DI water in wide-mouth plastic bottle. Bottled tightly capped and vigorously shaken for 5 min. Solution allowed to settle for 10 min prior to analysis/sampling.	pH, specific conductivity, alkalinity, temperature (all measured in-situ). Filtered (0.45 µm) leachate is analyzed for metal and anion concentrations.	Hageman (2004)
Colorado Department of Mines and Geology (CDMG) Leach Test modified from USGS FLT test	CDMG	Determine metal release from soils when exposed to natural waters	2 : 1	15 s	300 ml of DI water added to 150 ml of sediment sample. Stirred for 15 s and allowed to settle for 90 min prior to sampling.	pH and alkalinity are measured in-situ. Filtered (0.2 µm) leachate analyzed for metal and anion concentrations.	Herron et al. (2001)
Meteoric Water Mobility Procedure (MWMP) Modification from SPLP	ASTM 2002	Evaluation of mobility of constituents from mine waste by leaching with meteoric water	1 : 1	24 hr	5 L of Type 2 reagent grade water is percolated through 5 kg of sample in a 6" diameter column for 24 hours.	pH of the water is measured before and after contact with the sample. Filtered (0.45 µm) effluent is collected and analyzed for metal and anion concentrations.	ASTM E2242-07
Humidity Cell Tests	ASTM 2002	To simulate long term weathering reactions of mine waste material	NA	>20 weeks	Require 1kg sample crushed to < 6.3 mm. The sample is placed in a sealed plastic box. First dry air is passed over sample for 3 days followed by moist air for 3 days. Every 7th day the sample is flushed with 0.5 or 1 L of water.	Leachate is analyzed for pH, acidity, alkalinity, and electrical conductivity. Procedure also includes pre-leach and post-leach mineralogical and chemical characterization of sample.	ASTM D5744-96

Table 2.2 cont. Summary of Leaching Methods

Method	Agency	Original Purpose	Ratio (L:S)	Duration of mixing	Procedure	Measurements	Reference or Method
Passive Leach Method	USGS	Evaluation of mine waste leachate	20 : 1	1hr	100 g of mine waste sample was exposed to 2L of laboratory DI water in open 4L beaker. Samples are left at rest for 1 hr and then stirred for five minutes prior to sampling.	Conductivity and pH of leachate measured in-situ. Filtered (0.45 µm) effluent is collected and analyzed for metal and anion concentrations.	Fey et al. (2000)
National Cooperative Highway Research Program (NCHRP) method	NCHRP	Evaluation of leachate from materials used in highway construction.	4 : 1	24 hrs or 18 hrs	Crushed material is added to DI water at a ratio of 1 to 4 and agitated for 24 hours.	Filtered (0.45 µm) effluent is collected and analyzed for metal and anion concentrations.	Nelson et al. (2000)
Dutch column leaching test/ percolation test. Nederlands Normalisatie Instituut (NNI) & Comité Européen de Nomialisation (CEN)	NNI & CEN	Evaluation of leachate from building materials	10:1	3 wks	A 20 x 5 cm column is filled with approximately 500 ml of test material of any size below 4mm. Simulated rain water is flushed through the vertical column from bottom to top and samples are collected as a function of time/pore volume.	Leachate is analyzed for metals and anions.	NNI (1995) NEN-7343 prEN 14405 CEN TC292 WG6
The European pH-stat test	CEN	Evaluation of leachate from building materials	9:1	24 hr	8, 60g samples are placed in closed vessels. DI water is added until a L:S ratio of 9:1 is achieved. The pH is set at a pre-determined value (4, 5.5, 7, 8, 9, 10, 11, or 12) using an automatic pH-stat titrator assembly and acids or bases.	Filtered (0.45 µm) leachate is collected and analyzed for metal and anion concentrations.	PrEN 14405 CEN TC 292 WG6
The European shake test (the granular waste compliance leaching test). 4 variations exist.	CEN	Evaluation of leachate from building materials	2:1	6 hr then 18hr	100 g of sample added to a 1L bottle with 200 ml of rainwater and shaken for 6 hr. The solid is separated from the liquid via filtration and then added to a new bottle of 800 ml of simulated rain water and shaken for 18 hr.	Filtered (0.45 µm) leachate from both the 6 and 18 hr cycles is collected and analyzed for metal and anion concentrations.	EN 12457-3 CEN TC 292 WG2
TxDOT Soil pH Tex-128-E	TxDOT	Evaluation of soil pH	5:1	1 hr	Uses 30 g of minus 4.75 mm (No 4) material in 150 ml of 60ºC DI water. Stirred every 15 minutes for 1 hr prior to sampling.	Measured using a standard pH electrode	TEX-128-E
TxDOT Cl^- and SO_4^{-2} contents of soil Tex-620-J	TxDOT	Evaluation of soil chlorine and sulfate	10:1	15 to 18hr	Uses 30 g of pulverized material from a 300g minus 4.75 mm (No 4) split. 300 ml of DI water is added and stirred on a 150ºC hot plate.	Filtered (No. 42 size) leachate is analyzed for chlorine and sulfate.	TEX-620-J

A number of rapid geochemical leaching methods may provide a faster, cheaper, or more-reliable means of gathering the same chemical information that is obtained from the current suite of TxDOT soil electrochemistry methods. For example, the U.S. Geological Survey's Field Leach Test (FLT) has been shown to be effective for evaluating the geochemical properties of leachate from a variety of soils and rocks (Hageman, 2007). The procedure has been extensively tested and is comparable to the Environmental Protection Agency's synthetic precipitation leaching procedure (SPLP), and the European "shake test" recently standardized by the Comité Européen de Nomialisation (EN-12457-3; Hage and Mulder, 2004). The advantage of the USGS FLT is that it is quick, inexpensive, and produces a large enough quantity of leachate for any number of additional analytical tests. Moreover, the results provide high-quality geochemical data that are most-often indistinguishable from the data obtained from more rigorous (and expensive) leaching methods like column percolation tests (Hage and Mulder, 2004). Other investigators have also demonstrated that many of the more rigorous leaching protocols produce results that are similar to those from less detailed leach tests. For example, Nelson et al. (2000) show that the EPA SPLP is similar to the NCHRP leaching method.

Figure 2.2 illustrates the steps for a simplified leaching test (like the USGS FLT). The process can be broken into the following steps:

1. A rock sample is added to a given volume of distilled water in a reaction vessel.
2. The solution is allowed to mix for a given period of time.
3. After some settling time, in-situ parameters like pH, temperature, and conductivity (inverse of resistivity) are measured.
4. Samples of leachate are collected from the reaction vessels, filtered, and preserved for various laboratory analyses.

Geotechnical Properties of Backfill

The water permeability, aeration (air permeability) and water retention are widely recognized as backfill geotechnical properties influencing the corrosivity of the metallic earth reinforcements.

Water Permeability

Permeability refers to the propensity of a material to allow fluid to move through its pores. The primary concern with the permeability of the soil backfill is its effect on the corrosion process of the metallic earth reinforcements. Permeability is an important materials property during immersion conditions and especially during wet and dry conditions where corrosive moisture from condensation, leakage, or precipitation can be absorbed, retained, and concentrated with metal surfaces.

The permeability of a soil depends on a variety of soil characteristics including particle size, void ratio, mineralogy (in clays), fabric, and saturation. Additionally, the diameter of soil particles has been related to the permeability of a soil deposit. In particular, the permeability has been linked to D_{10}, where D_{10} is the equivalent diameter at which 10% of the soil particles are finer. For clean sands, Hazen developed the following relationship relating the permeability, k, to D_{10} (Lambe and Whitman, 1969):

$$k = C\, D_{10}^2 \qquad (2.8)$$

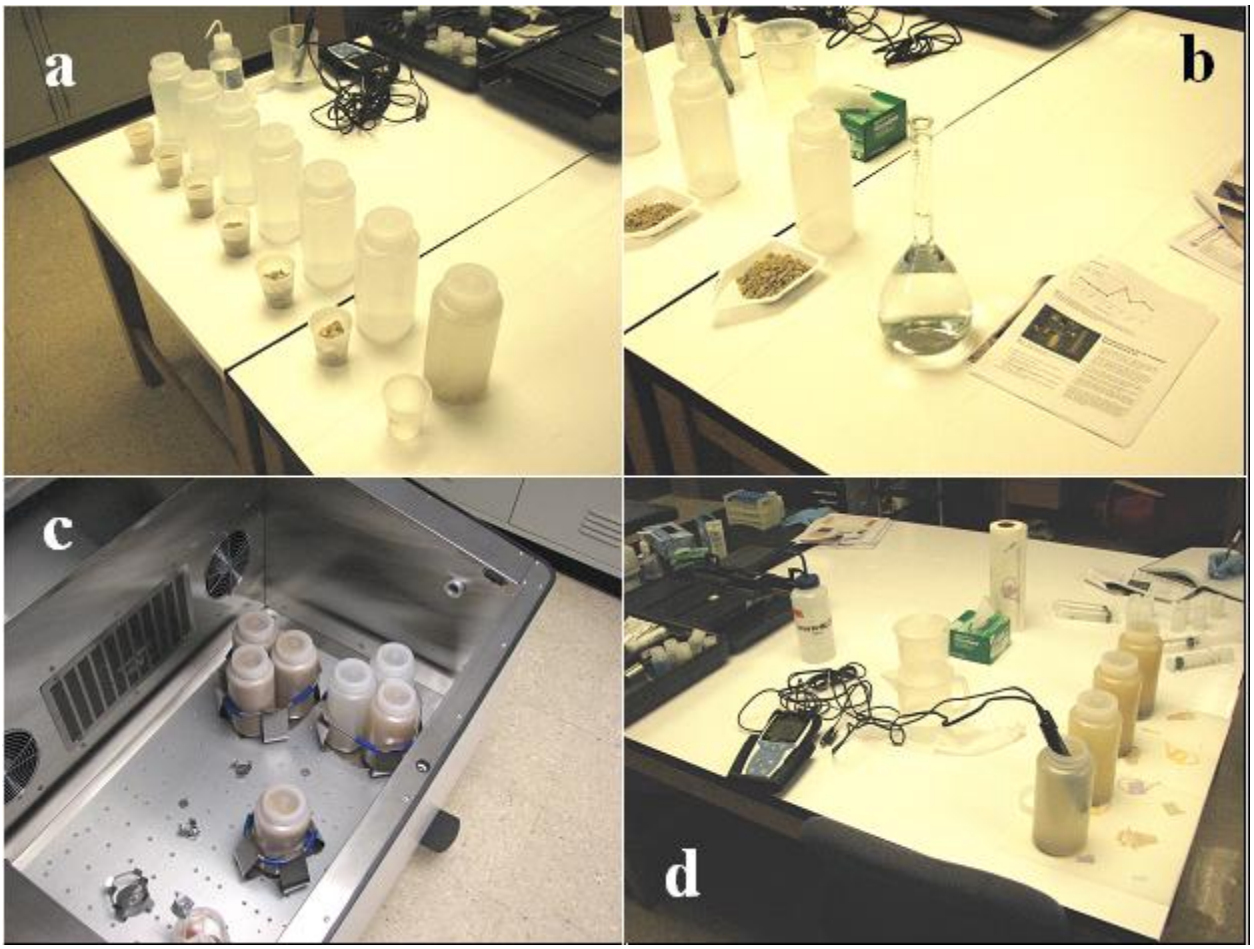

Figure 2.2 - Illustration of FLT Leaching Procedure

(a) measured amounts of rock are prepared, and (b) added to a measured volume of DI water. The samples are shaken (c) and then the in-situ parameters like pH, temperature, conductivity, and ORP are measured (d). Finally, samples are collected via syringe filtration for analytical analysis (not shown).

Soils with a wide gradation of particle sizes can pack more efficiently, leading to smaller diameter pore sizes which reduce the flow of fluid. The void ratio is another parameter which affects the permeability of a given soil. The void ratio is defined as the ratio of the volume of the voids to the volume of the solids; consequently, an increase in the void ratio, or void space, will lead to an increase in the permeability of a given soil (Lambe, 1951).

Fines contents and the type of fines are also important. Fines with Montmorillonite exhibit a much lower permeability than those with Kaolinite. The other major parameter influencing the measured permeability of a soil is the degree of saturation. Permeability is a direct function of the degree of saturation, with an increase in saturation causing an increase in permeability (Lambe, 1951). Table 2.3 lists some soil permeability limits for typical soils.

Aeration (Air Permeability)

Aeration affects the access of oxygen and moisture to the metal, consequently affecting corrosion. Oxygen causes corrosion by combining with metal ions to form oxides, hydroxides, or salts of metal. If these corrosion products are soluble or removed from the anodic areas,

corrosion proceeds, but if the products accumulate, they may act as a protective layer to reduce corrosion or may contribute to conditions that favor localized rather than uniform corrosion. Corrosion by differential aeration may result from substantial local differences in type and compaction of the soil or variations in the oxygen or moisture content resulting thereof. Such a phenomenon is generally associated with fine-grained soils (Elias, 2000).

Table 2.3 - Soil Permeability Coefficients and Relative Permeability

Soil	Permeability Coefficient, k (cm/sec)	Relative Permeability
Coarse gravel	$>10^{-1}$	High
Sand, clean	10^{-1}-10^{-3}	Medium
Sand, dirty	10^{-3}-10^{-5}	Low
Silt	10^{-5}-10^{-7}	Very Low
Clay	$<10^{-7}$	Impervious

A study conducted by the Nevada Department of Transportation found the use of uniformly graded, processed aggregate near the wall face can adversely affect the corrosion of reinforcements. The change in gradation and density, corresponding to differences in the porosity of the backfill, promotes development of macro-cells due to differences in oxygen and moisture conditions. Development of these macro-cells can promote corrosion of the reinforcements and the practice of placing more poorly graded backfill near the wall face should be avoided.

The particle shape and surface characteristics of soil should also be investigated along with the grain size distribution. It is this characteristic that can provide an indication of aeration level in a backfill material. Aeration affects the corrosion mechanism by creating aerobic or anaerobic conditions. The defining particle shape and surface properties are form, angularity, and texture. Each of these defining shapes and surface characteristics can be classified on a scale proposed by Al-Rousan (2005).

Morris and Delphia (1999) obtained results indicating that particle shape is a contributing factor in the compaction of cohesionless soils. Their results indicated that the maximum dry unit weight increases with increasing roundness, while the gradation of soil was shown to play a minor role in determining the compaction of cohesionless soils. Coarse backfills with good drainage and ample aeration may corrode steel at a much lower rate than clay and silt. Current geotechnical specifications do not take into account the effect of the aeration and porosity of backfill. Localized changes in the aeration, permeability, and compaction of the backfill surrounding the steel reinforcement may give rise to an oxygen concentration cell. The lower-oxygen area (normally at lower elevations where soil is more compacted) in contact with the steel can become anodic with respect to the steel in contact with the backfill of higher levels of oxygen. This results in corrosion and metal loss at the anodes (Davis, 2000).

Environmental Factors

Temperature is an important parameter in the investigation of soil corrosivity, because it can modify the interactions between the metal and the backfill (Akpofoure and Kehinde, 2006). Even though spatial and temporal temperature fluctuations within a single MSE site are thought

to be modest, the regional changes in the temperature among all the MSE sites in Texas may impact the rates of metallic corrosion.

The amount and frequency of precipitation controls the in-situ moisture content in the backfill and therefore plays a key role in soil corrosivity. When the moisture content of a backfill increases, the rate of corrosion usually increases (Elias, 2000).

Moisture Content

Soil structure, permeability, and porosity determine the moisture content of a soil. Corrosion rates will drop significantly when the steel structure is below a ground water table (GWT) and the water is relatively stagnant (low to no flow velocity) since free oxygen is much reduced. Where the moisture content of a soil is greater than 25% to 40%, the rate of general corrosion is increased. Below this value, a pitting type corrosion attack is more likely. The rate of corrosion of steel increases when soil moisture content exceeds 50% of saturation. This may be compared to the critical relative humidity that occurs above ground in atmospheric corrosion. Maximum corrosion rates seem to occur at saturations of 60 to 85% (Darbin 1986). This range of saturation for granular materials roughly corresponds to the range of moisture content required in the field to achieve needed compaction levels. A survey of 14 California sites found saturation levels in MSE fills to be between 30 and 95%, with most samples exceeding 65% (Elias 2000). Therefore the placement compaction requirements for MSE structures will be subject to the maximum corrosion rates consistent with all other electrochemical criteria.

Field Monitoring and Performance

Field monitoring of the on-site corrosion rate of reinforcing steel can be used to calibrate and verify the laboratory-based predictions and close the gap between the predicted and actual corrosion performance of earth reinforcements. North Carolina DOT (NCDOT) has conducted such a study. In 1990, NCDOT began to install monitoring stations during the construction of MSE walls and proceeded to routinely monitor the half-cell potentials of reinforcements and coupons (Medford, 1999). The performance of galvanized steel reinforcements of the NCDOT study along with a number of other similar investigations over 75 test sites throughout the United States and Europe are documented in Gladstone et al. (2006). They concluded that when good construction practice is implemented and AASHTO electrochemical requirements are satisfied, the amount of metal loss is far less than what is predicted by the AASHTO model indicating that the AASHTO specifications are conservative (Gladstone et al., 2006).

Similar conclusions may apply to TxDOT current practice since the AASHTO electrochemical specifications are similar to the ones in TxDOT current specifications. The lack of correlation may be a result of the inappropriateness of the threshold values or the effects of the "other influencing parameters" which are absent in the current specifications or both. While field monitoring is essential in establishing the correlation between the laboratory test results and field performance, it is most effective if the test plan is as comprehensive as possible to capture the effects of the influencing parameters.

Survey of Districts

A survey was conducted to identify the types of backfill to be used, and to suggest projects that can be incorporated in this study. The questionnaire, which was distributed statewide to ensure that the inference space of the materials within Texas is covered, is included in Appendix A.

Survey responses were received from the twelve districts. The responses can be summarized in the following manner:

- About 50% of the MSE walls have a Type B backfill and 44% Type A or Type D backfills.
- About 73% of the districts use limestone as aggregate in MSE walls.
- Only three districts use recycled materials, mainly asphalt pavement (RAP) materials.
- Only two districts use chemical stabilizers, mainly cement, in their backfills.

Figure 2.3 shows the frequency of each test used by the districts that responded to the questionnaire. The tests that are more frequently used are the pH (Tex-128-E), Resistivity (Tex-129-E) and Gradation (Tex-110-E). Some of the districts had a concern with the implementation of coarser gradations, the amount of finer material required for resistivity, sulfate and chloride testing requires crushing and in some cases that artificially elevates the sulfate concentration. Based on the questionnaire and interaction with the PMC, six materials and three sites were selected for this study as discussed in the next chapter.

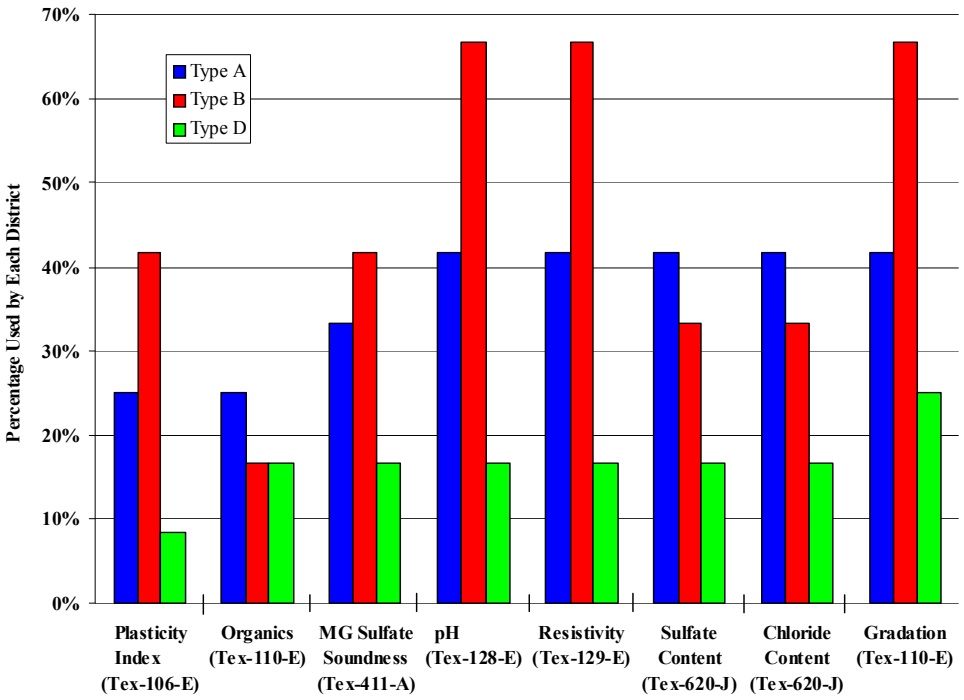

Figure 2.3 – Parameters used in Characterization of Backfills by Districts

Chapter 3 - Characterization of Backfill and Reinforcements

Introduction

This chapter contains the results from a number of tests to quantify the relevant parameters that would contribute to the corrosion of the metallic reinforcements and eventually to evaluate the adequacy of the current tests to predict the negative impact of these parameters. Six different backfill materials were sampled from six sources for the baseline study. The reported backfill types and aggregate types are presented in Table 3.1. In addition, a backfill material exhumed from a wall was tested as well.

Table 3.1 – Nature of Sampled Materials for This Study

District	Type of Backfill	Aggregate Type
Material A	Type D	Limestone
Material B	Type A	Limestone
Material C	Type D	Dolomite
Material D	Type D	Limestone
Material E	Type A	Limestone
Material F	Type D	Limestone

Geotechnical Characterization

The gradation curves for the seven materials are compared to the minimum and maximum limits specified in Item 423 for Type A and D backfills in Figure 3.1 and Table 3.2. Material D was the most uniform and the coarsest with 99.8% gravel. Materials B and E fall between Type A gradation limits while Materials A, D, C and F fall between both Type A and Type D gradation limits. Material B barely meets Type A gradation limits, the ½ in. sieve reached the maximum limit of 50%.

The constituents of the materials are shown in Table 3.3. All materials have gravel contents greater than 80%. Materials C and D had almost 100% gravel and no fines. Materials A, B, E and F had 6% to 22% sand and fine sand.

The plasticity index (PI) of each material was determined by Tex-104-E (liquid limit) and Tex-105-E (plastic limit). The results are shown in Table 3.4. Materials B, C and D were non-plastic. Materials A, E and F had a PI of about 4. Item 423 specifies a maximum PI of 6.

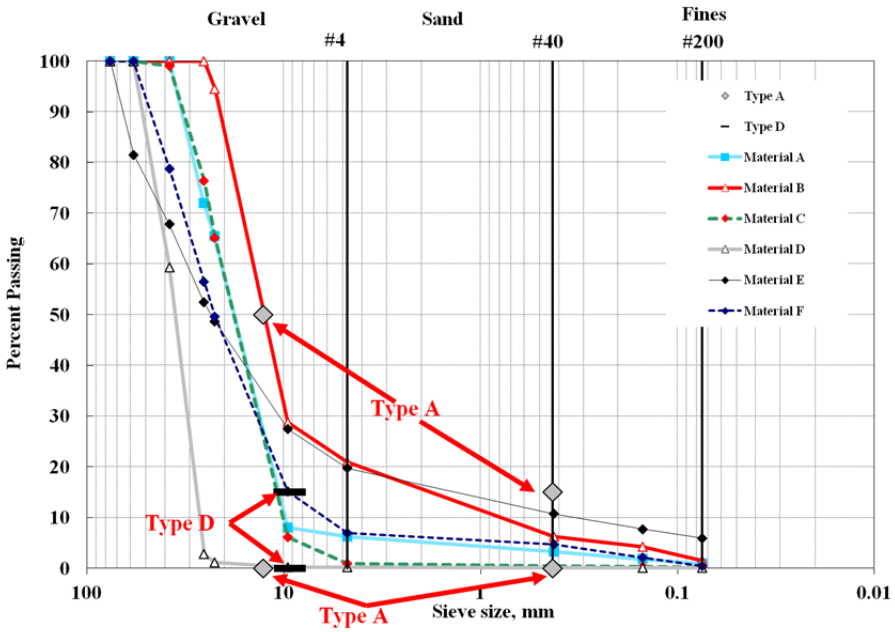

Figure 3.1 – Gradation Curves for all Backfill Materials

Table 3.2 – Sieve Analysis Results of Backfill Materials

Sieve Size	Percent Passing						Item 423			
							Type A		Type D	
	Material A	Material B	Material C	Material D	Material E	Material F	Min	Max	Min	Max
3"	100.0	100.0	100.0	100.0	100.0	100.0		100		100
2	100.0	100.0	100.0	100.0	81.5	100.0				
1.5	100.0	100.0	99.0	59.4	67.8	78.7				
1"	72.0	100.0	76.4	2.8	52.4	56.5				
7/8"	65.5	94.5	65.2	1.2	48.7	49.6				
1/2"	26.3	50.0	24.2	0.5	34.2	25.3	0	50		
3/8"	8.1	28.7	6.1	0.2	27.4	15.2			0	15
#4	6.3	20.9	1.0	0.2	19.7	7.0				
#40	3.3	6.3	0.4	0.2	10.7	4.7	0	15		
#100	1.8	4.2	0.3	0.1	7.7	2.1				
#200	0.9	1.5	0.2	0.1	5.9	0.5				

Table 3.3 – Material Constituents of Backfill Materials

Component	Percent of Total Materials					
	Material A	Material B	Material C	Material D	Material E	Material F
Gravel	94	79	99	100	80	93
Coarse Sand	3	15	1	0	9	2
Fine Sand	2	5	0	0	5	4
Fines	1	2	0	0	6	0

Table 3.4 – Atterberg Limits of Backfill Materials

Test	Material A	Material B	Material C	Material D	Material E	Material F
Liquid Limit	16	Non-plastic	Non-plastic	Non-plastic	15	22
Plastic Limit	13	Non-plastic	Non-plastic	Non-plastic	11	18
Plasticity Index	3	Non-plastic	Non-plastic	Non-plastic	4	4

The Wet Ball Mill Method (Tex-116E) was used to determine the resistance of aggregate to disintegration in the existence of water. The results are summarized in Table 3.5. The highest Wet Ball Mill (WBM) value was obtained from Material F. In contrast the materials with the least percentage loss were Materials C and D.

Table 3.5 – Crushing Potential of Backfill Materials

Parameter	Material					
	A	B	C	D	E	F
WBM Value (%)	11	6	1	1	22	30
AIV (natural aggregates)	19	11	9	13	25	28
AIV (crushed aggregates)	18	14	12	14	28	24
ACV (crushed aggregates)	29	22	16	26	37	34

Two alternate means of measuring the resistance of the aggregates to crushing are the aggregate crushing value (ACV) and the aggregate impact value (AIV) tests. The ACV gives a relative measure of the resistance of an aggregate crushing under a gradually applied compressive load, while the AIV provides the same information under a dynamic load. To perform these tests, adequate amount of materials passing the ½ in. sieve and retained on the 3/8 in. are either loaded to 90 kips (for ACV) or subjected to 15 blows of a 30 lb hammer. After appropriate tests, the material is retrieved and sieved. The AIV or the ACV is the percentage weight of materials passing a No. 8 sieve relative to the original weight of the specimen. The British Standard considers a material with ACV or AIV values of greater than 20 as crush susceptible.

The AIV and ACV values are also presented in Table 3.5. Since most materials were too coarse to provide enough natural materials passing the ½ in. sieve and retained on the 3/8 in. sieve for the ACV tests, the larger size aggregates had to be crushed. To ensure that the crushing process would not significantly impact these properties of the aggregates, AIV tests were performed on natural and crushed materials. There were reasonably small changes in the AIV's of the crushed and natural aggregates. Materials A, E and F were determined to be the most crush susceptible. Materials C and D had the most crush resistance values.

The optimum moisture content (OMC) and the maximum dry density (MDD) for each material obtained are shown in Table 3.6. We were unable to develop moisture-density curves for Materials B, C and D. These materials would not absorb any water and the compacted specimens would crumble as soon as they were extracted. Even though Materials A, E and F were very coarse, they yielded reasonable moisture-density curves. These materials that exhibited the highest crushing potential (see Table 3.6) severely crushed to finer materials during compaction. The optimum moisture contents for these materials ranged from 6% to 9%, and the maximum dry unit weights were 120 pcf and more. After compaction, these materials looked and behaved like a Type B material. On the other hand, the materials that could not yield a

moisture density curve provided a unit weight of 108 pcf and less. Even though the harder aggregates may be more expensive to acquire, their lower unit weights may have positive implication on the factor of safety of the walls.

Table 3.6 – Results of Moisture-Density Tests for Backfill Material

Parameter	Material					
	A	B	C	D	E	F
Optimum Moisture Content, %	9.0	N/A	N/A	N/A	6.0	8.3
Maximum Dry Unit Weight, pcf	120	108*	94*	95*	129	123

**** Dry unit weight at a moisture content of 3%.***

Geochemistry Characterization

The purpose of the geochemical characterization was to evaluate the materials using standard TxDOT methodologies to provide a baseline for comparison, and to compare the TxDOT methodologies to the USGS FLT method, which may be better suited for rapid chemical evaluation of coarser materials. Table 3.7 summarizes the results of tests for each of the selected backfill materials using Tex-128-E, Tex-129-E, and Tex-620-J, for quantifying the pH, resistivity, and chloride and sulfate contents, respectively. Most materials would not have passed the chloride or sulfate concentration criteria and samples from Materials A, C, E, and F also fail the resistivity criterion. The pH range for all samples is well within the 5.5-10 windows for acceptability.

Table 3.7 - Resistivity, pH, and Cl/SO4 Contents Measured Using TxDOT Methods.

Backfill Material	Resistivity (Tex-129-E), Ohm cm	pH (Tex-128-E)	Chloride (Tex-620 J), mg/kg	Sulfate (Tex-620 J), mg/kg
A	2322*	7.92	116.8	309.6
B	8815	8.79	326.0	151.6
C	1871	7.93	349.8	751.5
D	7740	8.69	611.3	460.7
E	2365	8.54	204.7	238.9
F	1967	8.14	91.5	64.7
TxDOT Limits	≥3000	5.5-10	≤ 100	≤ 200

The results of the resistivity tests performed on triplicate specimens of fine-grained fractions obtain from sieving and then on fine-grained materials obtained from crushing larger size aggregates are shown in Table 3.8. The average resistivity values of the crushed materials are consistently greater than those of the fines contained in the samples.

Table 3.8 – Resistivity Results for Backfill Materials

Parameter		Material					
		A	B	C	D	E	F
Natural Gradation	**Average**	2322	8815	1871	*	2365	1967
	COV	12%	11%	9%		9%	7%
Crushed	**Average**	4193	10105	3902	7740	4257	3161
	COV	7%	7%	27%	8%	2%	6%

**** Not enough materials***

Field Leach Testing (FLT)

The standard TxDOT methods used to evaluate the corrosive potential of backfill materials were originally designed for soils where only the smallest size fractions of backfill material are tested. Because coarse backfills often contain only a few percent fines (see Table 3.3), testing of these fine materials necessarily excludes the bulk of the rock material. In these cases, one is forced to make the assumption that the fines are chemically representative of the bulk rock. This assumption is likely to break down for field samples that are exposed to large amounts of chemical weathering. Conversely, the FLT method of testing does not exclude the coarse size fractions and thus may provide a more accurate assessment of the corrosive potential of larger backfill materials. The FLT method (as described in Chapter 2 and Hageman, 2007) utilizes a 50 g sample of backfill material that is added to 1000 ml of distilled water in a 1L plastic bottle. The solution is agitated for 5 minutes, and after some settling time, the pH and conductivity (inverse of resistivity) of the fluid are measured in-situ, while filtered samples are collected for laboratory analysis. During testing of the coarse materials, it was found that it was necessary to increase the mass of the sample from 50 g to 100 g in order to accommodate the largest pieces of rock without crushing. This solid/liquid ratio is identical to that used for the European "shake test" (EN-12457-3) and the TEX-620-J test for chloride and sulfate.

Leaching tests are sensitive to a variety of external parameters. For coarse-grained backfills the impact of grain size and leaching time are likely the most critical. Hence, the FLT testing was focused in three areas: (1) determining the effect of grain size on pH, resistivity, and chemistry, (2) determining the effect of leaching time of pH, resistivity, and chemistry, and (3) testing the validity of the assumption that the finest fractions of coarse backfill often used for TxDOT testing are chemically representative of the bulk rock.

Impact of Size Fractions and Leaching Time

FLT tests were performed on several sieve sizes of each of the six backfill materials and for a mixed grab sample (i.e., a sample that includes all sizes). Samples were collected and analyzed as a function of time for up to 200 hrs. Figure 3.2 presents the results of pH measurements for the FLT tests. The red lines in Figure 3.2 depict the pH measured using Tex-128-E. The results show that pH changes considerably among the tested size fractions and that pH generally decreases as a function of time for about 48 hrs. The reason for the pH-dependence of the size-fractions is likely two-fold: (1) the rate of chemical dissolution of the rocks increases with decreasing size, and (2) the chemistry of the size fractions may be different, particularly for the smaller sizes. The former changes in pH are a reflection of how fast the experimental system moves toward thermodynamic equilibrium. This includes the necessary equilibrium with atmospheric CO2 (10-3.5 atm in air). This is critical for the carbonate rock system because carbonates species (ultimately carbonate and bicarbonate) are being generated from the rock and the air, and it takes time for these to equilibrate (or at least to reach a steady state) at room temperature. The smaller size fractions would have a head start in reaching this steady state because they dissolve faster. Chemically driven changes in pH among the size fractions may be attributable to atmospheric interactions with SOx and NOx compounds that tend to breakdown the surfaces of reactive (e.g., carbonate) rocks. Similar chemical weathering reactions are responsible for the accelerated deterioration of building stones. These FLT experiments alone are not able to resolve the relative importance of these end-member possibilities; however, our comparison to lab-crushed materials (discussed below) pinpoints the role of chemical

heterogeneity in controlling pH. In general, the FLT pH measurements for the small size fractions are in good agreement with the TxDOT pH results (Figure 3.2). For example, at the 48hr mark the two methods have an average difference of less than 0.2 pH units if compared against the smaller size fractions of the FLT. The FLT test might be an attractive alternative to Tex-128-E for some applications.

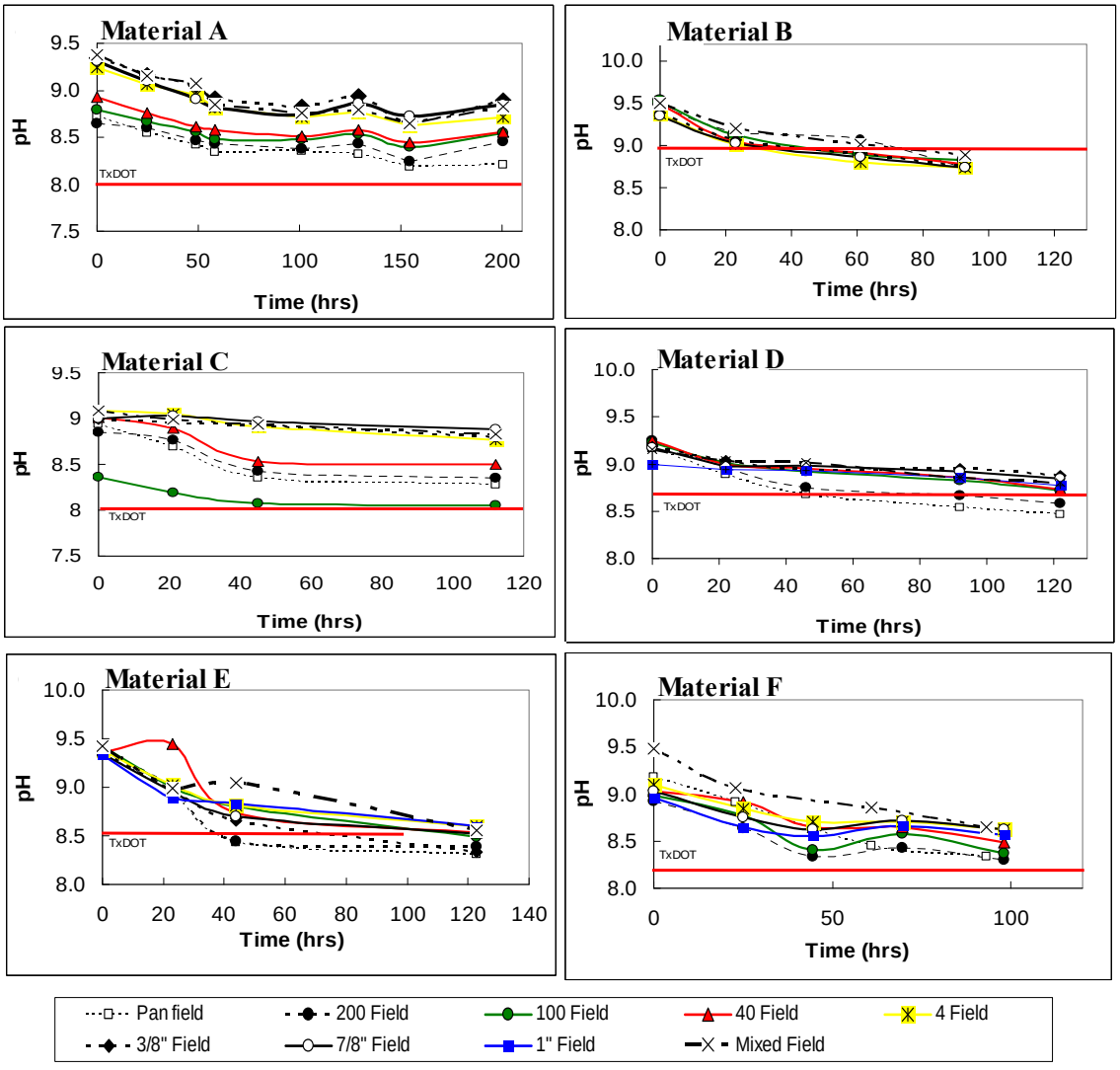

Figure 3.2 - pH of Different Size Fractions of Field Materials during FLT Testing as a Function of Time.

Figure 3.3 presents the results of resistivity measurements for the FLT tests. The red lines in the figure depict the resistivity measured using Tex-129-E. Unlike the pH tests, the TxDOT resistivity is not directly comparable to the resistivity in the FLT tests because of the different solid/liquid ratios used for each method. The results show that resistivity changes considerably among the tested size fractions, but that it remains relatively constant as a function of time. As with pH, the resistivity-dependence of the size fractions could be related to rates of leaching and/or the chemistry of the different size fractions. In most cases the Tex-129-E method

produced resistivity values less than all size fractions of the FLT method. However, for Materials B and D the Tex-129-E method resulted in higher resistivity values than the FLT method. The latter result is unexpected because the FLT method uses a much high liquid/ solid ratio, than the Tex-129-E method (Tex-129-E uses only enough water to saturate the soil). Therefore one would expect the FLT to have a lower concentration of ions relative to the amount of liquid and thus a higher resistivity. Further testing is necessary to evaluate this apparent contradiction and how the resistivity values relate to corrosivity.

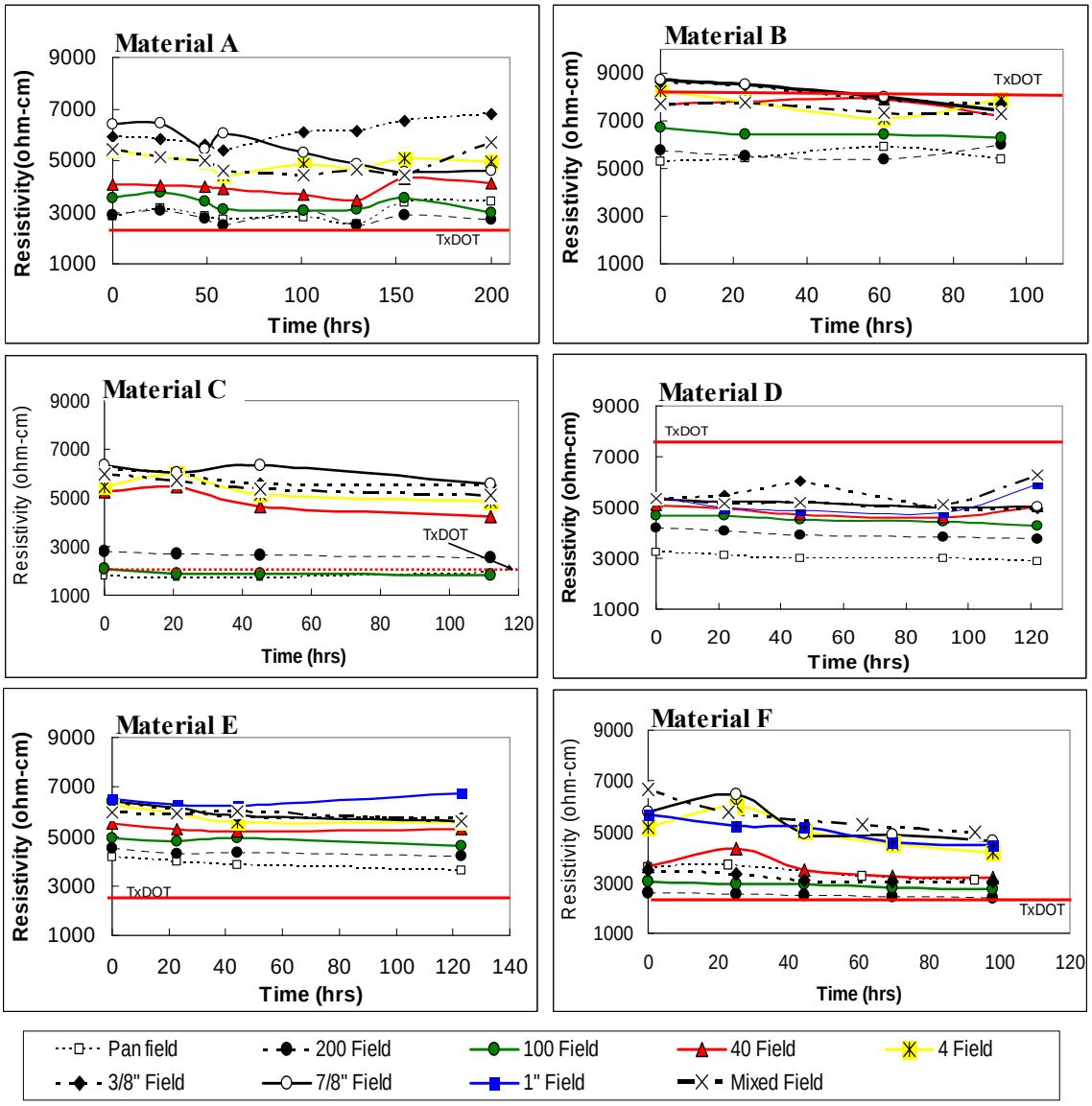

Figure 3.3 - Resistivity of Different Size Fractions of Field Materials during FLT Testing as a Function of Time.

In addition to the FLT testing of the sieved field samples, mechanically-crushed and sieved samples of the coarsest field fraction from each material (termed "lab-crushed" hereafter) were also tested. Because the smaller fractions were generated directly from the coarser fractions, the lab-crushed fractions should be chemically homogeneous. Therefore by performing FLT tests on

the lab-crushed fractions a better evaluation of the importance of chemistry and size fraction can be made. Any differences in pH, resistivity, or chlorine and sulfate concentrations among the lab-crushed size fractions can be attributed solely to rate differences (i.e., size differences).

As specified in Tex-620-J (for materials with a top size larger than No 4), lab-crushed material was used to determine the chloride and sulfate concentrations of the different materials. For comparison purposes, the chloride and sulfate concentrations of individual lab-crushed size fractions were measured using the FLT method. Table 3.9 presents the results of chloride and sulfate measurements for the FLT tests, as well as the chloride and sulfate values measured using Tex-620-J for comparison. The aggressive leaching at elevated temperature used for the Tex-620-J method results in larger concentrations of chloride and sulfate relative to the FLT tests conducted at room temperature (Table 3.2). It appears that Tex-620-J is not very representative of the likely chloride and sulfate concentrations of fluids in contact with these materials under normal temperature conditions, but instead provides arbitrary concentration values for comparative purposes. Additional testing will determine which method better predicts corrosive potential.

Table 3.9 - Chloride and Sulfate Contents of Different Size Fractions of Lab-Crushed Material Subjected to FLT Test.

Material	Chloride Concentration (mg/Kg)							
	Pan	200	100	40	4	3/8”	Mixed	TxDOT
A	140.9	141.2	147.1	135.2	152.2	128.1	129.9	116.8
B	305.9	312.4	285	249.2	238.3	239.3	244.9	326
C	286.4	272.8	274.7	249.1	254.4	250.5	250.9	349.8
D	309.1	282.7	269.5	246	257.3	233.9	241.9	611.3
E	171.9	150.7	136.7	116.1	-	-	110.1	204.7
F	209	213.4	165.8	143.2	103.5	101.1	111.5	91.5

Material	Sulfate (mg/Kg)							
	Pan	200	100	40	4	3/8”	Mixed	TxDOT
A	300.9	275.3	198.7	137.9	119.3	96.4	106.6	309.6
B	171.6	158.8	145.7	117.4	114.9	110.9	115.3	151.6
C	668.5	358	283.9	180	169.7	158.7	161.8	751.5
D	211.5	156.1	148.4	136.8	144.5	126.7	134.0	460.7
E	108	85.3	62.5	59.4	-	-	55.6	238.9
F	232.4	170	116.2	66.4	37.7	41.2	63.4	64.7

The lab-crushed materials can also be used to test the validity of the assumption that the finest fractions of coarse backfill from the field are chemically representative of the bulk rock. To do this the chemistries of the identical field and lab-crushed size fractions can be simply compared. If the chemistries are different, the assumption of chemical homogeneity among the sizes collected in the field breaks down. The initial (after 10 min.) FLT measurements of pH and resistivity for the field and lab-crushed samples are compared in Figures 3.4 and 3.5, respectively. The variations in pH and resistivity among the lab-crushed size fractions are a reflection of the differences in leaching rates. In general, the smallest fractions are less resistive

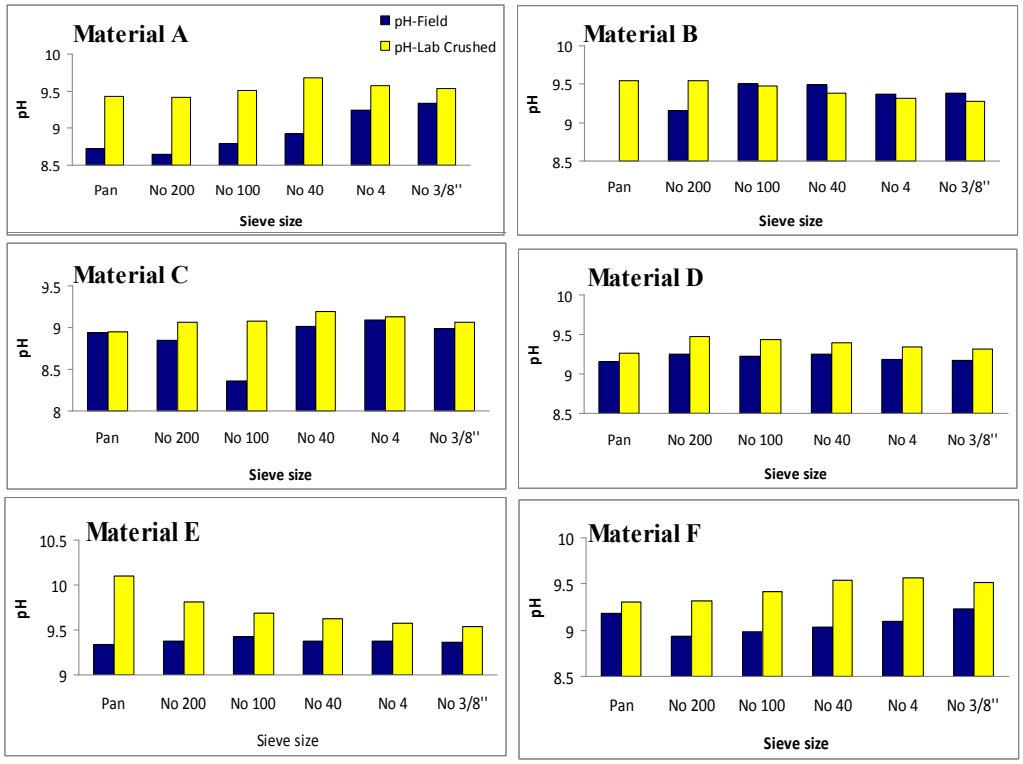

Figure 3.4 - Initial pH of Different Size Fractions For Lab-Crushed and Field Materials Determined Using USGS FLT Method.

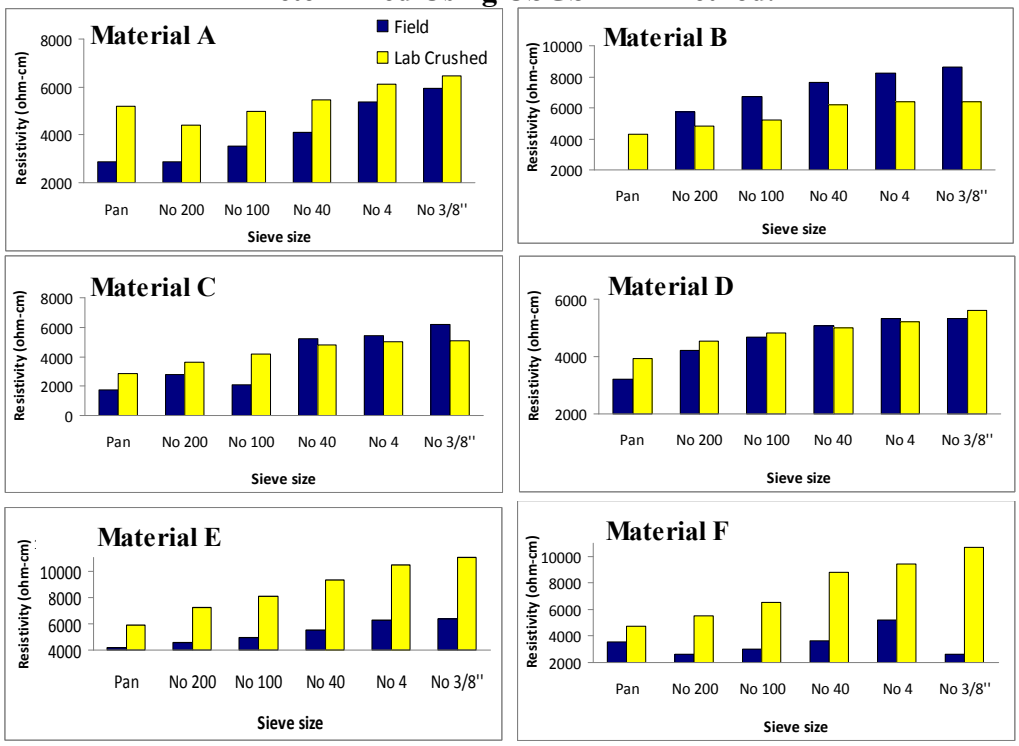

Figure 3.5 - Initial Resistivity of Different Size Fractions for Lab-Crushed and Field Materials Determined Using USGS FLT Method.

than the larger fractions because more ions have leached into solution from the smaller fractions. These differences become smaller with longer leaching times because the larger size fractions have a chance to leach more ions into solution essentially catching up to the smaller size fractions. Figure 3.6 is an example dataset from FLT testing of Material A that presents the pH of the different size fractions as a function of leaching time. Size-driven differences do not explain the discrepancies in pH and resistivity when comparing the lab-crushed vs. the field samples of the same sieve size. In most cases the pH of the samples collected in the field are lower than those of the lab-crushed samples of the same size fraction (Figure 3.4). The resistivity of the field samples is also lower (i.e., more ions are in solution) than compared to the corresponding lab-crushed fractions (Figure 3.5). Moreover, these differences are generally the greatest for the smaller size fractions and become insignificant for the larger size fractions (Figure 3.6). This demonstrates that the smaller size field fractions are chemically different than their lab-crushed counterparts. These chemical differences result in more ions in solution and lower pH values. We suspect that this is a reflection of the chemical weathering of field samples. SO_x and NO_x compounds in the atmosphere can react with carbonate rocks to produce reactive surface layers (typically of soluble sulfate minerals) that are easily abraded mechanically and easily leached chemically. Hence in field samples of coarse carbonate rocks, the finer fractions likely include some weathering products. This hypothesis was tested through our chemical analysis of the FLT tests as discussed below.

The concentrations of all major and trace elements in solution during the FLT experiments were measured in order to pinpoint the chemical differences. Table 3.10 compiles these chemical analyses for the individual size fractions for both field and lab-crushed samples. Elements Ca, Mg, Na, K, Al, SO_4, Cl, Ba, Sr, Li, and F were detected in the FLT leachate for all the materials and trace amounts of Cu, Fe, Rb, and Zn only for a few samples. The major cations for all the materials were always Ca and Mg and the major anions were always HCO_3/CO_3 (not measured, but can be assumed because these are carbonate rocks) and SO_4. These are typical element assemblages for the leaching of carbonate rocks. It is important to note that the SO_4 concentrations of the field samples in the PAN and No. 200 size fractions are 2 to 12.5 times greater than the corresponding lab-crushed fraction. Although present at lower concentrations, the NO_3 of the field samples in the PAN and 200 size fractions are also up to 6 times greater than the corresponding lab-crushed fraction. These observations support the hypothesis that the field materials are impacted by chemical weathering reactions largely involving SO_x and some NO_x compounds. This is a critical observation because the TxDOT pH and resistivity tests call for the use of fine-grained field materials. These field materials can bias the testing, resulting in pH and resistivity values that are not truly representative of the bulk rock. Additional testing will focus on finding the best testing methods to eliminate this bias.

Comparison of Test Results from Traditional TxDOT and Proposed Methods

The results obtained from the proposed procedure and those typically measured as per TxDOT specifications are compared in Figure 3.7. The following trends are observed from these results:

- The pH values measured with both methods pass the current criteria specified by TxDOT. However, the pH values from proposed method are greater than those measured with the traditional TxDOT method.
- The resistivity values from the two methods are different. All materials tested pass the current TxDOT specifications with the proposed method, while only two materials pass the current resistivity requirements under current TxDOT methods.

- The sulfate and chloride concentrations measured with the new method are lower than those measured by TxDOT method. Maintaining the same acceptance criteria, a number of materials that fail required TxDOT concentrations, pass based on the new method.

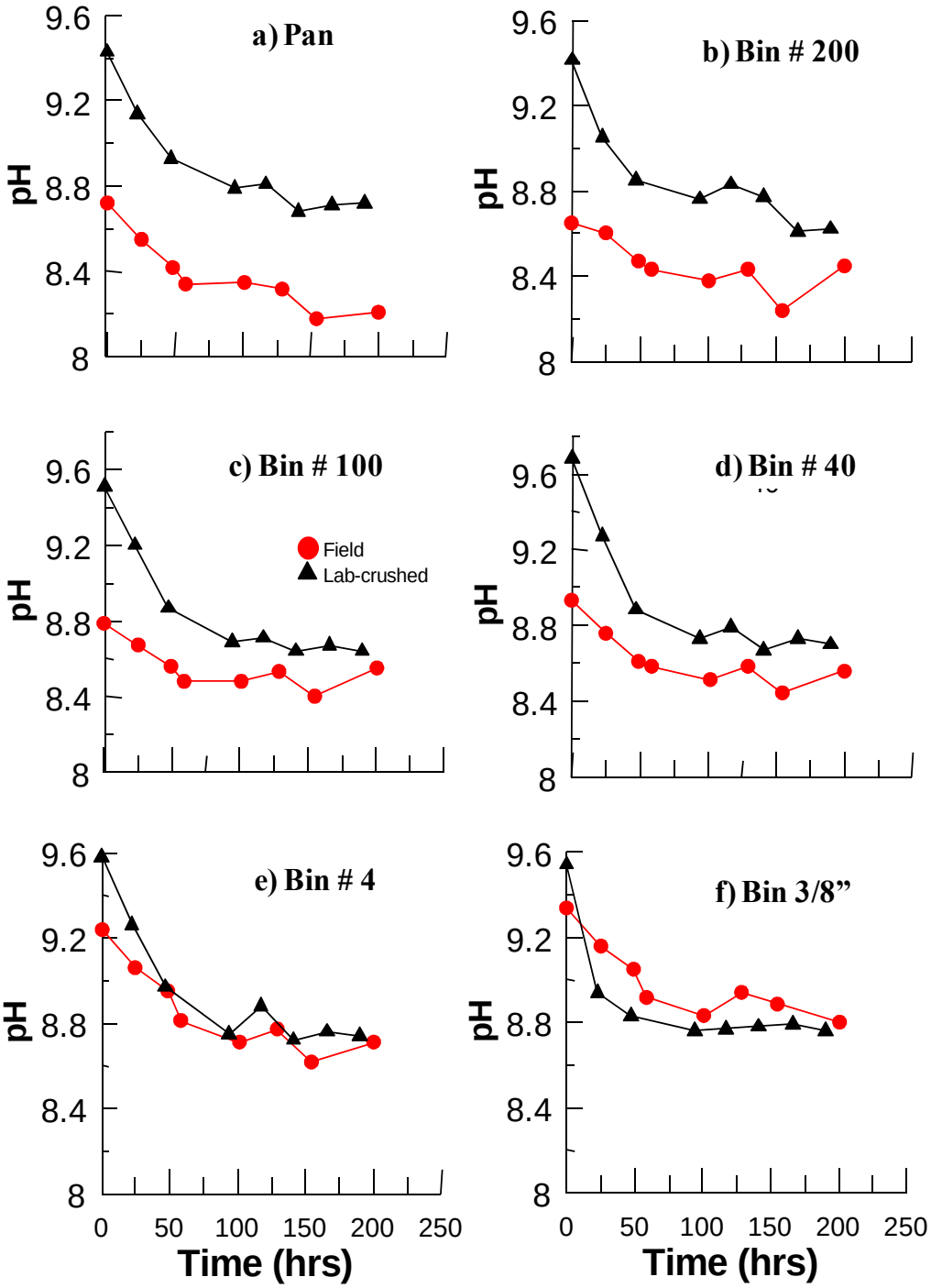

Figure 3.6 - pH of Different Sieve Sizes from Field and Lab-Crushed Material A as a Function of Leaching Time Using FLT Method.

Table 3.10a. Major and Trace Ion Concentrations of FLT Tests.

Material and Size	Ca (mg/kg)		Mg (mg/kg)		Na (mg/kg)		K (mg/kg)		SO4 (mg/kg)		Cl (mg/kg)		NO_3 (mg/kg)		Al (mg/kg)	
PAN	F	LC	F	LC	F	LC	F	LC	F	LC	F	LC	F	LC	F	LC
A	299.3	151.4	55.8	28.9	212.1	208.5	36.9	34.3	674.8	300.9	144.7	140.9	53.9	14.8	0.4	0.3
B	81.9	85.6	19.2	66.5	148.8	223.5	12.9	33.9	1358	171.6	235.5	305.9	19.2	13.4	0.1	0.3
C	531	519.1	84.8	80.9	185.2	122.8	58.9	40.5	2045	668.5	305	286.4	<4.0	8.4	0.6	0.9
D	222.9	519.1	37.3	25.2	251.3	256.4	47.6	44.7	561.1	211.5	277.7	309.1	<4.0	<4.0	0.4	0.8
E	103.1	-	27.7	-	274.1	-	21	-	204.6	108	324.3	171.9	23.4	22.3	0.3	-
F	175.4	-	25.3	-	326.4	-	16	-	562.5	232.4	521.4	209	75.2	22	0.2	-
No 200																
A	309	151.6	60.1	26.9	236.4	26.9	36.5	30.6	448.1	275	110.4	141.2	77.9	14.7	0.4	0.3
B	67.2	79.2	20.4	33.5	140.8	33.5	10.6	19.5	1989	158.8	239.4	312.4	22.5	13	0	0.3
C	263.3	257.7	44.7	41.3	164.5	41.3	38.9	27.3	905.1	358	277.3	272.8	<4.0	6.3	0.6	0.7
D	142.1	257.7	20.9	17	239.3	17	32.3	29.8	257.5	156.1	264.8	282.7	<4.0	<4.0	0.3	0.2
E	93.4	-	20.4	-	258.2	-	16.9	-	184.6	85.3	313.8	150.7	21.3	14.6	0.3	-
F	262.8	-	38.2	-	414.1	-	18.5	-	683.2	170	475.1	213.4	64.8	18.3	0.7	-
No 100																
A	219.9	122.6	45.5	20.6	204.1	206.3	27.6	27.3	118.2	200	144.8	147.1	76.2	13.4	0.2	0.4
B	60.8	88.7	16.7	28.8	129.2	196.7	10	17.2	286.8	145.7	167.1	285	26.1	<4.0	0	0.3
C	530	520.5	23.7	22.2	150.5	100.9	21.5	14.9	1782	283.9	239.1	274.7	<4.0	5.8	0.3	0.7
D	119.6	520.5	18.2	14.9	229.4	234.2	28.9	26.4	202.9	148.4	250.5	269.5	<4.0	<4.0	0.3	0.1
E	86.2	-	16.1	-	250.5	-	14.1	-	142.9	62.5	286.1	136.7	15.8	<4.0	0.1	-
F	262.8	-	30.3	-	398.9	-	12.9	-	424	116.2	293.8	165.8	36.4	<4.0	0.7	-
No 40																
A	183.1	105.4	34.1	14.9	189.1	207.9	21.1	25	273	140.6	139	135.2	55.9	9.3	0.3	0.3
B	63.5	85.5	10.4	11.4	136.6	187.1	5.3	9.1	79.6	117.4	145.7	249.2	<4.0	<4.0	0	0.2
C	81.5	85.9	12.6	12.1	124.4	91	18.2	12.7	199.3	180	240.7	249.1	<4.0	4.8	0.4	0.5
D	95.8	85.9	12.5	12.8	222.8	228.9	23.7	23	171.7	136.8	263.7	246	<4.0	<4.0	0.1	0
E	79.4	-	12.2	-	227.2	-	11.3	-	120.1	59.4	264.5	116.1	<4.0	<4.0	0.4	-
F	137.7	-	20.8	-	348.8	-	9.3	-	245.3	66.4	170	143.2	31.2	<4.0	0.3	-
No 4																
A	106.8	84.2	14.1	11	197.9	211.2	15.8	23.3	147.8	123	139.3	152.2	14.4	5.3	0.3	0.2
B	45.3	74.3	6.4	8.7	122.7	169.5	2	7.9	67.8	114.9	137.7	238.3	<4.0	<4.0	0	0.4
C	74.9	75.9	8.6	8	128.6	89.8	14.1	9.1	156.8	169.7	233.1	254.4	<4.0	4.5	0.4	0.5
D	-	75.9	-	11.1	-	221.2	-	21	150.4	144.5	268.5	257.3	<4.0	<4.0	-	0
E	78.1	-	8.3	-	201.5	-	8.6	-	104.1	-	235.9	-	<4.0	<4.0	0.2	-
F	94.5	-	10.3	-	255.1	-	7.5	-	145.3	37.7	100.6	103.5	<4.0	<4.0	0.3	-
3/8”																
A	80.6	72.3	8.7	7.7	201.5	191.4	16.7	21.1	106.2	97.9	131.6	128.1	5.1	4	0.3	0.1
B	52.1	70	7.7	8.7	128.8	171.1	2.7	7.4	92.5	110.9	141.1	239.3	<4.0	<4.0	<4.0	0.2
C	55.3	57.8	7.2	6.7	125.6	91.1	13.3	9	132.8	158.7	236.5	250.5	<4.0	4.6	0.2	0.3
D	95.2	57.8	11.6	10.1	418.5	206.7	26.5	18.7	135.7	126.7	247.2	233.9	<4.0	<4.0	0.2	<4.0
E	73.5	-	7.4	-	189.7	-	7.9	-	97.6	-	218	-	<4.0	<4.0	0.1	-
F	133.9	-	15.3	-	274	-	7.8	-	153.8	41.2	106.6	101.1	11.8	0	0.9	-

Table 3.10b - Major and Trace Ion Concentrations of FLT Tests.

Material and Size	Ba (mg/kg)		Li (mg/kg)		Sr (mg/kg)		F (mg/kg)		Cu (mg/kg)		Fe (mg/kg)		Rb (mg/kg)		Zn (mg/kg)	
PAN	F	LC	F	LC	F	LC	F	LC	F	LC	F	LC	F	LC	F	LC
A	0.3	0.1	0.1	0.1	0.9	0.8	3.5	3.2	<0.1	<0.1	0.1	<0.1	0.1	0.1	<0.1	<0.1
B	0.1	0.1	0.1	0.1	0.6	0.9	3.1	2.5	<0.1	0.1	<0.1	<0.1	0.1	<0.1	0.6	2.7
C	0.3	0.3	0.2	0.2	2.5	2.6	3.8	3.4	0.1	0.3	<0.1	<0.1	0.1	<0.1	0.1	0.7
D	0.5	0.8	0.2	0.2	9.3	4.5	4.8	4.5	0.1	<0.1	<0.1	<0.1	0.1	0.1	0.7	1.2
E	0.1	-	0.1	-	0.9	-	3.2	2.7	<0.1	-	<0.1	-	<0.1	-	0.4	-
F	0.7	-	0.1	-	2.4	-	9.1	9.6	0.1	-	<0.1	-	<0.1	-	0.1	-
No 200																
A	0.3	0.1	0.1	0.1	0.9	0.7	3.7	2.6	<0.1	<0.1	<0.1	<0.1	0.1	<0.1	<0.1	<0.1
B	0.1	0.0	0.1	0.1	0.5	0.7	2.2	2.4	<0.1	0.1	<0.1	<0.1	0.2	<0.1	0.1	0.4
C	0.2	0.2	0.2	0.1	1.5	1.6	3.7	2.6	<0.1	0.2	<0.1	0.2	<0.1	<0.1	0.1	0.6
D	0.5	0.2	0.1	0.1	2.9	3.7	2.8	2.7	<0.1	<0.1	<0.1	<0.1	0.1	0.1	0.6	0.1
E	0.1	-	0.1	-	0.8	-	2.5	2.0	<0.1	-	<0.1	-	<0.1	-	0.1	-
F	0.7	-	0.2	-	3.5	-	9.9	7.4	0.2	-	<0.1	-	<0.1	-	1.2	-
No 100																
A	0.2	0.1	0.1	0.1	0.5	0.5	3.8	2.1	<0.1	0.8	<0.1	<0.1	<0.1	<0.1	<0.1	<0.1
B	0.0	0.0	0.1	0.1	0.3	0.7	2.2	2.1	<0.1	<0.1	<0.1	<0.1	0.1	<0.1	0.6	1.0
C	0.2	0.2	0.2	0.1	1.1	1.2	4.8	1.9	0.1	0.3	<0.1	<0.1	<0.1	<0.1	1.4	1.9
D	0.3	0.2	0.1	0.1	2.5	2.8	2.1	2.2	<0.1	<0.1	<0.1	<0.1	<0.1	0.2	0.3	<0.1
E	0.1	-	0.1	-	0.7	-	2.1	1.4	<0.1	-	<0.1	-	<0.1	-	0.6	-
F	0.7	-	0.2	-	2.8	-	8.6	4.8	0.1	-	<0.1	-	<0.1	-	0.9	-
No 40																
A	0.2	0.1	0.1	0.1	0.4	0.4	3.5	1.3	<0.1	1.1	<0.1	<0.1	<0.1	0.1	<0.1	<0.1
B	0.0	0.0	0.1	0.1	0.3	0.5	0.8	1.3	<0.1	0.1	<0.1	<0.1	0.2	<0.1	0.3	4.0
C	0.1	0.1	0.2	0.1	0.5	0.5	0.8	1.3	0.3	0.3	0.1	<0.1	<0.1	<0.1	0.7	0.8
D	0.2	0.1	0.1	0.1	1.5	1.5	1.7	1.4	0.1	0.1	<0.1	<0.1	0.1	<0.1	0.3	0.1
E	<0.1	-	0.1	-	0.5	-	1.5	<1.0	<0.1	-	<0.1	-	<0.1	-	0.5	-
F	0.7	-	0.1	-	1.8	-	4.6	1.6	0.1	-	<0.1	-	<0.1	-	0.7	-
No 4																
A	0.1	0.0	0.1	0.1	0.3	0.4	1.6	1.1	<0.1	<0.1	<0.1	<0.1	<0.1	0.1	<0.1	<0.1
B	0.1	0.0	0.1	0.1	0.3	0.4	0.0	1.2	0.1	<0.1	<0.1	<0.1	<0.1	<0.1	1.0	0.8
C	0.1	0.1	0.2	0.1	0.4	0.4	0.9	1.2	0.1	0.1	<0.1	<0.1	<0.1	<0.1	0.4	0.6
D	-	0.1	0.0	0.1	0.0	1.0	1.3	1.2	0.3	0.2	<0.1	<0.1	<0.1	0.2	1.4	0.8
E	<0.1	-	0.1	-	0.5	-	0.9	<1.0	<0.1	-	<0.1	-	<0.1	-	1.1	-
F	0.5	-	0.1	-	0.9	-	2.0	<1.0	0.1	-	<0.1	-	<0.1	-	1.2	-
3/8”																
A	0.1	0.0	0.1	0.1	0.4	0.4	1.0	1.0	<0.1	<0.1	<0.1	<0.1	<0.1	<0.1	0.1	0.2
B	0.1	0.0	0.1	0.1	0.3	0.4	0.0	1.2	0.1	0.1	<0.1	<0.1	0.1	<0.1	0.7	0.8
C	0.0	0.0	0.2	0.1	0.4	0.4	0.0	0.0	0.1	0.2	<0.1	<0.1	<0.1	<0.1	0.7	0.9
D	0.2	0.1	0.2	0.1	1.2	0.9	1.4	0.0	0.2	0.2	<0.1	<0.1	<0.1	0.1	0.6	0.5
E	<0.1	-	0.1	-	0.5	-	1.1	<1.0	<0.1	-	<0.1	-	<0.1	-	1.0	-
F	0.4	-	0.1	-	1.5	-	2.2	1.1	0.3	-	<0.1	-	<0.1	-	2.6	-

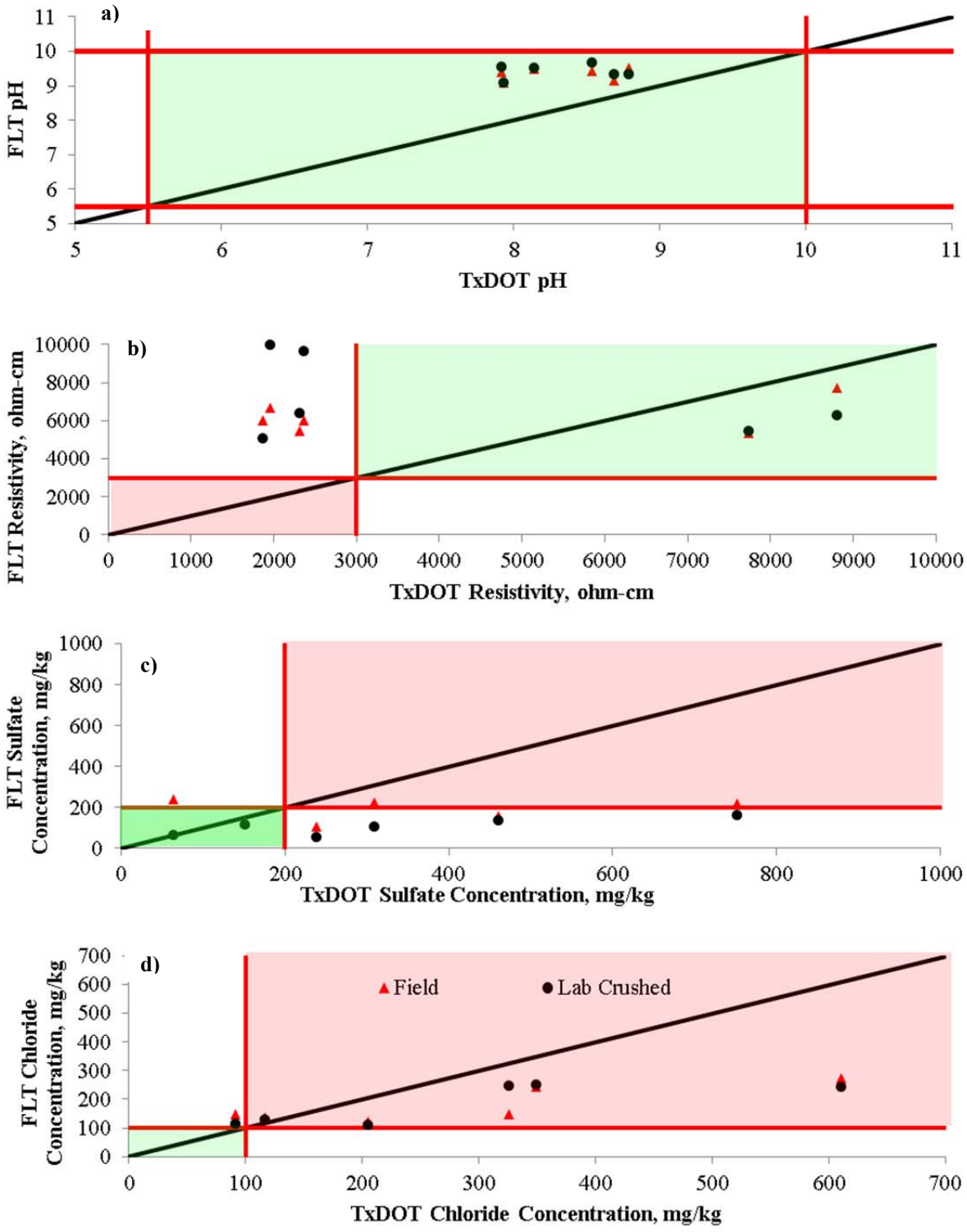

Figure 3.7 – Relationships between Parameters Measured with TxDOT and Proposed Methods

Metallurgical Characterization

The metallic reinforcements containing a galvanized coating were metallographically prepared for characterization with a scanning electron microscope (SEM). The metallographic preparation consisted of polishing a cross-section of the reinforcement with 600, 800, and 1200 SiC grit paper followed with final polishing with alumina particles (i.e., 1 μm). A few samples were etched with nital (nitric-ethanol solution) to discern grains as shown in Figures 3.8 and 3.9. The SEM image indicates an α-phase typical for low carbon steel (0.30 wt% C) with the indentations showing where prior inclusions were positioned. The inclusions are normal for the carbon steel though if unprotected they may serve to initiate pitting corrosion. However, with the protective zinc layer, the carbon steel would be less susceptible to pitting corrosion. The zinc layer of the

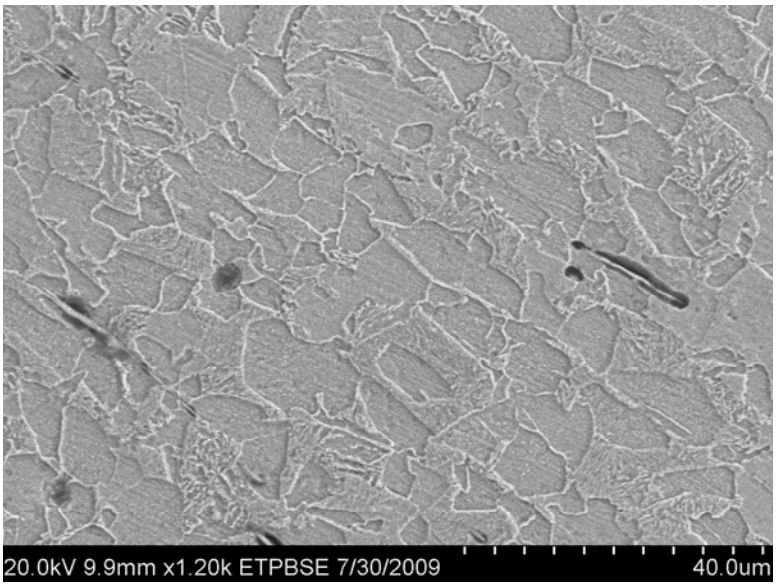

Figure 3.8 – Scanning Electron Microscope Image of Galvanized Steel Indicating an α-phase of Metallic Reinforcement.

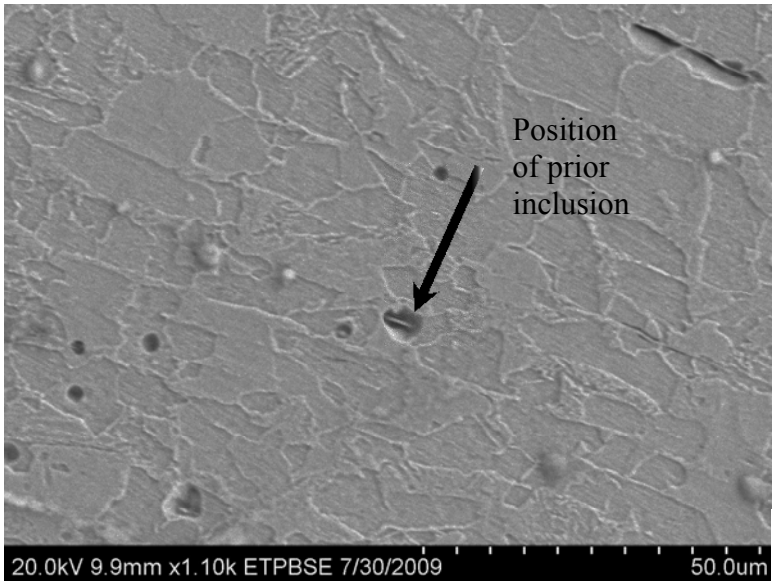

Figure 3.9 – Scanning Electron Microscope Image of Galvanized Steel with Regions of Prior Inclusions.

galvanized steel ranged from 74 to 124 μm with metallurgical phases apparent on a SEM image, as shown in Figure 3.10. The phases formed are the Zn layer, or eta (η) phase, with a minor solubility of Fe, the zeta (ζ) intermetallic layer (or $FeZn_{13}$ phase), delta (δ), and a thin layer consisting of gamma phases (Γ and Γ_1) adjacent to the Fe substrate. The microstructure follows the primary phases of the Zn-Fe phase diagram, as critically reviewed by Marder (2000).

With the zinc coating essentially consisting of three thick primary phases (i.e., Zn, $FeZn_{13}$ and δ), and a thin layer of the gamma phases, one would anticipate a change in the corrosion measurements, which could mark the different characteristics in dissolution of the metallic reinforcements. The differing corrosion rates would then reveal the state of the galvanized steel in the soil. For example, the chloridechlorine from the solution reacted with Zn to form probably a Zn oxychloride changing the outer microstructure with a cracked region, as shown in Figure 3.11.

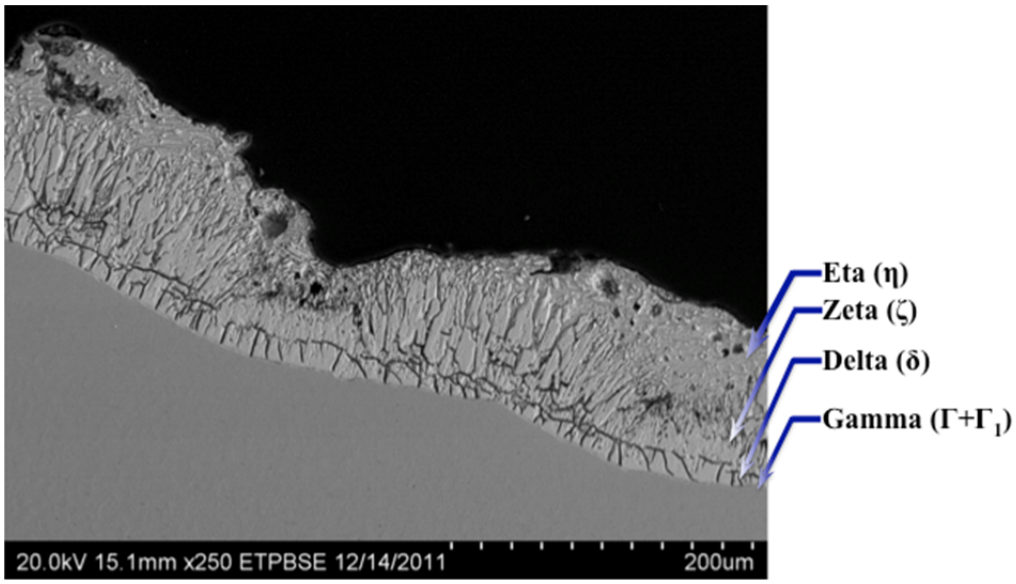

Figure 3.10 – Phases on Fe Substrate from Scanning Electron Microscope Image of Zinc Layer

Yadav et al. (2004) reported that chloride solutions contacting a Zn surface, analyzed via Raman spectroscopy and X-ray diffraction, detected $ZnCl_2 \cdot 4Zn(OH)_2$, ZnO, $Zn(OH)_2$, and $ZnCl_2$, as corrosion products of galvanized steel. Their corrosion products also depicted cracking which was probably a result of the differences in thermal expansion between the precipitated salts and Zn.

The wire mesh consisting of carbon steel welded together and then coated subsequently with liquid zinc to form the galvanized mesh was also characterized in the scanning electron microscope (SEM). The SEM images depicted the weld with a crack emanating from the welded region, but the crack was filled with a protective Zn layer, as shown in Figure 3.12. The crack was buried underneath a protective Zn, or eta (η) phase, approximating 1.3 mm deep. The Zn reacted with the carbon steel as previously explained with the zeta (or $FeZn_{13}$) and delta phases, though the separate layers barely discernible, appear adjacent to the Fe phase.

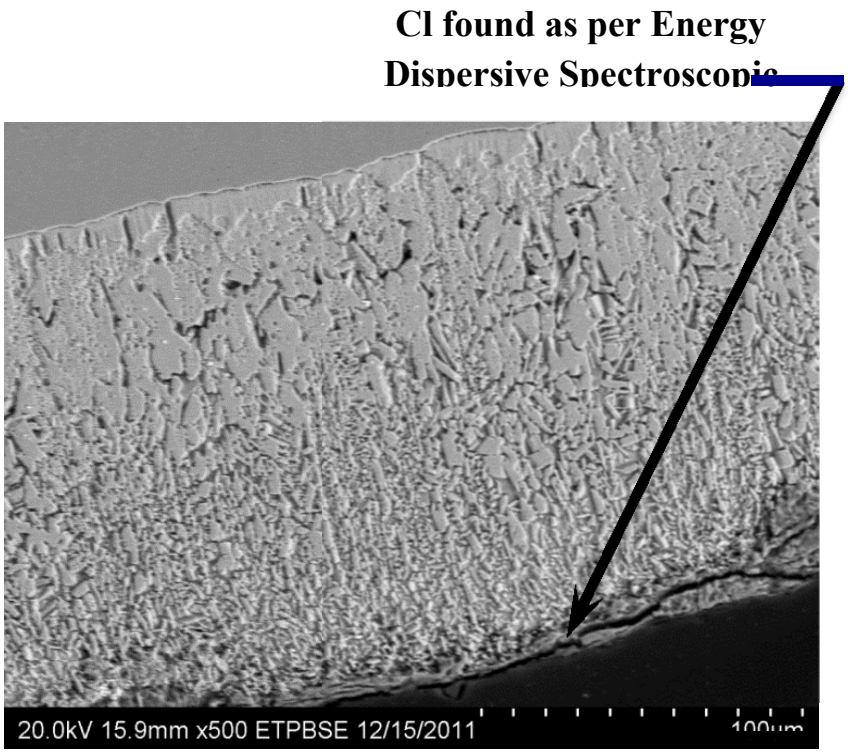

Figure 3.11 – Scanning Electron Microscope Image Showing Corrosion on outer Zn Layer with Chlorine Detected via Energy Dispersive Spectroscopy.

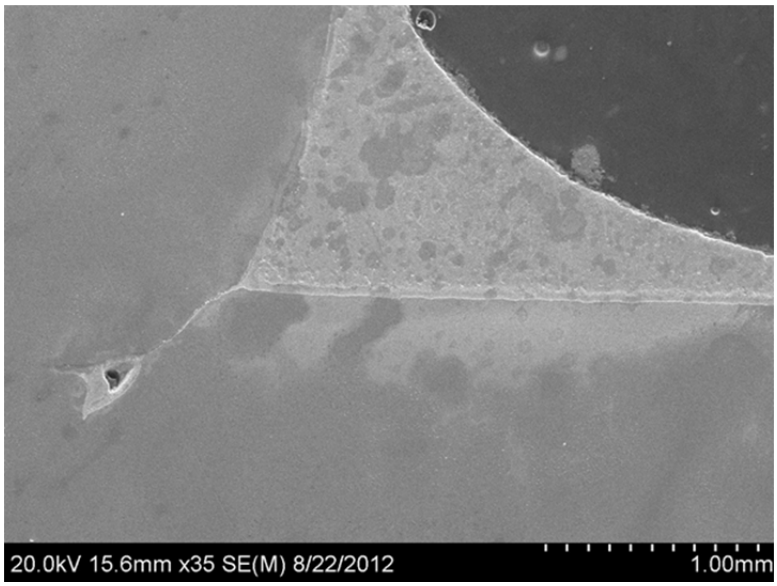

Figure 3.12 – Scanning Electron Microscope Image Showing Zn Layer on Welded Region of Wire Mesh.

Chapter 4 – Laboratory Monitoring

Specimen Preparation

In order to observe the impact of different MSE wall construction materials on the corrosion of the galvanized metal reinforcements, a lab setup was used to monitor the changes in the geochemistry and corrosion rates of the different materials with time. Figures 4.1 and 4.2 show how the specimens were prepared. Resistivity probes, a piece of reinforcement material and a corrosion coupon that would emulate an electrochemical cell were embedded within each specimen. A more detailed description and fabrication of the corrosion coupons will be covered in Chapter 5. Several holes were drilled in the plastic cylinder to allow proper electrical connections of the resistivity probes and the corrosion coupons in the specimen. Another hole that was drilled at the base of each cylinder was used to accommodate a drainage hose.

The specimens were subdivided in the following three different moisture conditions: Wet and Dry, Always Wet and Always Dry. For the Always Wet group, the specimens were filled with water, covered with plastic to minimize evaporation, and topped off with water when necessary. For the Always Dry group, the specimens were simply covered with plastic and no water was ever introduced to them. For the Wet and Dry group, a time frame of a week was used to define a wet-dry cycle. The specimen was filled with water on the first day and left for two days for the water to infiltrate the specimen. On the third day, the specimen was allowed to drain and dry for the following five days. The wet-dry cycle was repeated on these specimens throughout the entire length of the project. Considering the number of materials involved as well as the three moisture conditions mentioned, 80 specimens were prepared for the execution of this part of the project.

Data Acquisition System

Considering the number of specimens, the length of time of the project and the different signals to monitor, an automated data acquisition system was built to constantly monitor all test specimens. Figure 4.3 shows the data acquisition system used during this project. The data acquisition system consisted of an uninterruptible power supply (UPS), a computer with a National Instruments data acquisition card (NI PCI-6014), a function generator (Tektronix CFG250) to provide a constant sinusoidal signal for the resistivity probes and a box where all the specimens were connected using RJ45 connectors. This box contained the necessary circuitry to programmatically select each of the cylinders at a predetermined interval. The box also included a buffer circuit to amplify the current and voltage signals from the corrosion coupons, and a

precision resistance to measure resistivity during their respective cycles. A program using National Instruments LabVIEW software was created to continually read signals in two segments. In each of the segments, the program cycled through each of the 80 specimens to take measurements at 15 second intervals, essentially taking 20 minutes for the entire segment. The resistivity probes were used during the first segment to measure the resistance of the specimens. In the second segment, the signals from the corrosion coupons were measured.

Figure 4.1 – Pictures of a Cylindrical Specimen Being Prepared.

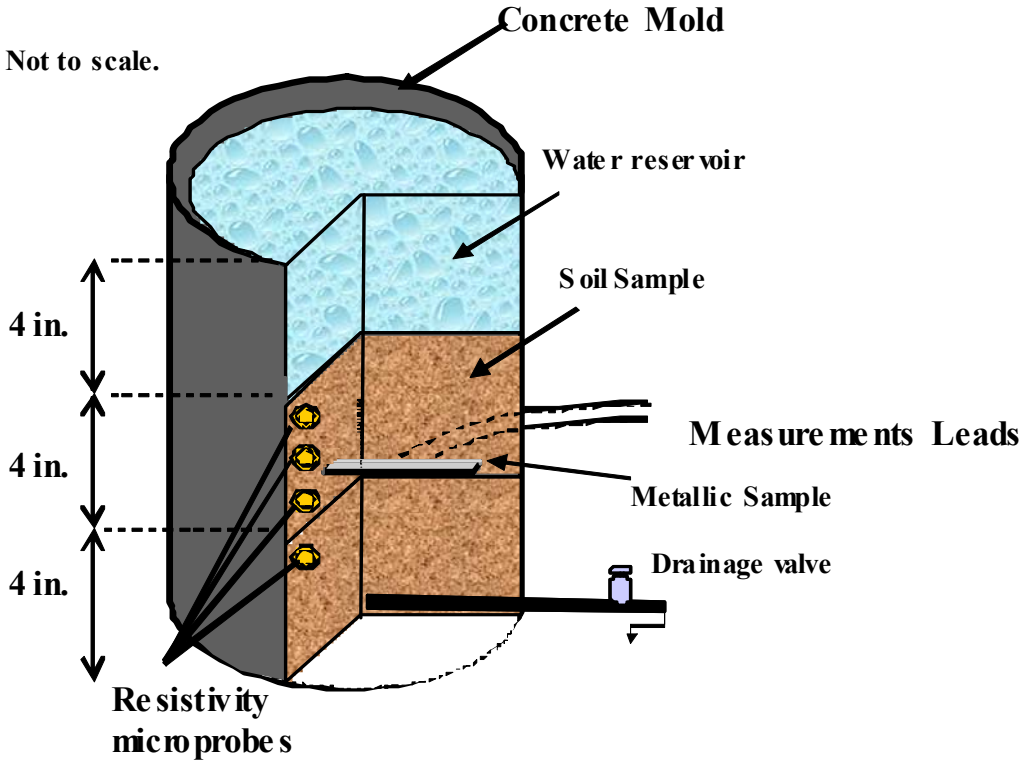

Figure 4.2 – Graphical Layout of Specimens Prepared for Project 0-6359.

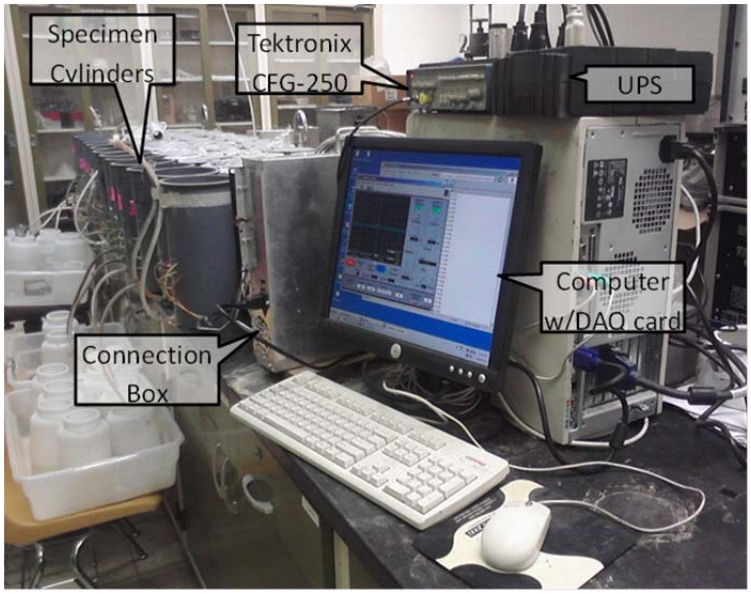

Figure 4.3 – Data Acquisition System Used for Project 0-6359.

Data Logging Program

The data-logging program consisted of a virtual instrument that would continually measure the DC and AC contents of the signals of the active channels (Figure 4.4). It used a clock to precisely determine the exact interval between each measurement and it also generated the digital control signals needed to automatically cycle from specimen to specimen.

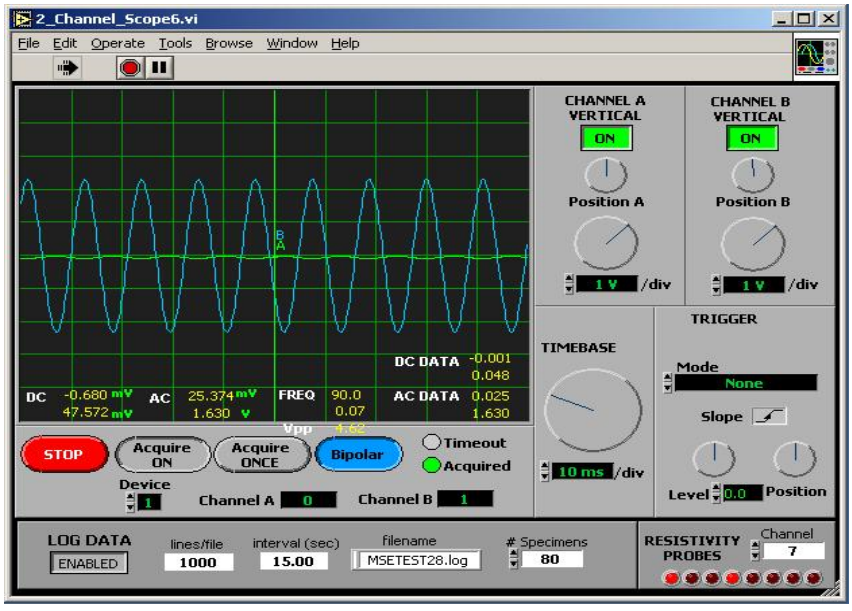

Figure 4.4 –Data-Logging Program Used for Project 0-6359.

Typical Results

Since the two cycle segments read different sensors, the values of interest differed. For the resistivity probes, the important values measured were the root mean square (RMS) of sinusoidal signals; while, for the corrosion coupons, the direct current was measured with time. To better handle the collected data, an Excel spreadsheet was developed that allowed us to select from different materials, at different time periods and present the information from the sensors in graphical form. This spreadsheet allowed us to compare the behavior of the data from multiple materials and to record the trends being developed as the project progressed further.

Figure 4.5 shows the case where resistivity was measured from three different specimens for a length of 10 weeks under differing conditions. For the Wet-Dry cycling, the resistivity decreased sharply with the addition of water and remained low while water immersed the specimen. The resistivity increased as the specimen dried during the five days after draining the water. For the Always Wet specimen, the resistivity remained more or less at a constant low resistivity. The Always Dry specimen shows resistivity values that start at a level that is similar to the wet specimens but then increase with time.

Figure 4.6 shows the corrosion coupons current for the same specimens and time period as the ones from Figure 4.5. In this case, the Wet-Dry specimen also shows much more activity than the Always Wet and the Always Dry specimens. Figure 4.7 shows the voltage in the corrosion coupons for the same specimens and time period as the ones from Figure 4.5. As with the current graphs, the Wet-Dry specimen shows more activity than the other two specimens. Further interpretation of these results is provided in the following chapters.

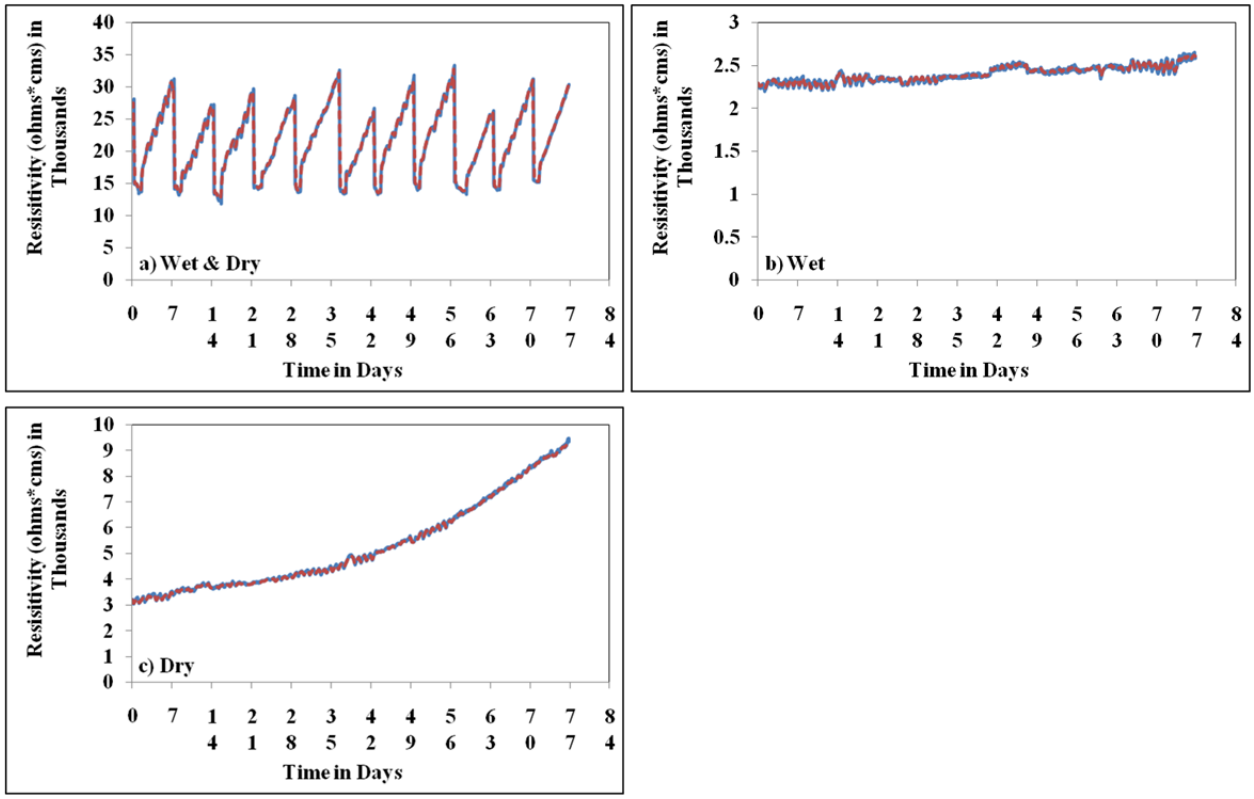

Figure 4.5 – Typical Resistivity Data from Lab Specimens.

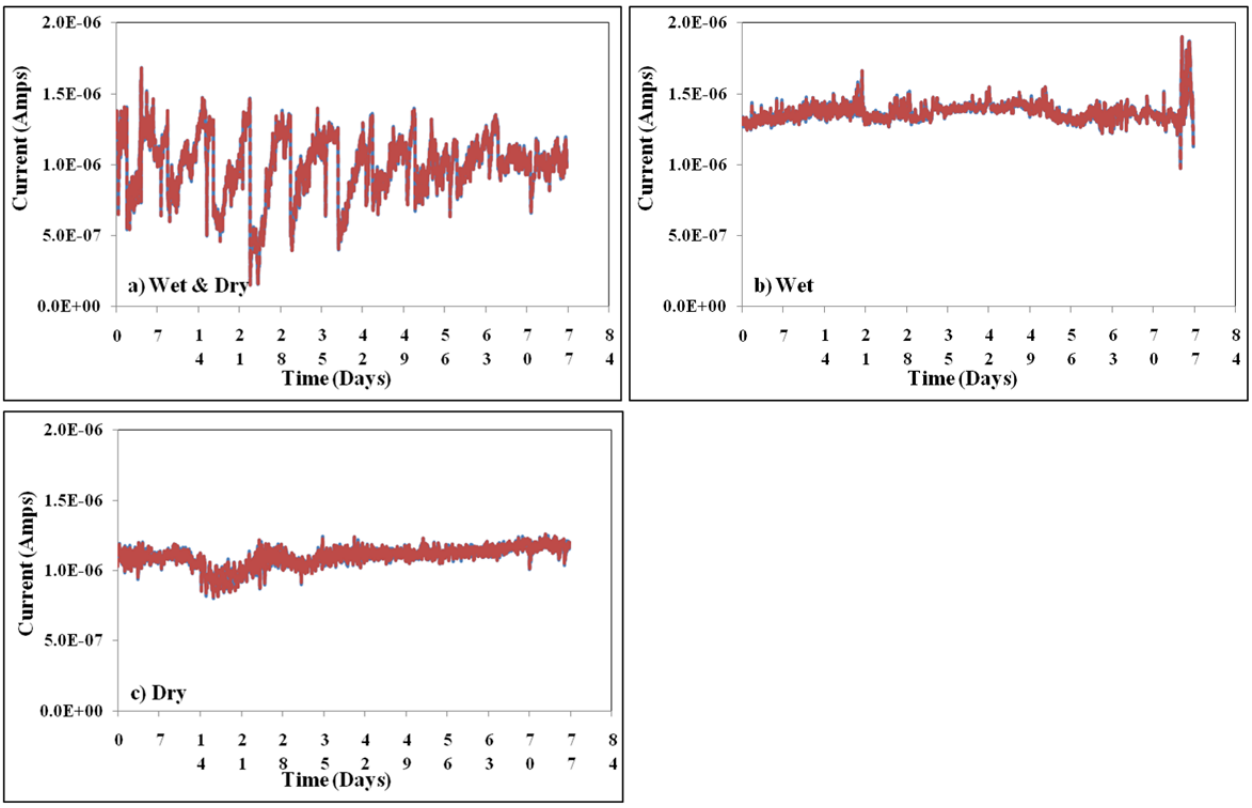

Figure 4.6 – Typical Current Data from Corrosion Coupons.

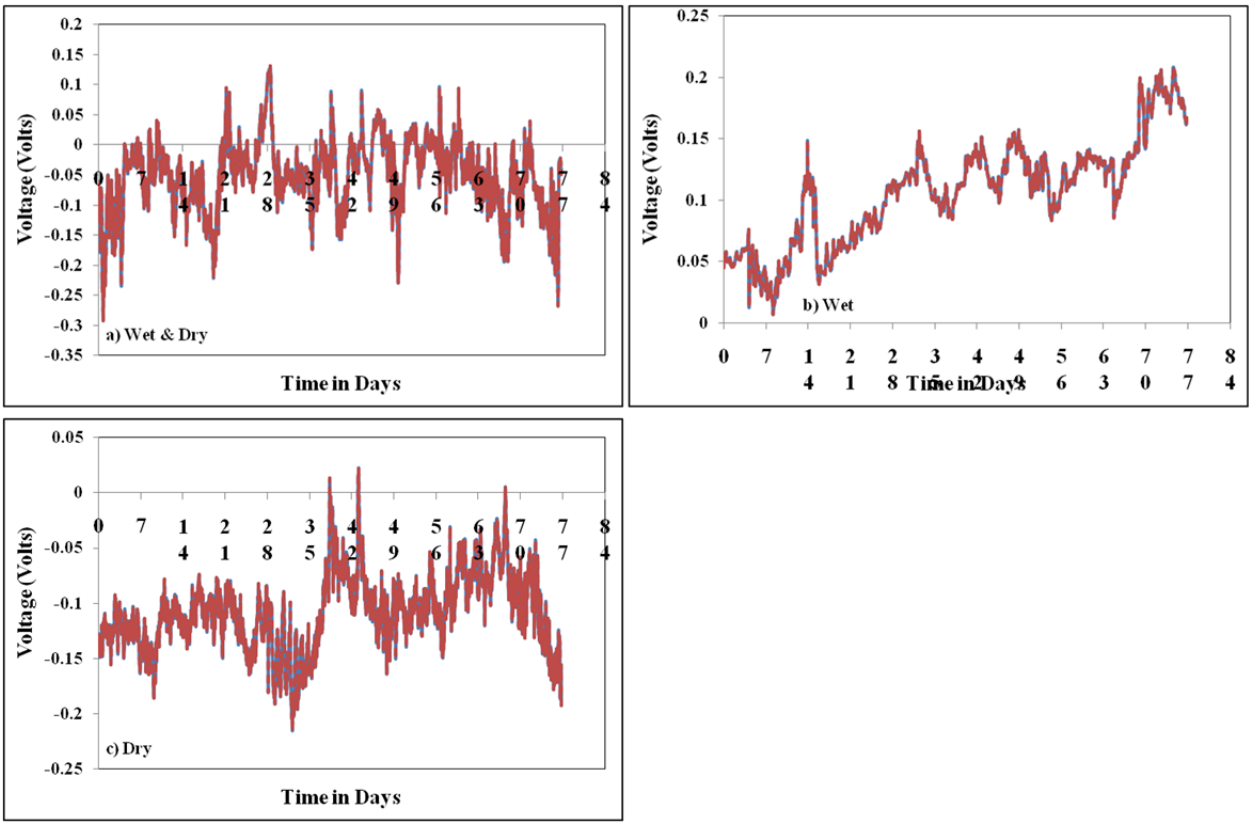

Figure 4.7 – Typical Voltage Data from Corrosion Coupons.

Chapter 5 - Corrosion Studies

The laboratory corrosion studies consist of three techniques primarily to determine 1) the long-term integrity of galvanized steel by monitoring passively the dissolution, 2) the mechanistic aspect of the electrochemical reactions of the solution/metal interface, and 3) the traditional polarization scan to establish guidelines for long-term corrosion tests, as shown in Figure 5.1. The first technique uses electrochemical noise to monitor the effect of the soil geochemistry creating the solution for the dissolution of the Zn coating with time primarily for use in field applications. In a simplistic view, the current transient (i.e., amps versus time) shows the dissolution of the metal (Zn or Fe) into solution by an increasing current, which subsequently decreases as a result of an oxide reforming on the surface. The second technique uses electrochemical impedance spectroscopy to characterize the effect of the chloride solution on the Zn surface, the Zn/Fe couple and the Fe substrate. The impedance obtained at the highest frequency determines the solution resistance and impedance at the lowest frequency is related to the polarization resistance, of which the reciprocal is proportional to the corrosion rate. The third technique uses the traditional polarization scan to give long-term guidelines for corrosion tests, but the scan is usually limited to assumptions of uniform corrosion. In this chapter, the experimental methodologies of the three techniques are described and the results are subsequently analyzed.

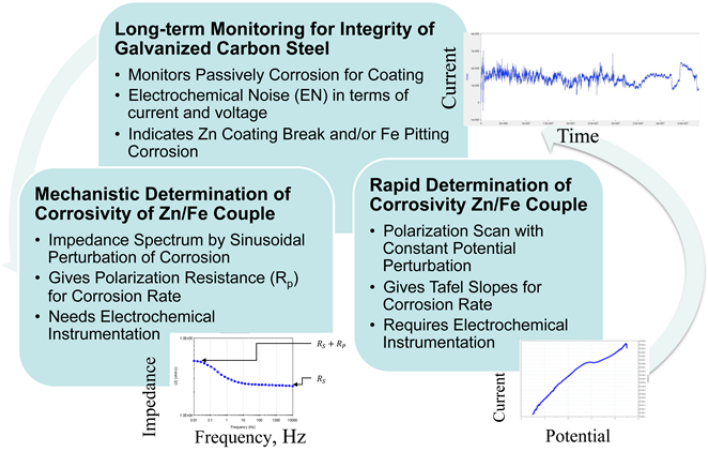

Figure 5.1 – Experimental Triad of Electrochemical Techniques Used to Assess Corrosion of Galvanized Steel.

To calculate the corrosion rate of the galvanized steel embedded in soil, the corrosion rate of galvanized steel immersed in NaCl solution was first related to its conductivity in a laboratory measurement by using primarily electrochemical impedance spectroscopy. The subsequent relationship of NaCl-solution conductivity to corrosion rate was then used to acquire the corrosivity of a leach-liquor generated as the water permeates the soil. The conductivity of each

backfill was measured as the corrosion coupons, for example, were embedded in soils, which are either continuously wet or undergo a wet/dry cycle.

Galvanized Steel Electrode Preparation

The galvanized steel reinforcement was cut into sections avoiding ribs or scratches to machine into electrodes. The sides of the section of galvanized steel segments were chosen, and then the sections were machined via computer numerical control (CNC) in a Hass super mini-mill. The CNC mill was programmed to create an area of 0.4 x 0.2 in. by using a ¼ in. four flute end-mill made of tungsten carbide in a cobalt matrix. Coolant was used during the whole CNC machining process to avoid the heating of the material, which would change the microstructure of the metal such as grain size and consequently the corrosion characteristics. The spin and feed rates of the CNC were also fixed to ensure the zinc coating was not damaged during the machining process. Figure 5.2 shows how the plate looked after the CNC process was completed.

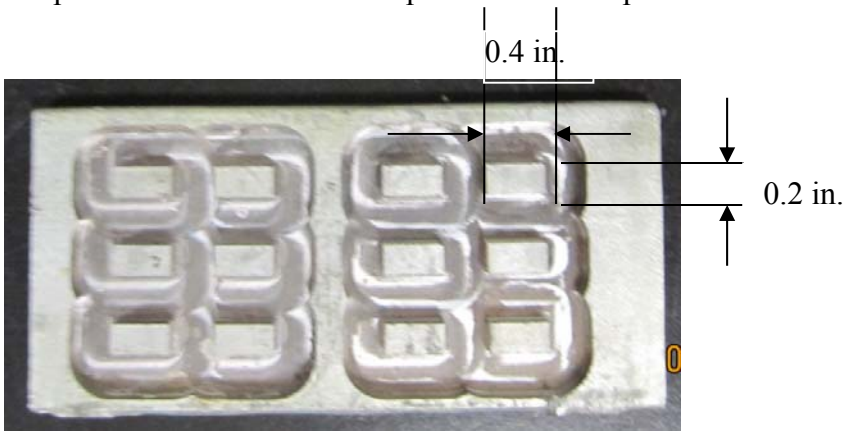

Figure 5.2 - Galvanized Steel Plate after CNC Machining.

After CNC machining of the galvanized steel plates, the electrodes were cut with a water-cooled, abrasive wheel and detailed with a grinder. The galvanized steel electrodes were subsequently machined to a height of 0.170 in. This machining step ensured that the electrode fitted into the Delrin pocket with a depth of 0.20 in. along with the copper cable used for data acquisition. The machining of the height of the electrode also allows the copper wire to have contact with steel instead of zinc, which improves the conductivity between the electrode and the wire.

Delrin Coupon Preparation

A 1.25 in. diameter Delrin rod was cut into segments of 2 in. of length and the sections were then machined with a CNC mill programmed to create a ridge of 0.02 in. and 3 pockets of 0.4 x 0.2 in. and 0.2 in. in depth. The Delrin rod was faced with a 1 in., two-flute end-mill, and the pockets were machined with 0.25 in., four-flute end-mill. The coupon was then detailed with a 1/8 in., four-flute end-mill. During the machining of the Delrin coupon, coolant was used to prevent the Delrin from burning.

After the 2 in. Delrin sections were machined on both sides, they were cut in half with a vertical saw to create two separate Delrin coupons. The final height of the Delrin coupons was machined with a milling machine. The reason for reducing the height in the laid machine before using the milling machine is due to the elasticity of the material. The material was slowly fed into the milling machine to minimize overheating and damage. Finally, the holes to insert the copper

cables into the Delrin coupon were machined with a milling machine and a 1/16 in. bit, as shown in Figure 5.3.

Figure 5.3 – Views of a Finished Delrin Electrode Holder.

Electrode Coupon Assembly

Before the working electrode was press fitted into the Delrin holder, the edges of the working electrode were slightly ground to facilitate the electrode pressing into the Delrin pockets. The electrodes and Delrin were cleaned in an ultrasonic cleaner with acetone for 30 min. to remove any contaminants remaining from the machining process. The copper wire was inserted into the coupon and spread inside the pocket to ensure good contact with the electrode. Prior to press-fitting of the electrode, two drops of epoxy were poured into the coupon's pocket to seal the electrode sides and prevent crevice corrosion. The electrode was press fitted carefully so the Zn coating on the galvanized steel was not damaged during the process. After the electrodes were press fitted, pressure was applied with a hydraulic press to ensure the electrodes are driven to the bottom of the Delrin pocket. Finally the electrodes were cleaned with a cotton cloth saturated with acetone to remove any epoxy that may have extruded onto the electrode's surface. After allowing the epoxy to dry for 2 to 3 hours, the cables were also sealed with epoxy to prevent corrosion during the experiments.

Electrode Positioning Structure

For the electrochemical impedance spectroscopy and polarization scans, a Plexiglas structure was designed to accommodate the electrodes inside a 1-liter beaker glass, as shown in Figure 5.4. The Plexiglas structure fixed the position of the Pt counter electrode along the same plane of the reference electrode placed (1.725 cm) opposite the working electrode. With the spacing between the counter electrode and working electrode fixed, the ohmic potential drop is easily calculated if needed.

Polarization Scan Experiments

Polarization scans were acquired for aqueous solutions ranging from 0.0001 M to 0.1 M NaCl for the calculation of corrosion current rates, as well as to compare with chloride contents obtained from field data. The electrode potential measured between the working electrode and the reference electrode was perturbed at a 0.1 mV/s scanning-rate during for which the resulting current response was measured between the working electrode and counter-electrode. The polarization scans were performed with galvanized steel as the working electrode, Ag/AgCl saturated with KCl as the reference electrode and a Pt wire as the counter-electrode.

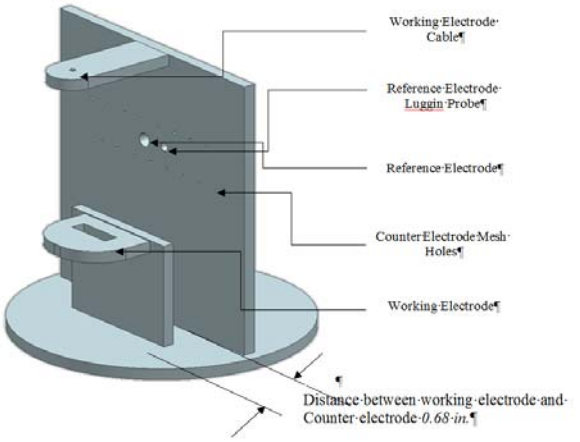

Figure 5.4 - Electrode Positioning Structure.

Electrochemical Impedance Spectroscopic Experiments

The technique of electrochemical impedance spectroscopy (EIS) was used to obtain the solution resistance, as well as the polarization resistance. The reciprocal of the polarization resistance is ultimately related to the corrosion rate of the Zn surface. The electrochemical impedance experiments characterize the electrochemical behavior with the use of an equivalent circuit representing the metal/solution interface and interphase. In an EIS measurement, the working electrode was perturbed with a sinusoidal potential with frequencies from 10^{-2} to 10^{4} Hz and the subsequent current response was measured. As explained in the results section, a one-time constant circuit can represent the capacitance of the electrode interphase, an electrolytic resistance, R_s, between the reference electrode and the working electrode, and charge-transfer (or Faradaic) impedance, or polarization resistance (R_p), caused by a charge transfer reaction.

The setup for the electrochemical impedance experiments used the same electrode structure (Figure 5.4) as the polarization scan experiments with main components of the experiment shown in Figure 5.5. For the reference electrode, a Pt electrode contained in a Luggin-probe was connected in parallel to an Ag/AgCl reference with a 100 μF capacitor. This modification to the reference electrode allows the stabilization of the electrochemical impedance measurements at high frequencies. The necessity for this modification was brought upon by problems such as the phase shift introduced by the potentiostat and problems at high frequencies due to the resistance and capacitance of the fiber tip of the reference electrodes (Mansfeld, Lin, Chen, & Shih, 1988).

Electrochemical Noise Experiments

The setup for the electrochemical noise experiments consisted of three galvanized steel electrodes working as the reference electrode, the counter-electrode and the working electrode. Current was measured between the working electrode and counter-electrode; the potential was measured between the working electrode and the reference electrode. The electrode signals were amplified with two separate circuits, as shown in Figure 5.6. The circuit to acquire the voltage noise signals included a 10 MΩ connected to the working electrode to dissipate probable parasitic capacitance. The voltage signal obtained between the working and reference electrodes is then connected to a buffer amplifier to simplify data acquisition. The circuit to acquire the current noise signals used the counter-electrode being grounded. The current signal then passed through an operational amplifier with a 10 MΩ resistance. The resultant signal finally passed through a buffer amplifier to improve the data acquisition.

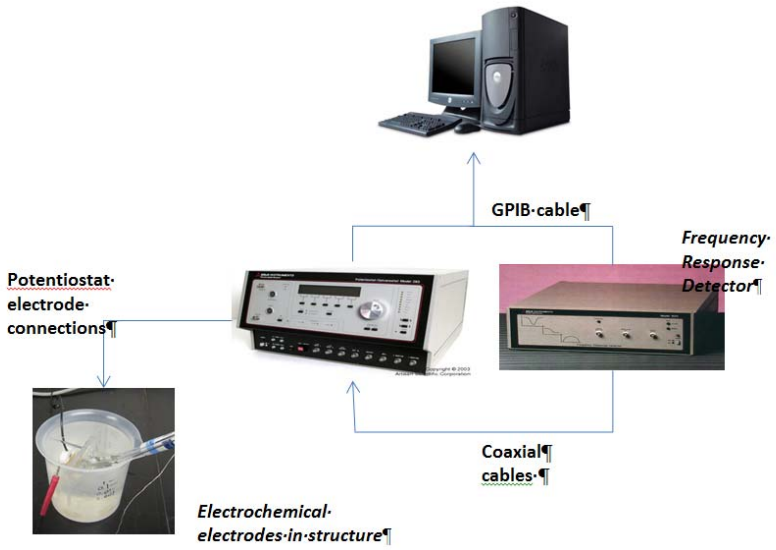

Figure 5.5 – Potentiostat, Frequency Response Detector and Electrochemical Cell with Electrodes.

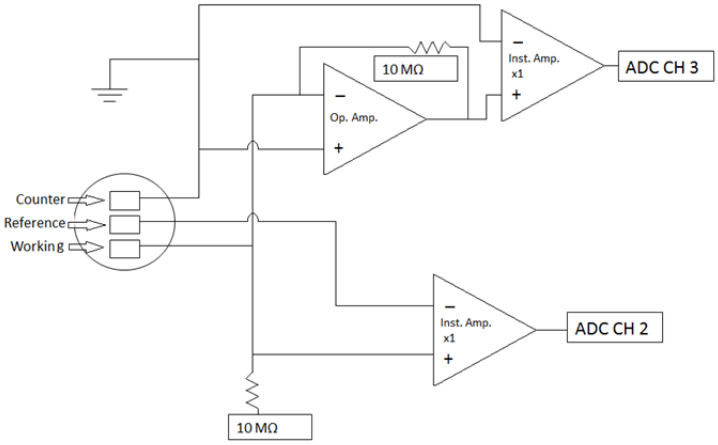

Figure 5.6 - Circuits Used to Acquire Current and Voltage of Electrochemical Noise.

The electrochemical noise analysis was acquired from the current transients indicating the dissolution of the surface with positive amperage and surface repassivation by the current returning to approximately its preceding value. For noise analysis, the data must have an order of a power of 2, so the number of sample data was chosen to be 1024 to simplify the analysis and obtain a clearer spectrum. As a typical acquisition, the current noise data for four samples buried in Material F soil are shown Figure 5.7. Additional current transients for the galvanized steel embedded in soils collected from six Texas sites are appended. Specimens 1 and 3 were underground during the wet/dry cycle experiment for about 1 year and specimens 2 and 4 were exposed to soil with the similar wet/dry cycle for two years. The rate of acquisition of the current for electrochemical data was 40 minutes (or 2400 s) amounting to $4(10)^{-4}$ Hz.

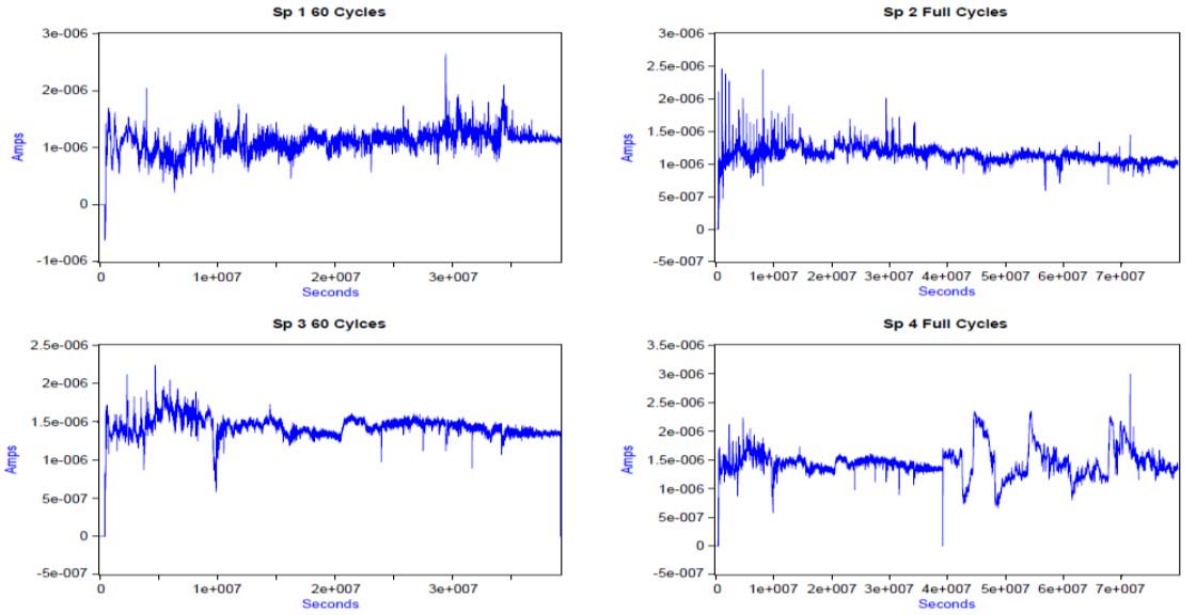

Figure 5.7 – Typical current transient of electrochemical noise for Material F.

Chapter 6 – Laboratory Geotechnical, Geochemical and Corrosion Results

The laboratory corrosion experiments on the 80 specimens described in Chapter 5 were continued for about two years. About half of the specimens were retired after approximately one year and the other half after two years. The specimens were separated into three categories: (1) always wet, (2) wet-dry and (3) dry. The results obtained from the geotechnical, electrochemical and corrosion aspects of these experiments are described below.

Geotechnical Engineering Aspects

The main focus of the geotechnical engineering aspects was to monitor the impact of changes in properties with time especially changes in gradation and migration of aggregates.

The typical change in gradation for Material A due to compaction is shown in Figure 6.1. The significant difference in the gradation is appreciable. To better demonstrate these changes in gradation, the before and after gradations for all materials after one year and two years are cross-plotted in Figure 6.2. The changes in gradations between the first and second year for a given material is minimal, indicating that most changes are due to the compaction efforts. Also there is a close correlation between the hardness of the materials as judged from data in Table 3.5. As such, it may be prudent to encourage the utilization of harder aggregates for coarse backfills.

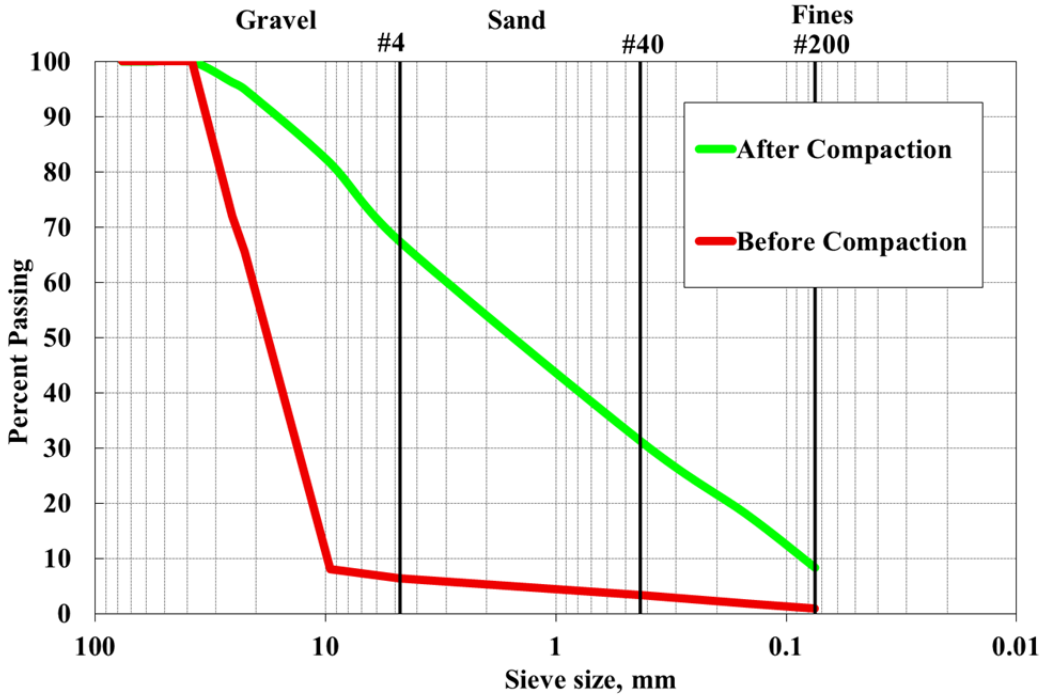

Figure 6.1. – Comparison of Gradation Curves of Material A before and after Compaction

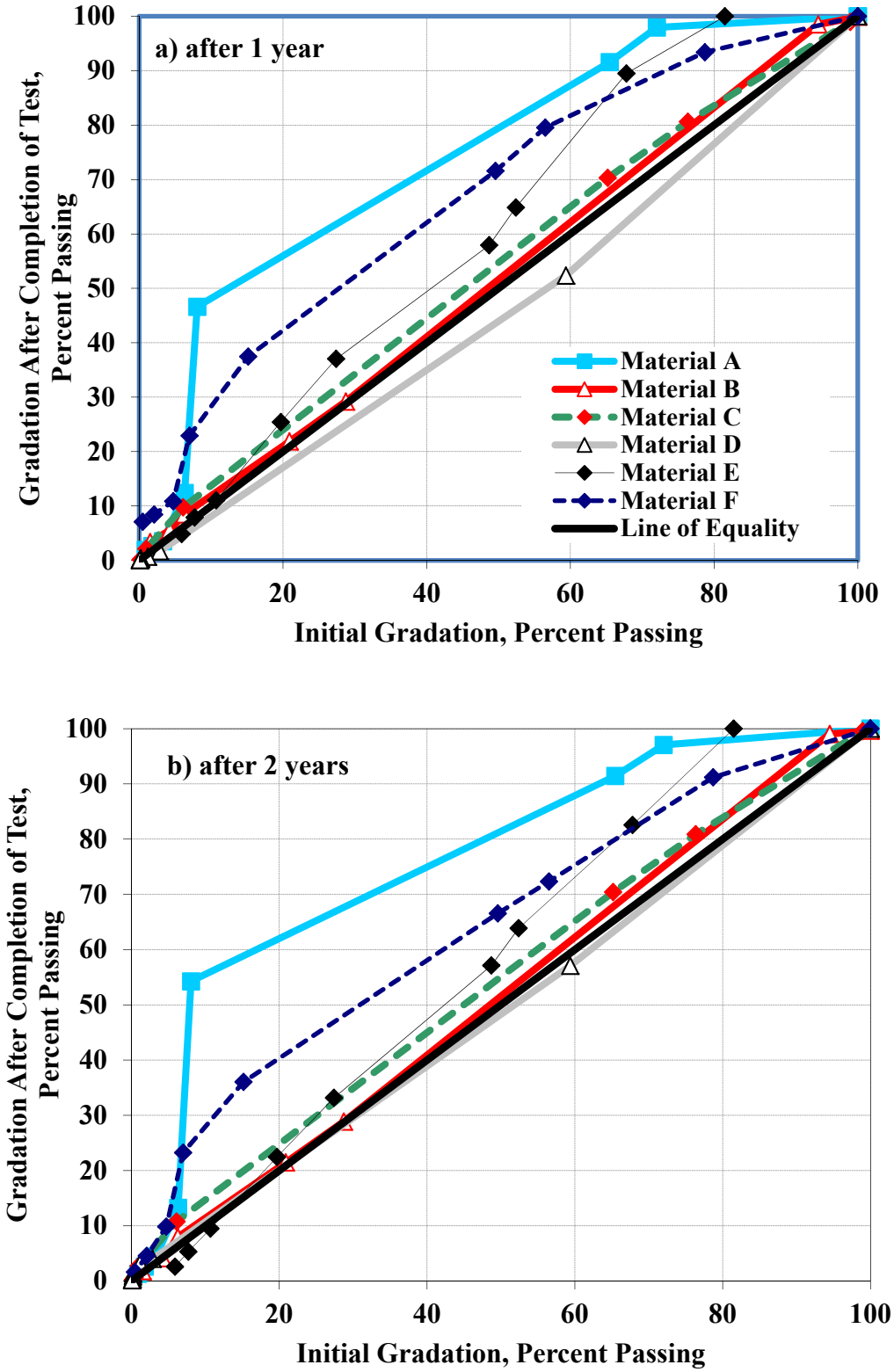

Figure 6.2. – Changes in Gradations of Materials Tested in This Study

Figure 6.3 demonstrates typical migration of finer aggregates for always wet and wet and dry specimens. As reflected in Figure 6.3a, almost all fine-grained materials have migrated toward the bottom of the specimen, while this is a less of an issue for the always wet specimens. The always dry specimens looked more uniform.

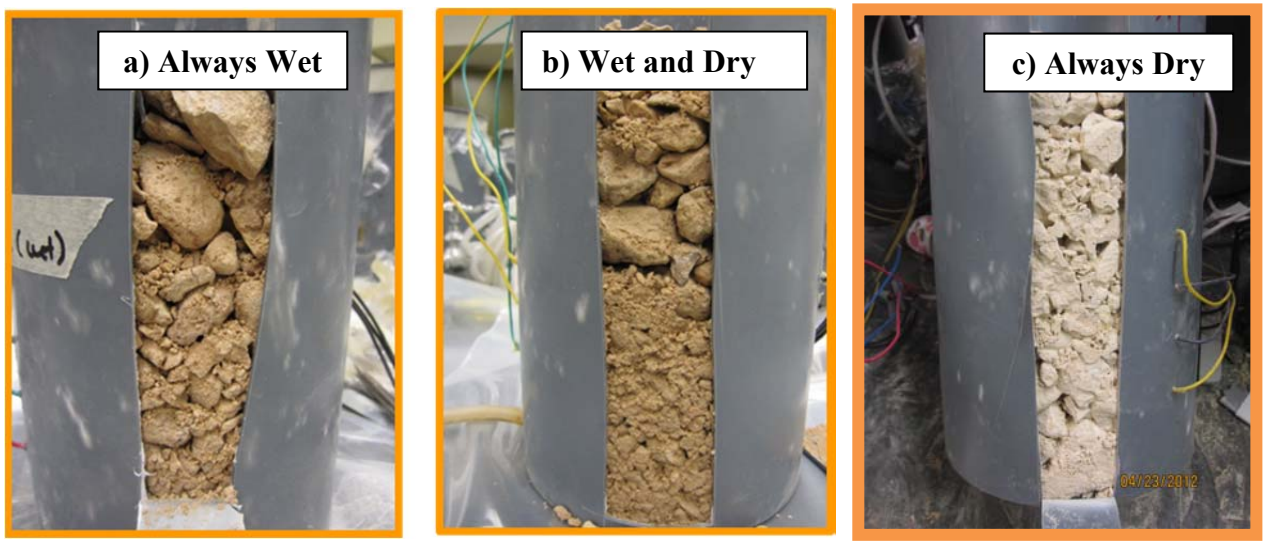

Figure 6.3 – Migration of Fine-Grained Materials due to Introduction of Water

Geochemical Aspects

The main focus of the geochemical aspects of this study was to evaluate the changes in the ions within the solution created by leaching the aggregates. To that end, adequate amount of drainage fluids from the specimens subjected to wet/dry cycles were sampled and tested to obtain their sulfate chloride and other relevant cations and ions. Small amounts of fluid from the always wet specimens were also extracted regularly for similar tests.

The variations in the concentrations of sulfate with time are shown in Figure 6.4 for all materials. For the wet/dry specimens, the sulfate concentrations became negligible after a few cycles, whereas the sulfate concentration increases almost gradually for the always wet specimens. The figures also contain the sulfate and chloride concentration obtained from the traditional TxDOT approach and the proposed FLT tests. After a few weeks, these values fall in between the concentrations of the always wet and wet and dry conditions. As reflected in Figure 6.5, the same patterns are apparent for the chloride concentrations.

The soil resistivity values are shown in Figure 6.6 for all materials. The minimum and maximum values correspond to the variation in resistivity under dry and wet conditions. As water leached and depleted the salts (e.g., chloride and sulfate salts) from the soil, the resistivity increased with increasing time (or weeks). The change of soil resistivity represents the readily dissolvable salts (e.g., chloride and sulfate salts) entering into solution as cations and anions though salt characteristics may affect their dissolution, as well as soil porosity, causing the resistivity to rise, drop or plateau.

The pH values measured from the extracted fluids are shown in Figure 6.7 for all wet-dry materials. The pH values are not significant probably as a result of the dissolved ions having low

concentrations. Finally, the conductivity values of the fluids were determined as the most significant parameter for estimating the corrosion of the materials. The measured conductivity values for the wet/dry and always wet specimens are shown in Figures 6.8 and 6.9, respectively. The sulfate and chloride concentrations from the wetted soils of Materials C and F were significantly more than the other four materials, and consequently, the ionic content caused higher conductivities for materials C and F than for the other four materials, as shown in Figure 6.9. Further analyses of these results are given in the next section.

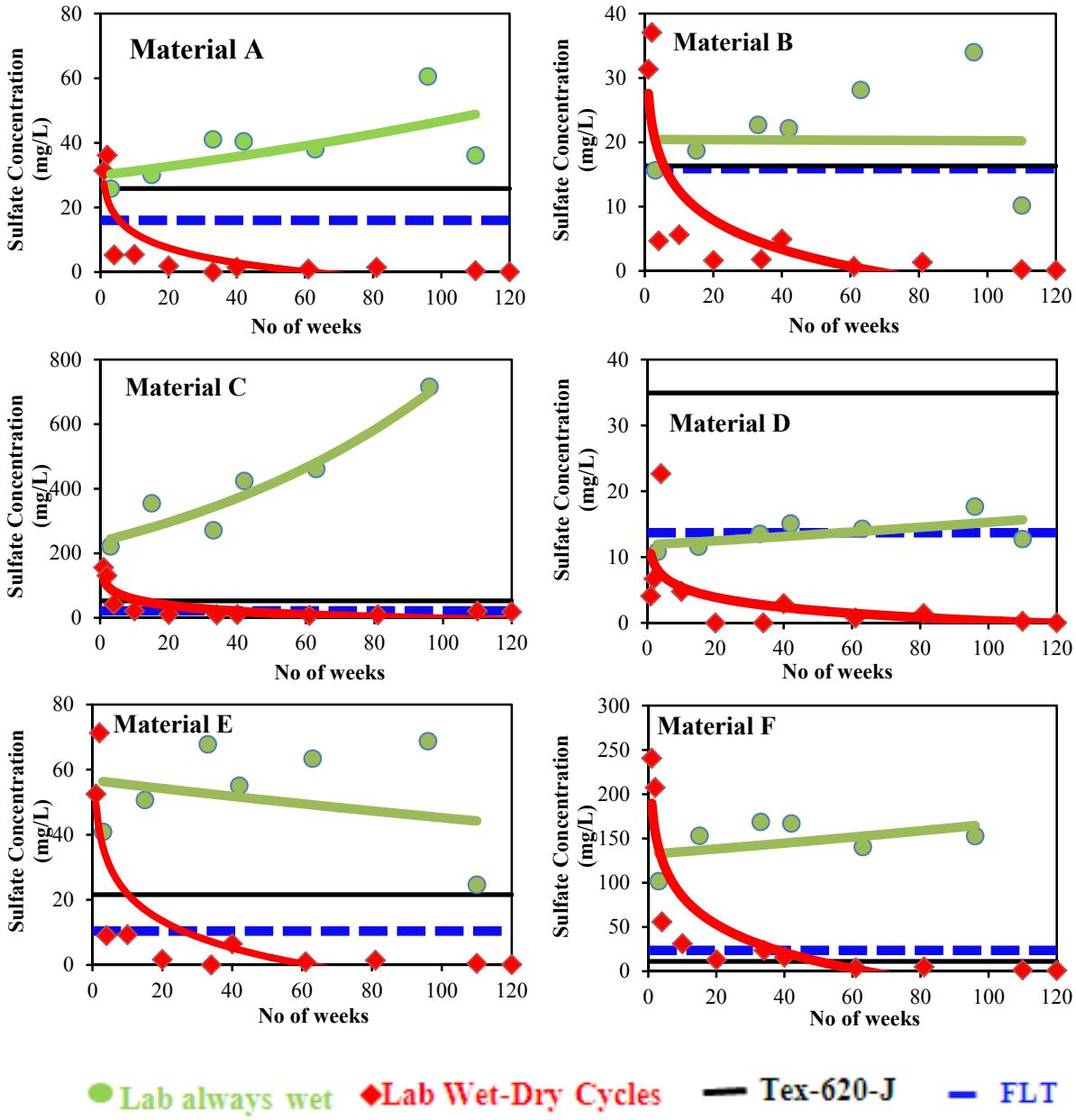

Figure 6.4 – Variations in Sulfate Concentration with Time

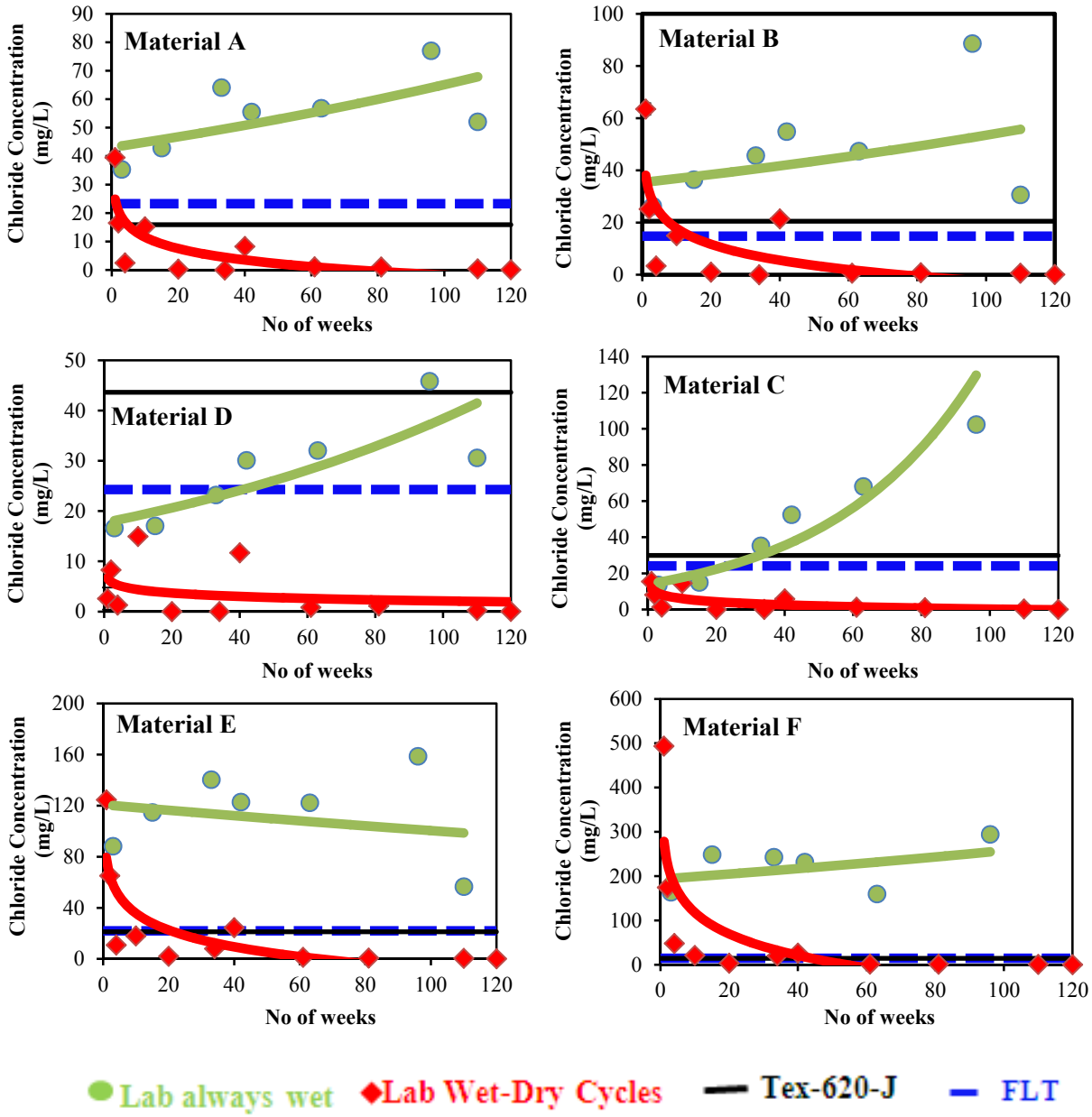

Figure 6.5 – Variations in Chloride Concentration with Time

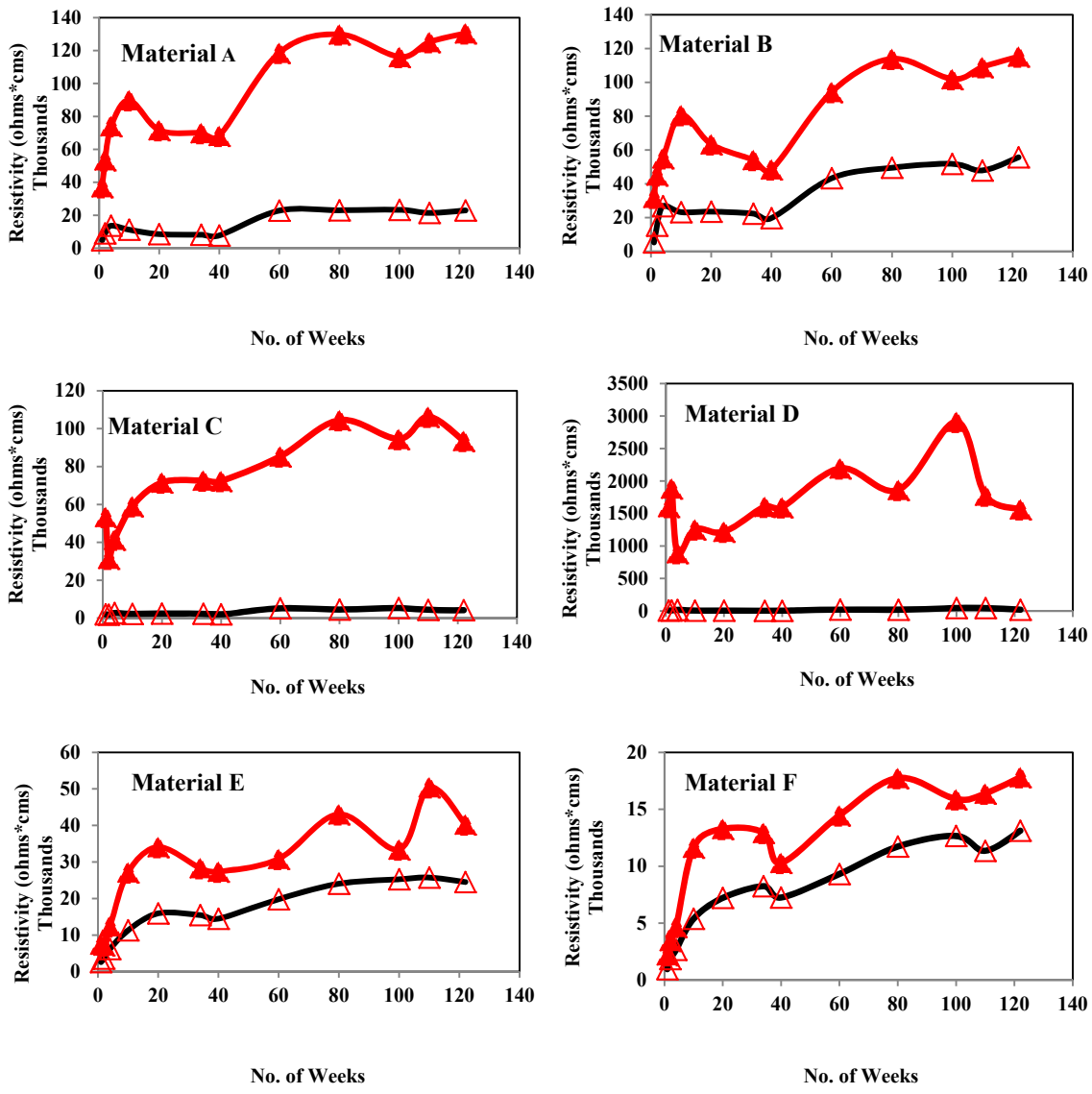

Figure 6.6 – Variations in Soil Resistivity with Time

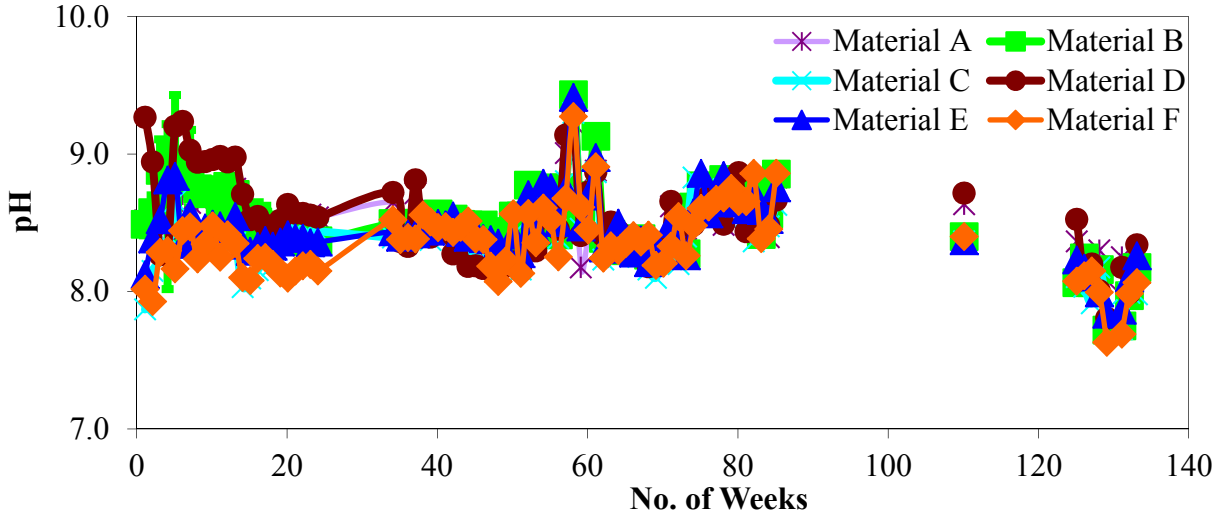

Figure 6.7 – Variations in Fluid pH with Time

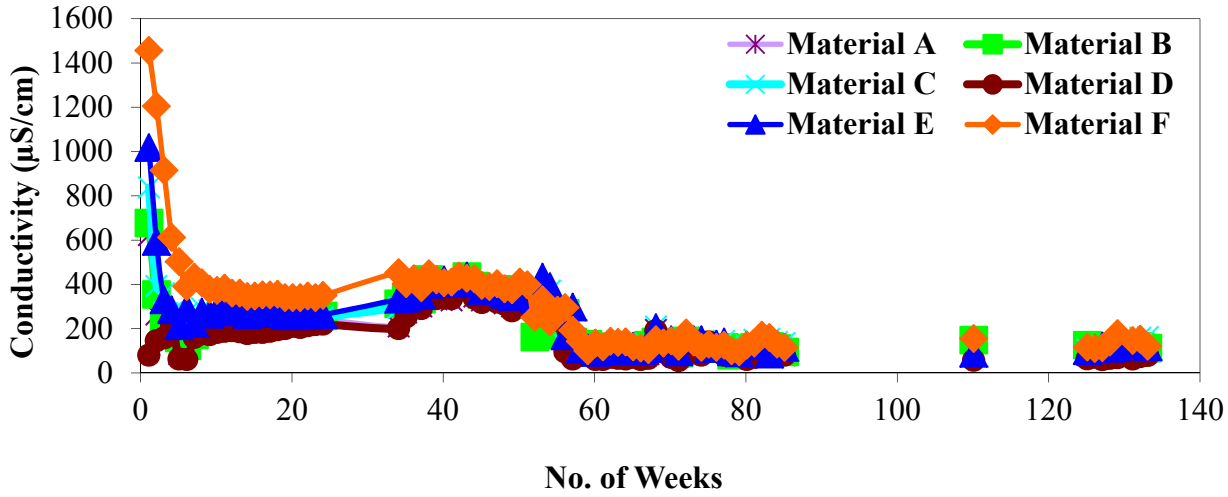

Figure 6.8 – Variations in Fluid Conductivity with Time from Wet/Dry Specimens

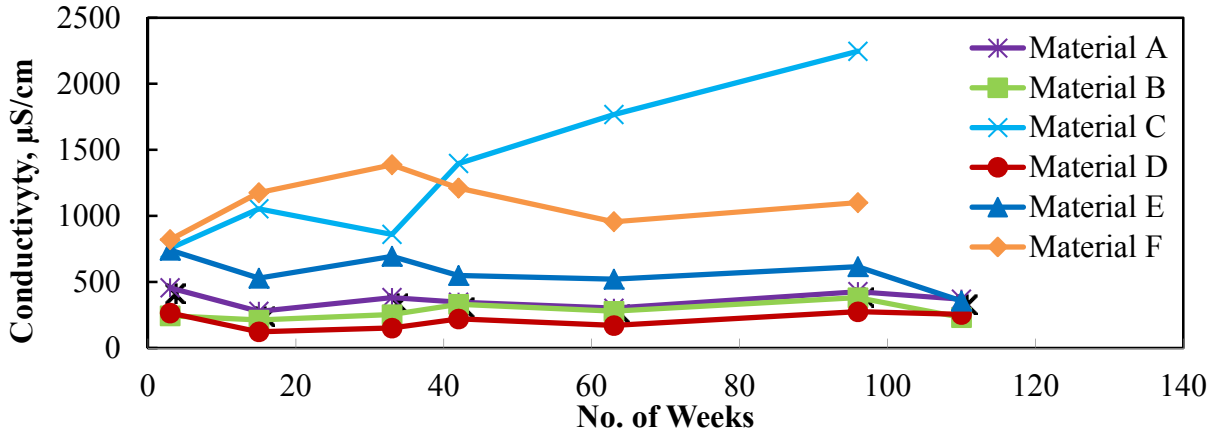

Figure 6.9 – Variations in Fluid Conductivity for Wetted Soils

Corrosion Aspects

The first aspect of the corrosion study was to qualify and quantify the corrosion of the reinforcements exhumed from the 80 laboratory samples. Chlorine was detected on the outer region of the zinc layers of the coupons in the wet/dry specimens. The chlorine is associated with the $ZnCl_2 \bullet Zn(OH)_2$ compound, as identified by Yadav et al. (2004).

With an energy dispersive spectrometer attached to the SEM, an elemental distribution (or dot mapping) of Zn, O, Cl and S along the Zn/Fe interfacial region was acquired. As an example, the results from corrosion coupons embedded in Material F subjected to 60 and 120 wet/dry cycles are depicted in Figures 6.10 and 6.11, respectively. The upper left image shows the microstructure of the Zn layer on the Fe substrate for Figures 6.10 and 6.11. Although the microstructure is clearly reduced from previous microstructures (e.g., Figure 3.10) as evident from the micron bar, the focus of the depiction, here, is more on the elemental distribution. The Zn distribution was denser near the Fe substrate with a more open distribution indicating a porous morphology created after Zn reacted from the dissolved oxygen in the leach-liquor to form ZnO, as further evident by the oxygen distribution (lower left image). Chlorine was found within the porous ZnO region near the Zn layer attesting to the Zn oxychloride formation. Zinc chloride ($ZnCl_2$) may also form, but the chlorine distribution beyond the Zn/ZnO interface seems to favor oxychloride predominance. For dot mapping acquired from a typical sample from Material F, the same elemental distribution of the oxygen, chlorine and sulfur within the corroded Zn layer are shown for microstructures in Figures 6.10 to 6.12. The oxygen and chlorine distribution are more obvious on the lower left images of Figure 6.12.

A swelling of the Zn layer was clearly evident for the coupon embedded for 27 months, or the full wet-dry cycles, as shown in Figure 6.13. Although the sample was obtained from Material E, the swelling probably resulted from the galvanic Zn/Fe coupling as suggested by Yadav et al. (2004). The Zn/Fe coupling decreases corrosion and Zn serves as the sacrificial corroding surface protecting any exposed Fe sites. Chlorine concentrated again near the Zn/Fe interface, but the sulfur penetrated less into the porous ZnO layer, as indicated by the lower elemental sulfur distribution near the Fe substrate.

Electrochemical Impedance Spectroscopy

The rate of corrosion of the reinforcement was related to the measured fluid conductivities (Figure 6.8) with the aid of electrochemical impedance spectroscopy (EIS). To understand the use of EIS in corrosion measurements, the present section describes results acquired by perturbing the working electrode with a sinusoidal voltage causing a sinusoidal current response and their ratio (i.e., perturbed voltage/measured current) gives impedance. The EIS measurements were analyzed with the aid of Bode plots, which were interpreted with the aid of equivalent circuits to discern corrosion behavior, as shown in Figure 6.14. For example, the solution with a resistance of 2.30 $(10)^4$ ohm contacts the Zn surface, which is simulated with an effective capacitance (C_{eff}) of 163 μF and a polarization resistance (R_p) of 2.74 $(10)^4$ ohm. The RC equivalent circuit, or one time constant, demonstrates the simulation of the corroding Zn surface with the reciprocal of R_p related to the kinetics of corrosion. A more expanded view of the corrosion behavior can be explained as Zn oxide formed on the surface of the Zn coating and represented as a R_{ox}-C_{ox} adjacent to the solution resistance as shown in Figure 6.14.

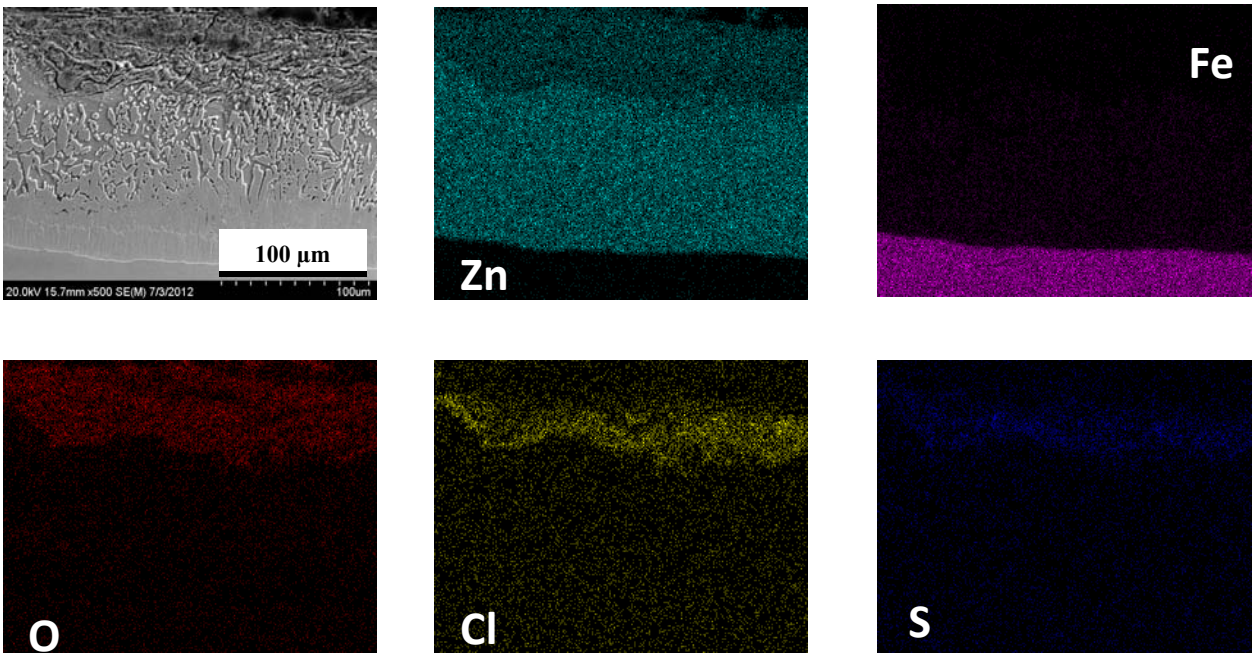

Figure 6.10 - Elemental Distribution of Zn, O, Cl and S Found within Zinc Coating Adjacent to Fe Substrate from Scanning Electron Microscope Image after 60 Wet/Dry Cycles from Material F.

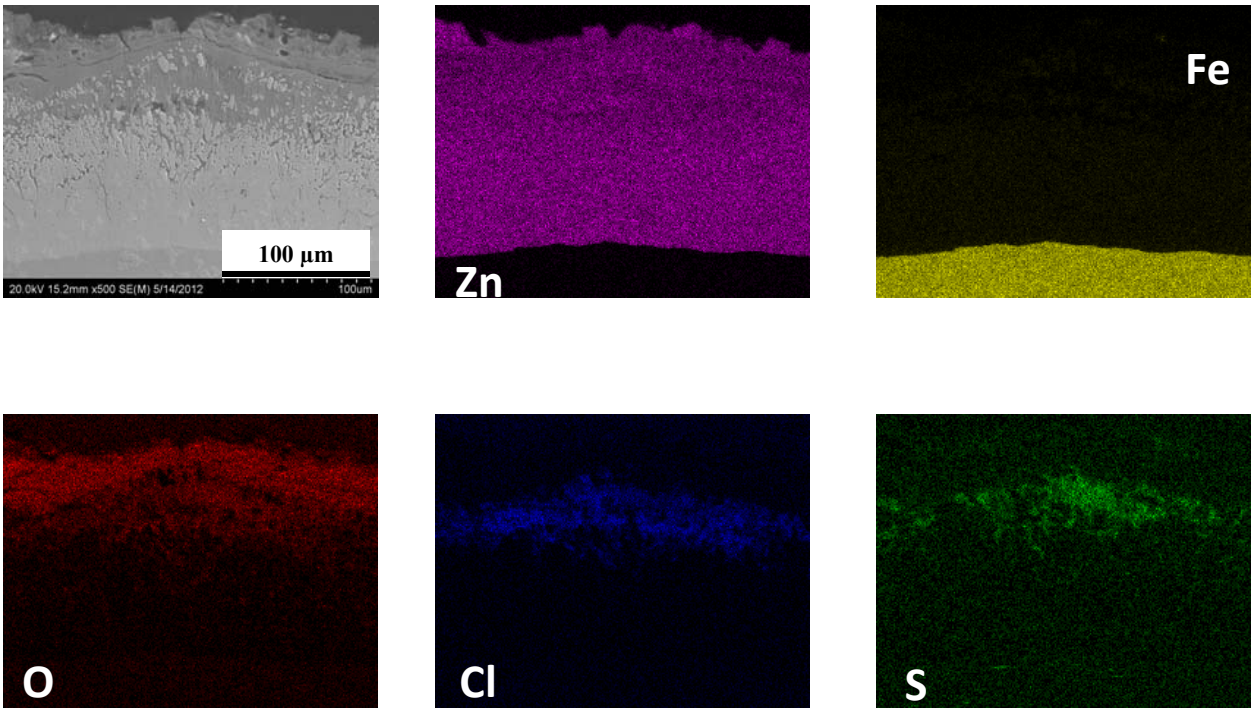

Figure 6.11 – Scanning Electron Microscopic Image and Dot Mapping of Zn, O, Cl and S within Zinc Coating Located on Fe Substrate after 120 Wet/Dry Cycles from Material F.

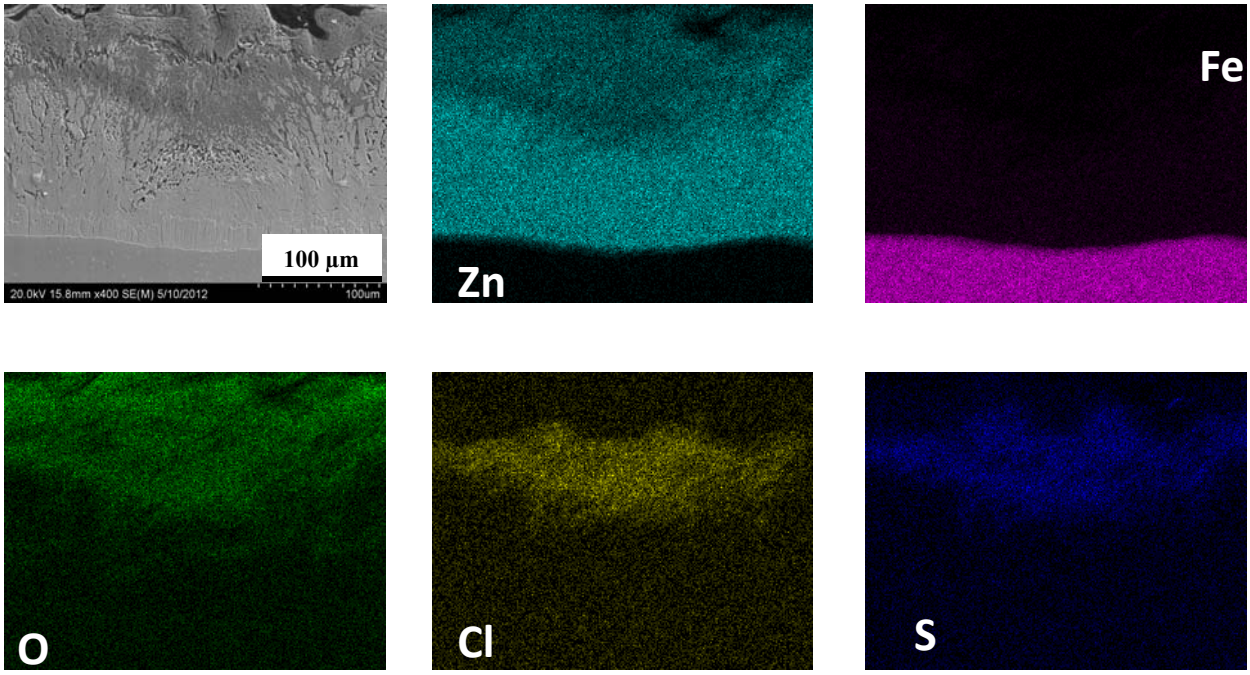

Figure 6.12 – SEM-EDS of Zn Layer Acquired from Sample Exposed to Material F after a full Wet-Dry cycling.

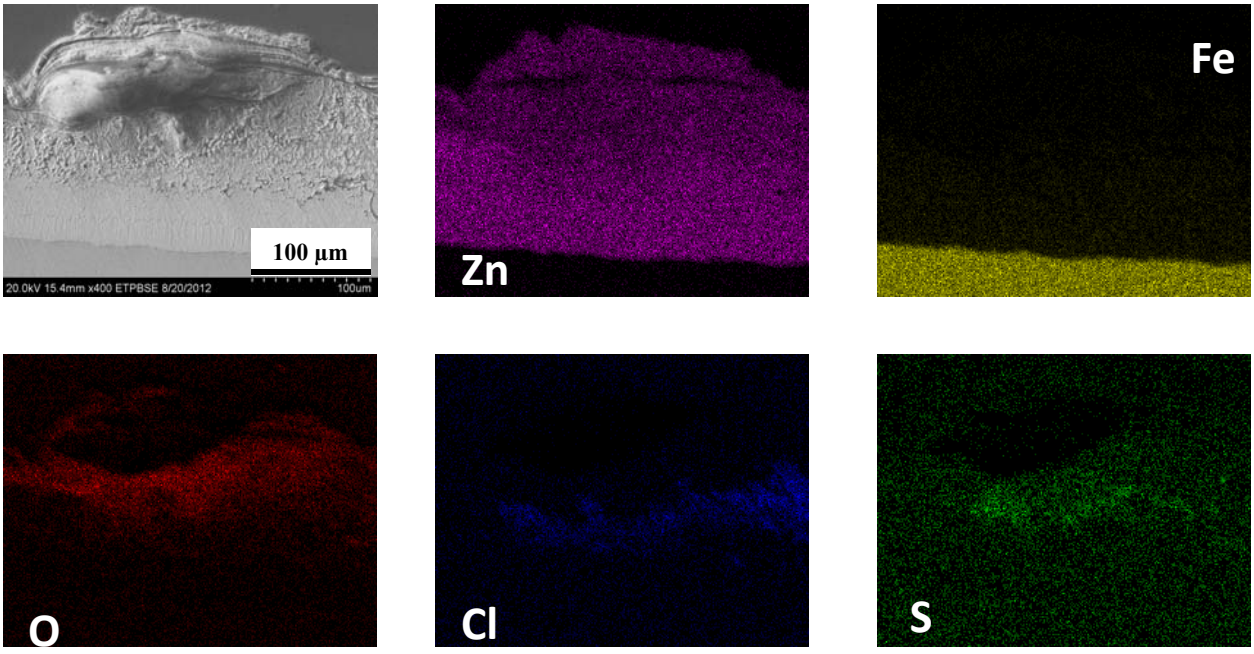

Figure 6.13 – SEM-EDS of Zn Layer Acquired from Sample Exposed to Material E after a full Wet-Dry cycling.

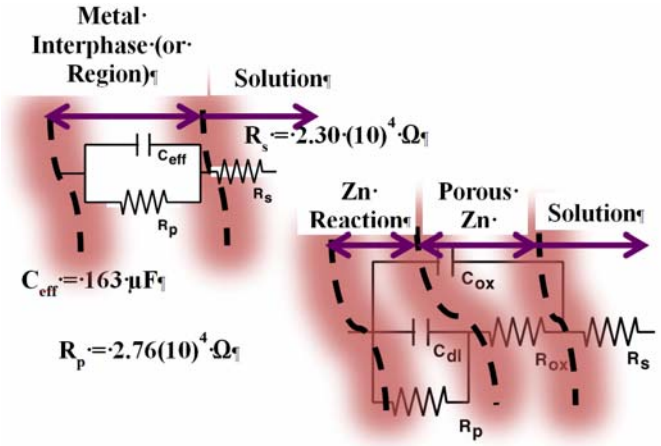

Figure 6.14 – Two Possible Equivalent Circuits Simulating the Corrosion Process along Zinc Layer.

Electrochemical impedance spectroscopy was performed for galvanized steel electrodes immersed in aqueous solutions containing 0.0001, 0.001, 0.01 and 0.1 M NaCl. To mimic the real time corrosion behavior of the galvanized steel in the soil, special attention was given to the results at the lowest molarity possible (0.0001 M NaCl), since it was the closest to the chloride content of the soil. From the Bode plots acquired from EIS measurements of the foregoing NaCl solutions, the polarization resistances were then used to find the corrosion rates, as explained below.

The low conductive solution may introduce experimental artifacts to the measured impedance, because the coupling capacitance of the working electrode to the counter electrode may affect impedance at the high frequency limit, which determines usually the electrolyte resistance (Chechirlian et al., 1990). To remove the effect of a low conductive solution, Orazem et al. (2006) suggested a relationship according to in Equation 6.1 to calculate an adjusted impedance ($|Z|_{adj}$), which then determined the polarization resistance.

$$|Z|_{adj} = \sqrt{\left(Z_r - R_{s,est}\right)^2 + \left(Z_j\right)^2} \qquad \phi_{adj} = \tan^{-1}\left(\frac{Z_j}{Z_r - R_{s,est}}\right) \tag{6.1}$$

The electrolyte resistance ($R_{s,est}$) was measured with an external conductivity sensor (EC500) and subtracted from the real impedance to determine an adjusted impedance (Z_{adj}) with respect to frequency. A modified Bode representation then determined to differ only slightly from the real impedance, as shown in Figure 6.15.

Bode plots were obtained for the NaCl contents ranging from 0.1 to 0.0001 M NaCl with a typical plot shown in Figure 6.16. The Bode plots, which are included in Appendix C, were reproduced several times to verify results and averaged at each molarity to provide a more accurate result. The solution resistance decreases linearly on a logarithmic plot with increasing NaCl content, as shown in Figure 6.17. The resistivity with respect to the solution molarity was calculated by dividing the solution resistance acquired from EIS measurements by the spacing between the working electrode and the reference electrode. A solution resistance of $2.1(10)^4$ ohm/cm was acquired from Material F after 24 months of wet/dry cycles. Hence, the solution resistance of a leach-liquor acquired from the Material would compare to a 0.0001 M NaCl solution.

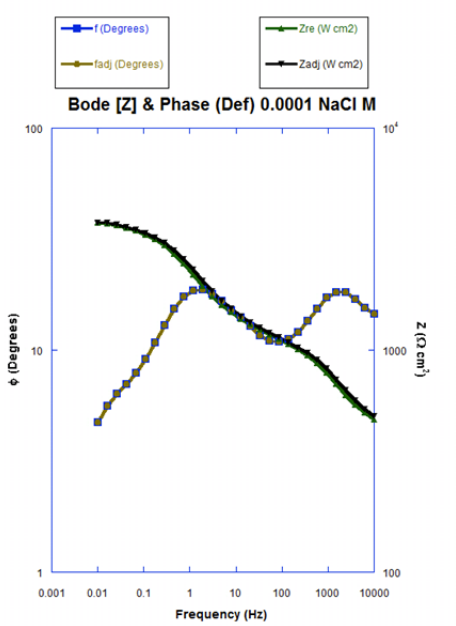

Figure 6.15 - Adjusted Impedance and Phase Angle Incorporating Resistance of a Low Conductive 0.0001 M NaCl Solution.

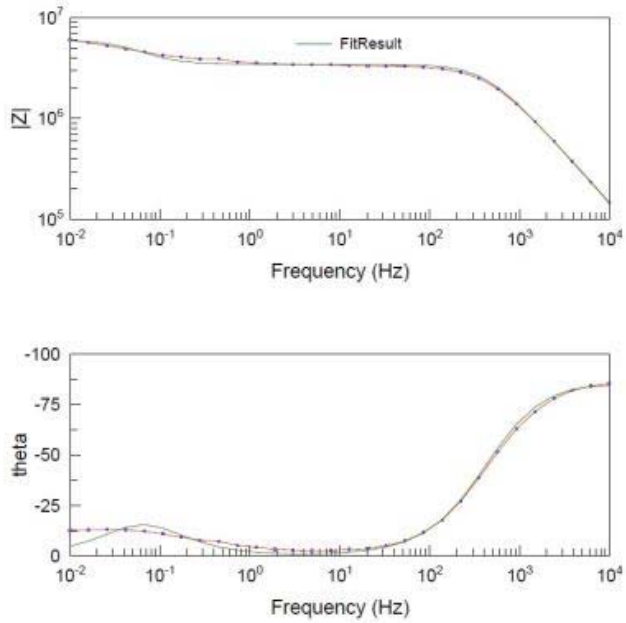

Figure 6.16 - Bode Plot of Galvanized Steel Immersed in a 0.0001 M NaCl Solution

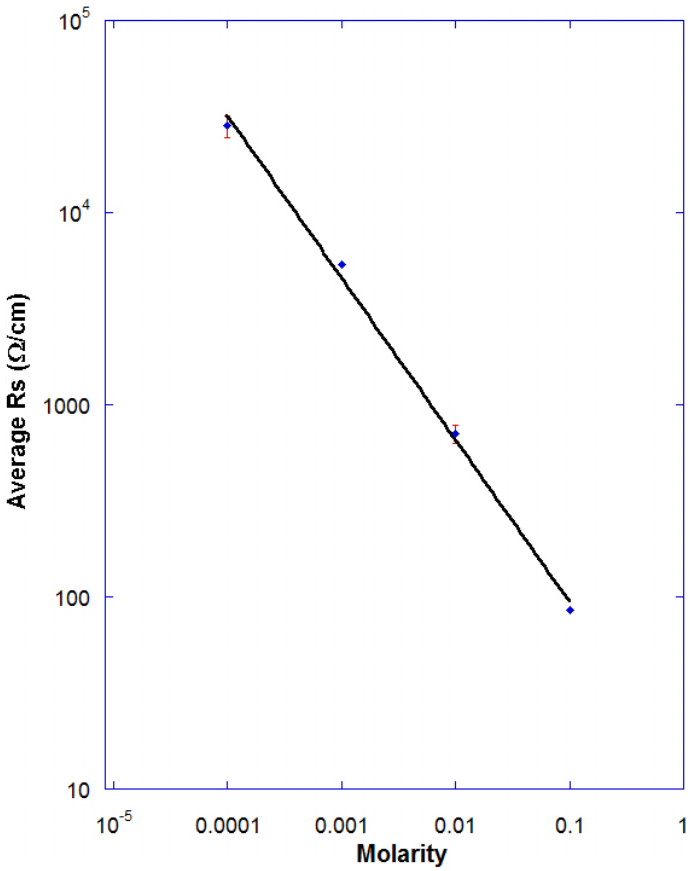

Figure 6.17 - Effect of NaCl Concentration on Solution Resistance.

Electrochemical impedance spectroscopy (EIS) measurements were used to determine the solution resistance. The EIS measurements usually give N_{yquist} diagrams in ohms for the imaginary and real parts though normalized units of ohm/distance (Macdonald, 1991). The solution resistance from the EIS measurements and divided by the spacing (i.e., 1.75 cm) between electrodes with an electrode area of 1 cm^2 compared well with a conductivity sensor, as shown in Table 6.1.

Table 6.1 – Comparison of Solution Resistance from EIS Resistivity and Conductivity Sensor

NaCl Molarity (M)	Average Solution Resistance from EIS (R, ohm)	Normalized Average Solution Resistance (ohm/cm)	Specific Conductance* determined from EIS (κ, µS/cm)	Specific Conductance from Conductivity Sensor (κ, µS/cm)
0.0001	2.30E+04	1.33E+04	24.8	25.2
0.001	4.60E+03	2.67E+03	124	126
0.01	7.71E+02	4.47E+02	741	751
0.1	8.95E+01	5.19E+01	6384	6477

* Conductance (1/ρ) determined from resistivity (ρ) calculated from solution resistance (R) with electrode spacing of 1.75 cm and an electrode area of 1 cm^2 ($\rho = RA/l$)

The polarization resistance (e.g., Table 6.2) obtained from the Bode plots represents the kinetics of the dissolution of the Zn after the solution permeates the porous ZnO product layer. In addition, chloride ions were actually the aggressive ions corroding the underlying Zn surface. The distribution of oxygen and chlorine as found in the dot maps acquired form energy dispersive spectroscopy (Figures 6.10 - 6.13) infers that an oxychloride corrosion product formed near the Zn surface. The resistive and capacitive components simulating the Zn dissolution from NaCl solutions were acquired from equivalent-circuit models using Zview software (Scribner and Associates, Charlottesville, VA) with typical values shown in Table 6.2. The equivalent-circuit models simulated two time-constants – a resistive (R_{ox}) – capacitive (C_{ox}) for the Zn oxide and a R_p-C_{dl} for the dissolution, as shown in Figure 6.14.

Table 6.2 - Values for Equivalent Circuit 0.0001 M NaCl Solution

Element	Abbreviation	Value
Solution Resistance	R_s, ohm	8272
Zn Oxide Capacitance	C_{ox}, F	1.10E-10
Zn Oxide Resistance	R_{ox}, ohm	3.44E+06
Double Layer Capacitance	C_{dl}, F	1.27E-06
Polarization Resistance	R_p, ohm	2.53E+06

Polarization Scans

Polarization curves (e.g., Figure 6.18) were obtained for four molarities to calculate the corrosion rate of galvanized steel with the EIS measurements. The water used for the acquisition of the polarization curve was the same (deionized) water used for the real-time corrosion of the galvanized steel embedded in soil. The polarization scans were acquired at a low scan rate (0.1 mV/sec) to allow the half-reactions to achieve steady-state on the surface of the galvanized steel. The slopes consisting of potential difference versus log i were acquired for the anodic side of the polarization scan according to the following equation (Prentice, 1991):

$$\frac{\Delta V}{\log|i|} = b_a \tag{6.2}$$

A similar slope was acquired for the cathodic side of the polarization curve. The slopes were then used to calculate the "k" constant.

$$k = \frac{b_a b_c}{2.303(b_a + b_c)} \tag{6.3}$$

For a 0.1 M NaCl solution, though slightly higher the slope agreed with Walter (1976) in his analysis of Zn corrosion in aerated acidic chloride solution who acquired a Tafel slope of 29.5 mV/decade of current (2.3 RT/F). The "k" constant along with the inverse of the polarization resistance determined the current density, i_{corr}, according to the Stern-Geary equation incorporating the polarization resistance (R_p), as reported by Macdonald (1991) and Mansfeld and Lorentz (1991) as shown in Table 6.3. The polarization resistance was acquired from electrochemical impedance spectroscopy as explained earlier. The "k" constant was then substituted into the following equation along with values of the polarization resistance (R_p):

$$i_{corr} = kR_p^{-1} \tag{6.4}$$

$$\dot{\delta} = \left(\frac{M_{Zn}}{nF}\right) i_{corr} \tag{6.5}$$

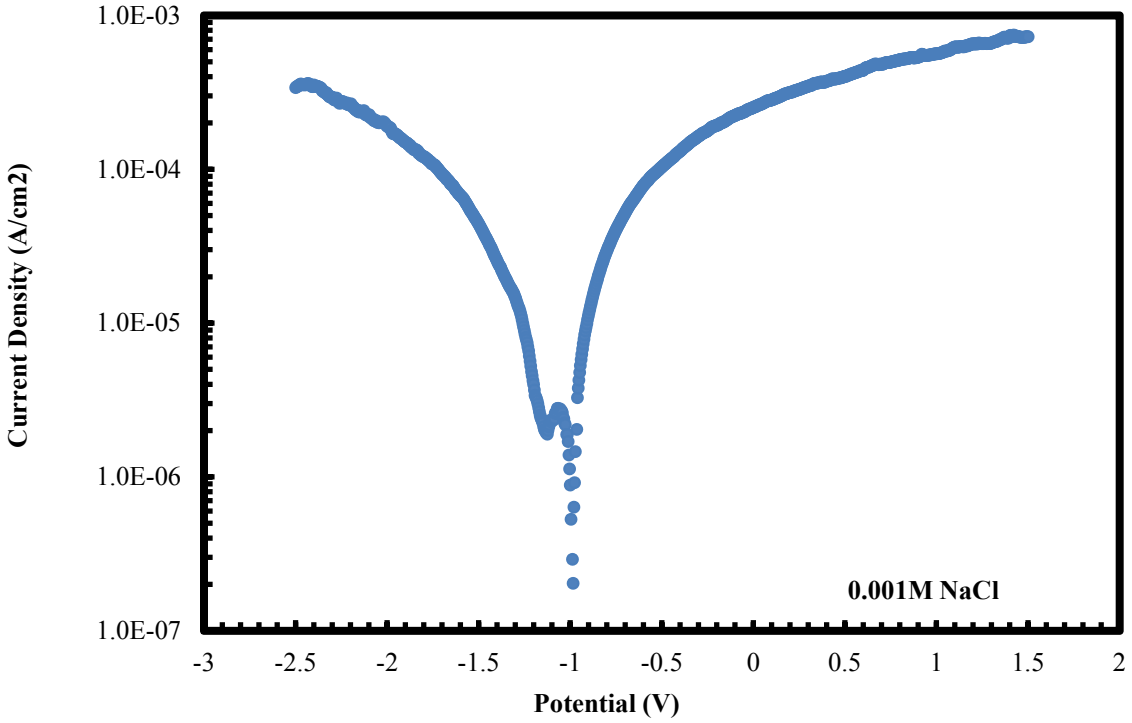

Figure 6.18 - Polarization Scan of Galvanized Steel Immersed in a 0.001 M NaCl Solution.

The corrosion rate of Zn ($\dot{\delta}, \mu m/yr$) was determined from the atomic weight of Zn (M_{Zn}, 65.4), corrosion current density (i_{corr}, A/cm^2), number of equivalents (n =2), and Faraday's constant (96487 C/equivalent), as explained by Kaesche (1985). The corrosion rate of Zn for the NaCl solutions are summarized in Table 6.3.

Table 6.3 Corrosion Rate Results for Galvanized Steel at Different NaCl Molarities.

NaCl Molarity	b_a (V/decade)	b_c (V/decade)	R_p (Ω-cm^2)	k	i_{corr} (A/cm^2)	mils/yr	µm/yr
0.0001	0.027	0.044	2.54E+06	0.0073	2.86E-09	0.0017	4.29E-02
0.001	0.02	0.059	8326	0.0065	7.79E-07	0.459	1.17E+01
0.01	0.047	0.01	2516	0.0036	1.42E-06	0.839	2.13E+01
0.1	0.05	0.01	1761	0.0036	2.05E-06	1.21	3.08E+01

With the current density (i_{corr}) for each NaCl solution (Figure 6.19), the corrosion rate was also calculated for the galvanized steel, as shown in Figure 6.20. In addition, the conductivity of a NaCl solution, which is the reciprocal of the solution resistance (Figure 6.21), was related to the corrosion rate of the galvanized steel.

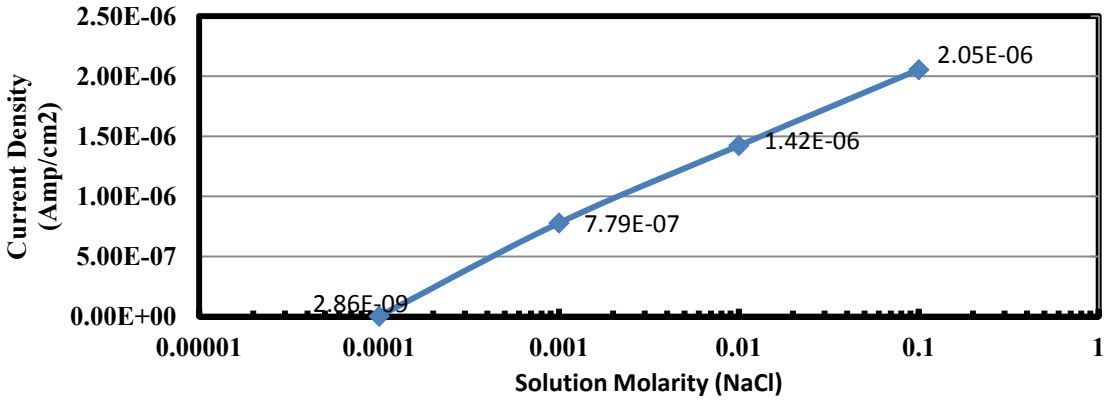

Figure 6.19 – Variation in Current Density with NaCl Content of Solution

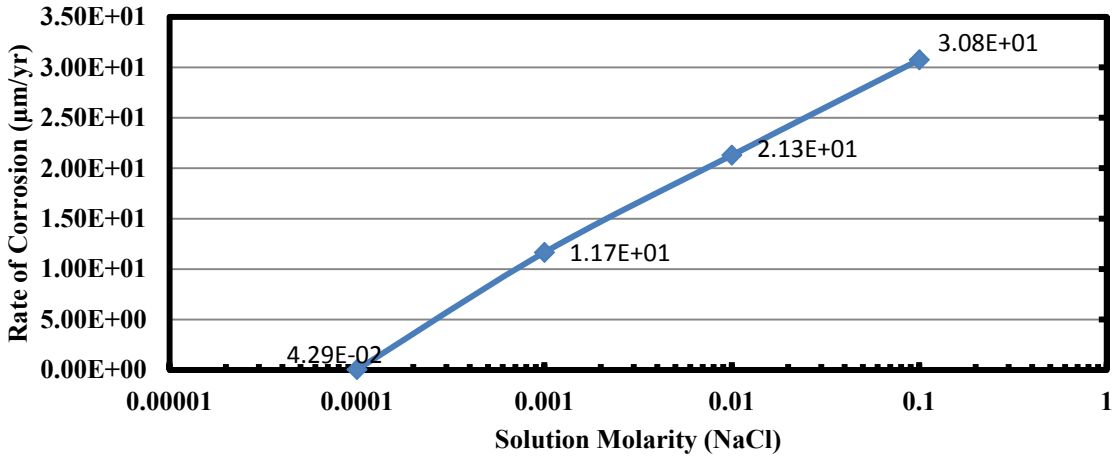

Figure 6.20 - Effect of NaCl Concentration on t Corrosion Rate of Galvanized Steel as Determined from EIS and Polarization Scans

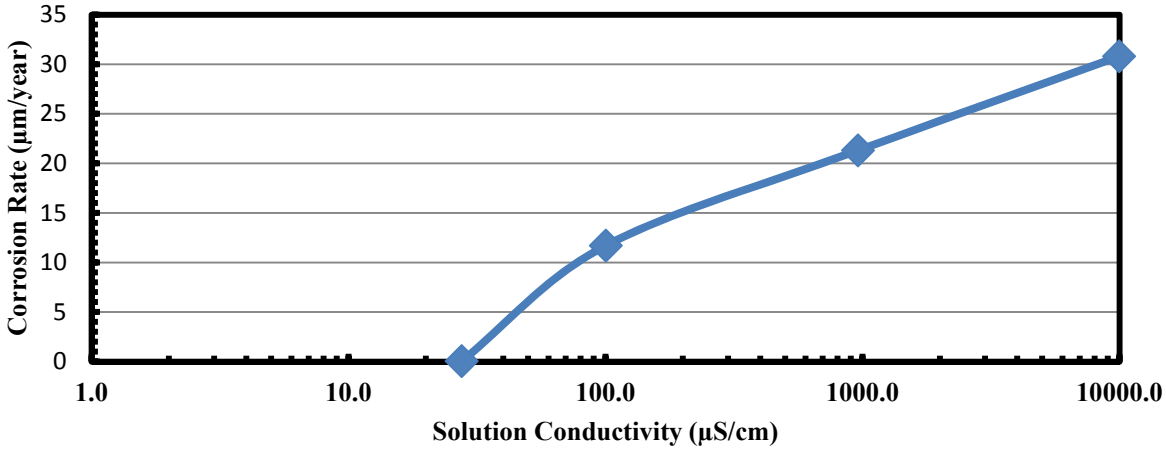

Figure 6.21 – Relationship between Solution Conductivity Related and Corrosion Rate of Galvanized Steel

The conductivities of the leach-liquors were also measured for each wet/dry and always wet specimen at regular intervals as shown in Figure 6.8. The conductivity-corrosion rate relationship (Figure 6.21) from the NaCl solutions was then used to determine the corrosion rate of galvanized steel embedded in each material as shown in Figure 6.22. All coupons of galvanized steel show a significant initial corrosion rate, though the rate was highest for the coupon embedded in Material F. The lapse of time without measurement was primarily from problems with the data logging circuit, which were corrected, as shown in Figure 6.22. For the first year, the predicted corrosion rate hovers about 15 µm/yr, which agrees with Elias (2000) model of 15 µm/yr for the first two years, though the corrosion rate seems to plateau to approximately 7 µm after the first year.

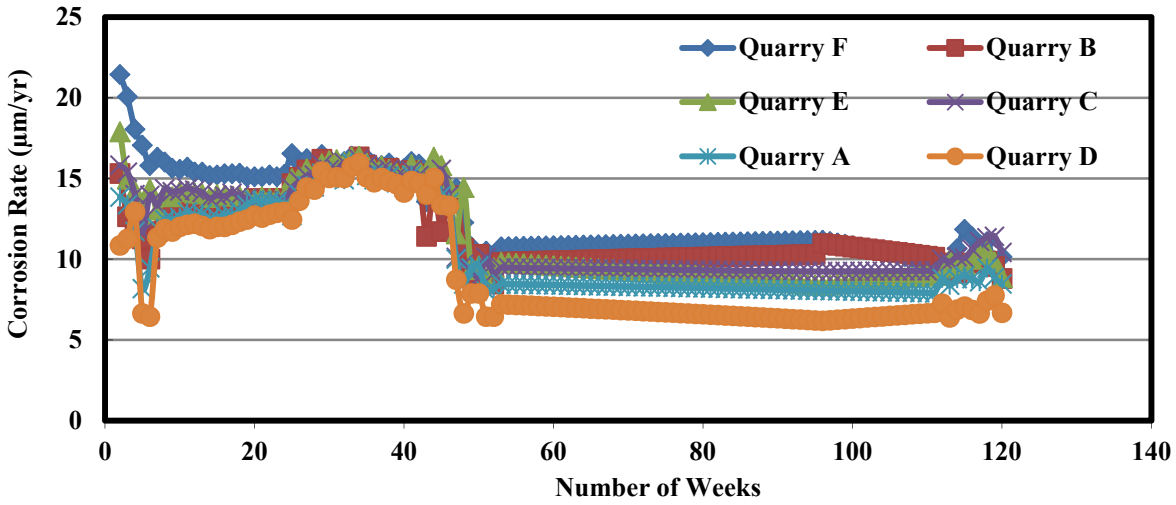

Figure 6.22 – Average Corrosion Rate of Embedded Coupons in Wet/Dry Specimens

Corrosion Monitoring with Electrochemical Noise

The current and potential transients were measured for corrosion coupons embedded as explained in Chapter 4 and with the circuit of Figure 5.6. The current transients represent the actual Zn surface reacting with ions of the leach-liquor, especially chloride ions, which attack most metals. The current usually indicates the dissolution of the metal surface by a sharp spike and then decreases or returns sharply to eventually a plateau current suggesting usually oxide reformation returning to steady-state dissolution of the ZnO. The current spikes or current noise was measured without electrical or mechanical perturbation and the current displays the minor reactions occurring on the surface, as shown in Figure 6.23. The current transients were recorded for approximately two years and were analyzed by calculating the power spectral density (PSD), as described in the present section. The PSD was calculated through fast Fourier transform (FFT) and maximum entropy method (MEM) shown in Figures 6.24 and 6.25, respectively. The foregoing methodologies follow the recommendations by Cottis (2001), Huruna et al. (2003) and Bertocci et al. (1997). The number of data samples chosen was 1024 to simplify the analysis and obtain a clearer spectrum. The current noise data for four samples embedded in Material F are shown in Figure 6.24. Additional current transients for the galvanized steel embedded in soils collected from other materials are included in Appendix C.

Specimens 1 and 3 were subjected to the wet/dry cycles for about 1 year and specimens 2 and 4 for 27 months. The rate of acquisition of the current for electrochemical data was 40 minutes (2400 sec).

With a fast Fourier transform, the current transients were converted into a PSD as a function of frequency, Hz, and then transformed into a current PSD divided by the frequency (or A^2/Hz), as shown in Figure 6.24. With a maximum entropy method (MEM) technique using an order of 1000, which indicates the number of coefficients or terms in the equation, the PSD lowers the fluctuations and smooths the PSD, as shown in Figures 6.25 and 6.26. However, the PSD-MEM shifts the PSD (A^2/Hz) to lower values compared to the PSD-FFT with increasing order.

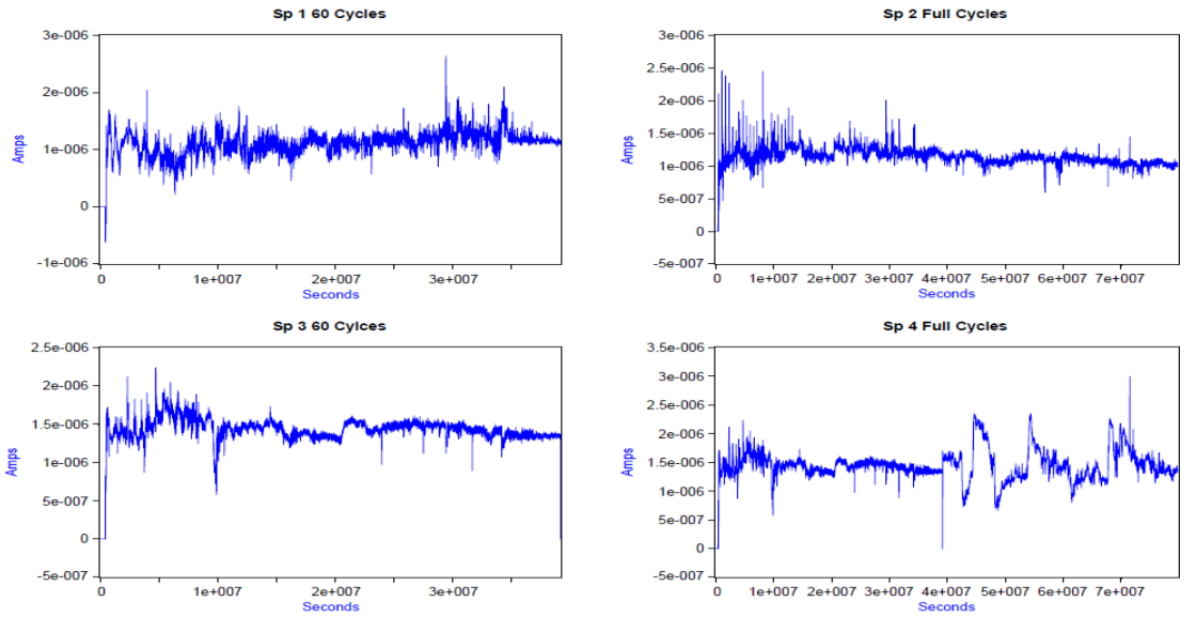

Figure 6.23 - Current Transients Acquired from Material F after 60 cycles (or 12 months) and Full Cycles (or 27 Months).

A relationship between the PSD-FFT and corrosion rate of the galvanized steel was sought by examining the value of the A^2/Hz near the low frequencies, which corresponds to long-term corrosion. For example, after approximately 27 months (i.e., 840 days) amounting to 72.6 Ms, the frequency becomes 10^{-8} Hz near which an average value of the A^2/Hz can be acquired for five data points of Figure 6.27. To determine the change in the average value (or plateau) over time, the data of 840 days were divided into five segments corresponding to increments of 168 days. The variation of the PSD-FFT among the five segments shows some overlap as shown in Figure 6.27. However, the plateau for each segment initially decreases with time and then seems to level out even though the standard deviation of the plateau (or average) is dramatic, as shown in Figure 6.28.In comparison with the corrosion rates (Figure 6.22), the PSD-FFT plateau value of greater than $3(10)^{-8}$ A^2/Hz would indicate a significant corrosion rate. The decreasing trend of the PSD-FFT with exposure time to wet/dry cycles (Figure 6.28) compares similarly with the corrosion rate shown in Figure 6.22. For a passive monitoring system for corrosion, the analyses using PSD-MEM can give a smoother fit and lower standard deviation for the electrochemical

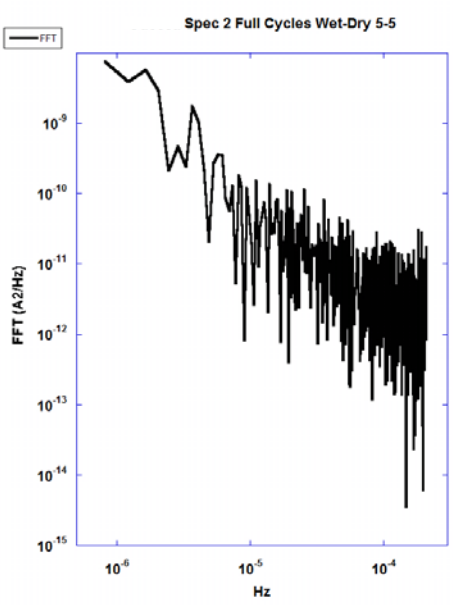

Figure 6.24 Current PSD Acquired through a FFT Technique for Material F Data.

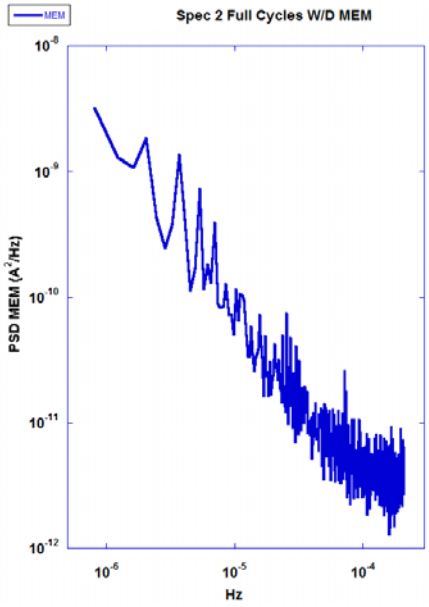

Figure 6.25 - Current PSD Acquired through a MEM Technique of order 1000 for Material F Data.

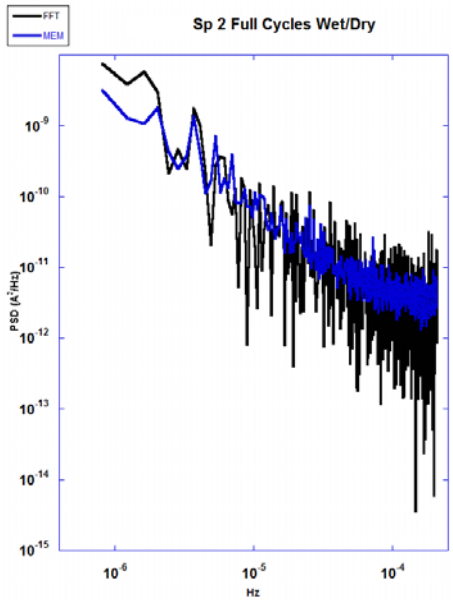

Figure 6.26 - Current PSD Overlapping FFT and MEM Techniques of Material F Data.

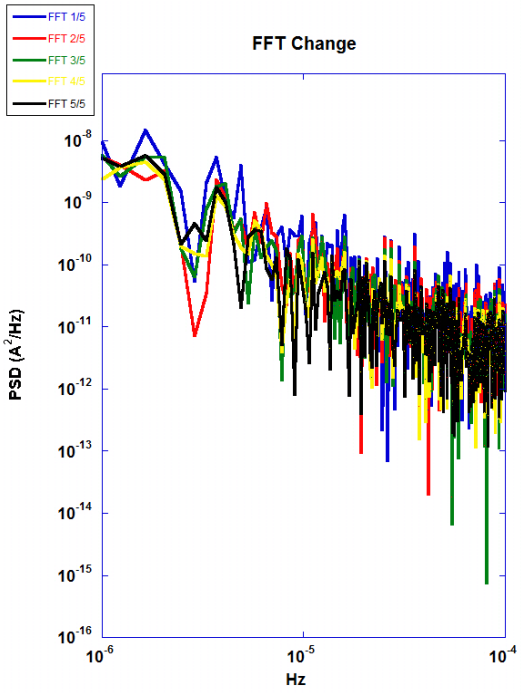

Figure 6.27 - PSD acquired from FFT Analysis for Wet/Dry Cycles from Material F of Specimen 2 from Five Segments at 168-Day Increments.

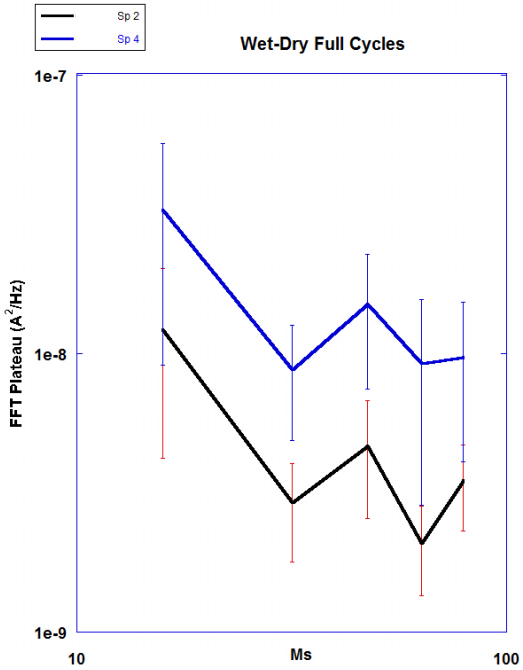

Figure 6.28 - Plateaus of PSD-FFT Divided in Five Increments (i.e., 168-Day Increment) for Wet/Dry Cycles for Specimens 2 and 4 from Material F.

noise data, but the PSD values would need confirmation with a PSD-FFT analysis. Future studies should compare accelerated corrosion rates with the passive corrosion tests. However, the present analysis suggests that the conductivity-corrosion rate relationship gives significantly less fluctuations than the PSD-FFT.

Validation of Corrosion Models

In the present section, the corroding thickness of the galvanized steel is summarized for the quarries investigated. In addition, a corrosion prediction model is developed from the corroding Zn thicknesses.

The thicknesses of the corroding zinc layer were determined with time by integrating the corrosion rate data of Figure 6.22. The Zn acquired a constant rate of corroded thickening for approximately the first year, followed by a dramatic decrease of the thickening rate, as shown in Figure 6.29.

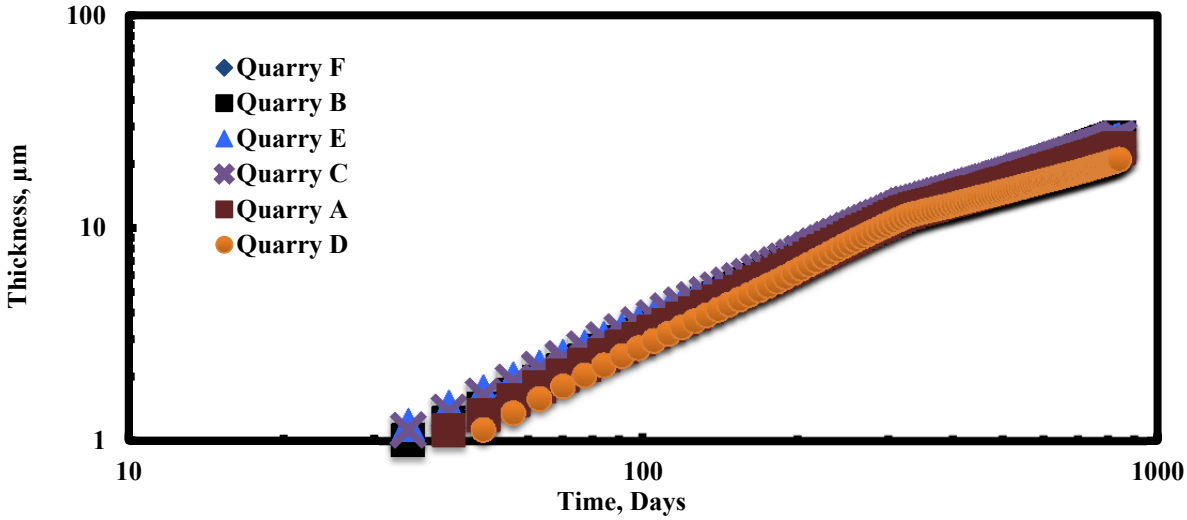

Figure 6.29 - Calculated Corroded Thickness for Wet/Dry Specimens.

Previous analysis of the corrosion of MSE amounted to a corroding thickness (δ) according to the following equation:

$$\delta = A\, t_1^B \tag{6.6}$$

With the result of calculated corroded thickness, the prediction model followed more closely a two-stage corrosion with the initial time increment having a corrosion rate different from the second time increment. For the time greater than t_1, the two-stage corrosion model for the first two years according to the data is:

$$\delta = A t_1^{B_1 - B_2} t_2^{B_2} \tag{6.7}$$

For the time less than t_1, $B_2 = 0$ and essentially follows the initial equation though B_1 would be slightly greater than the slope predicted by Elias (2000) for a 50 to 100% saturation for

galvanized steel with a slope of 0.65 (or $\delta = 25t^{0.65}$ as average and $\delta = 50t^{0.65}$ for maximum). The average of the slopes of the lines acquired in Figure 6.29 give the following relationship:

$$\delta = A t_1^{1.1-0.74} t_2^{0.74} \quad (6.8)$$

The foregoing two-stage corrosion prediction model is shown in Figure 6.30. For designing a MSE considering an anticipated corrosion, the maximum thicknesses should be used and has been determined from the wet/dry specimens, as shown in Figure 6.30. At the end of 840 days, the maximum predicted thickness was 29 µm for a range of thickness of 21 to 29 µm. A comparison of the average and maximum corroding thicknesses show that the two trends curiously meet, but afterwards they both have decreasing trends or corrosion rates (i.e., slopes) for the corrosion of the Zn layer.

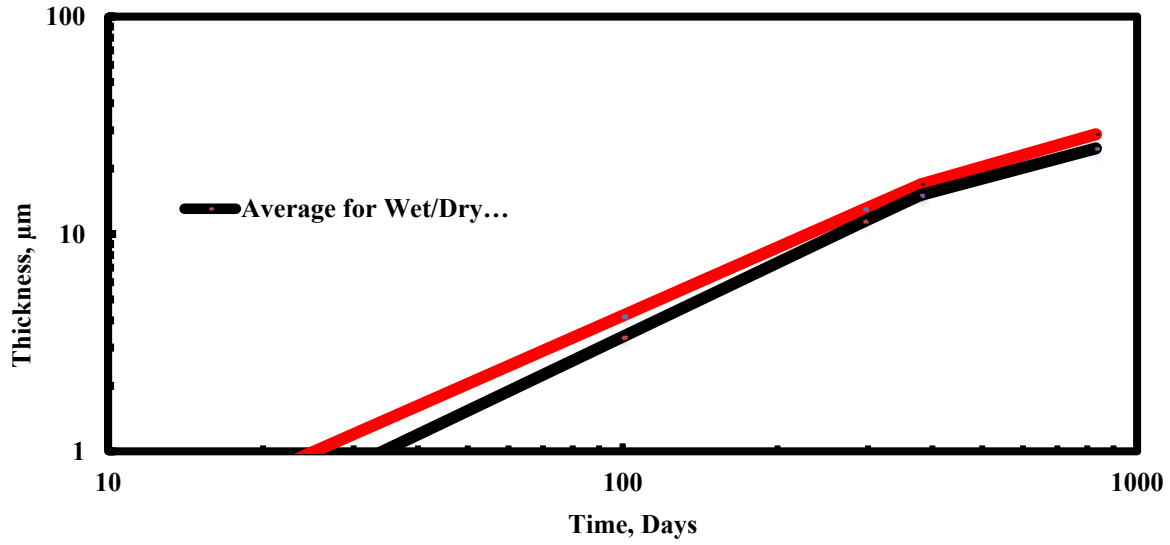

Figure 6.30 - Average Corroding Thickness for Embedded Galvanized Steel as Acquired from Figure 6.29 for Average and Maximum Thicknesses.

For the calculated corroded thickness for galvanized steel embedded in wet soils, the data are shown in Figure 6.31. The conductivities for each of the solutions taken from the wetted soils were calculated from the ions measured and then the conductivities were used to determine the corrosion rate. After 770 days, the calculated thicknesses ranged from 26 to 40 µm among the six quarries. The calculated thicknesses of specimens from wetted soils are slightly greater than the samples acquired from wet/dry soils and may be a result of the calculated conductivities for each leach-liquor.

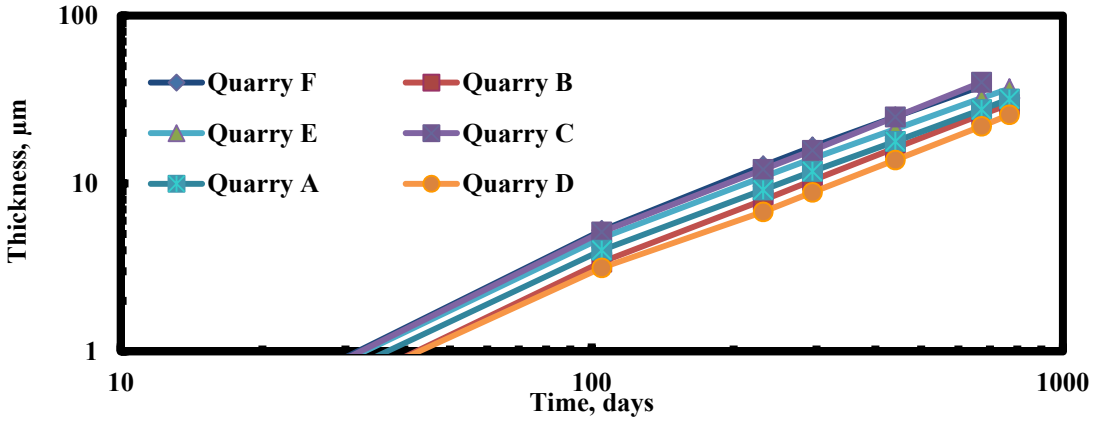

Figure 6.31 - Calculated Corroded Thickness for Specimens Embedded in Wet Soils

The corroded thicknesses were also measured for galvanized steel embedded in wet soils and wet/dry cycled soil by examining the SEM microstructures and plotted in Figure 6.32. The corroded thicknesses were acquired from galvanized steel exposed after 12 months and after 27 months. The low concentrations of ions in the leach-liquor cause low corroding rates as also reported, for example, by Elias (2000) and Sagues et al. (1998). However, the corroded thicknesses were calculated by assuming that the total Zn layer was 120 µm. The initial Zn layer thicknesses usually averaged approximately 120 µm, though the Zn thicknesses may vary from 80 to 150 µm. Elias (2000) reported a maximum loss of 86 µm for a 75-year life.

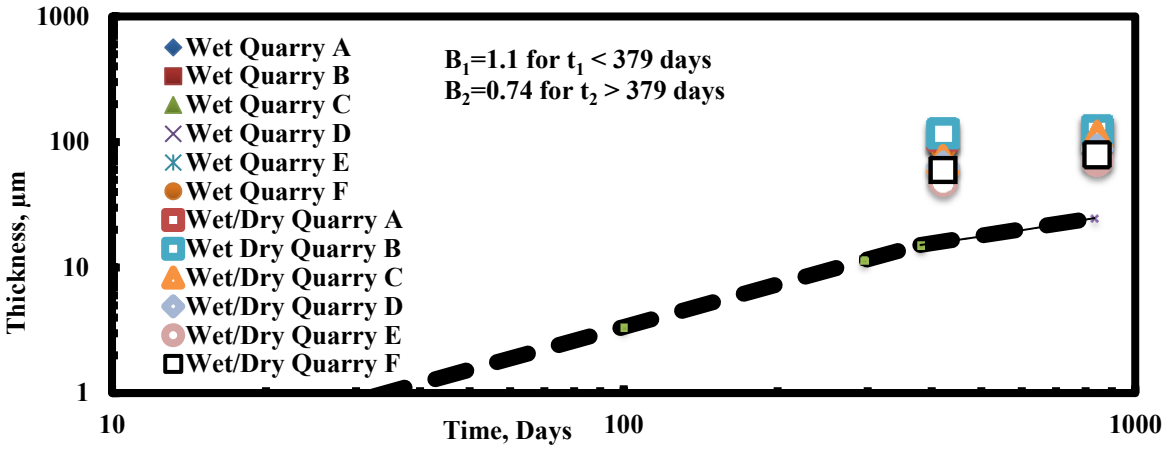

Figure 6.32 – Comparison of Measured and Calculated Corroded Thicknesses of Galvanized Steel for Always Wet and Wet/Dry Specimens

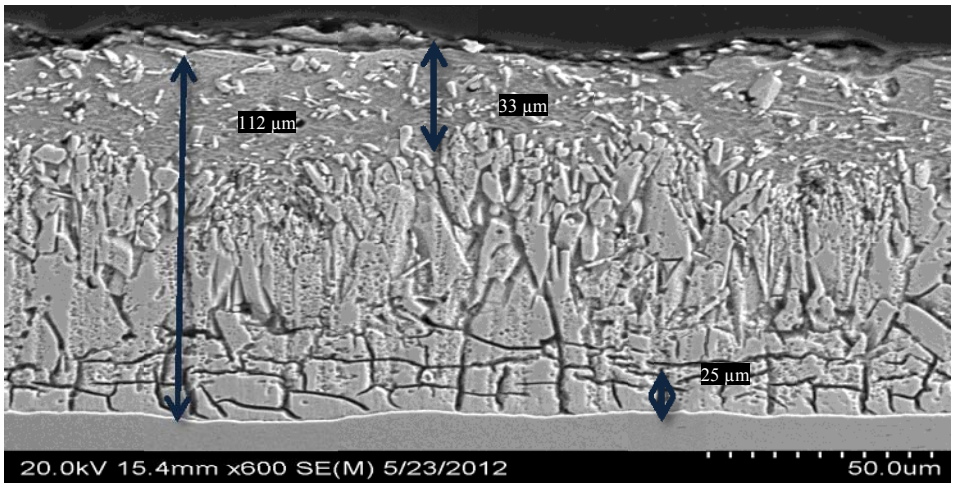

Figure 6.33 - Microstructure of Zn Layer with the corroded thickness of 33 µm for a total original Zn layer of 112 µm.

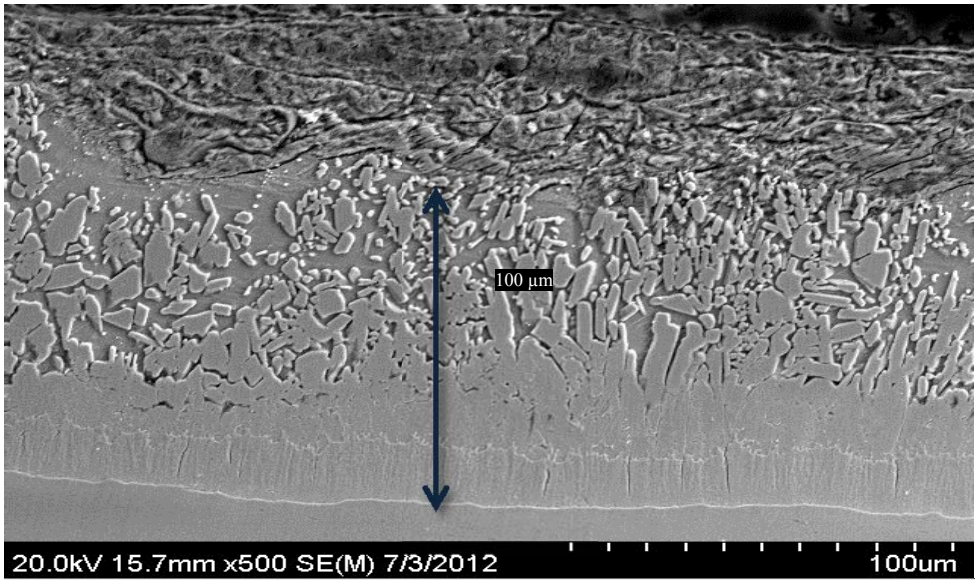

Figure 6.34 - Microstructure of Zn Layer after Exposure to an always wetted soil.

With the measured Zn layer in a region sometimes slightly less than 86 µm or near it (e.g., Figure 3.9), an increased Zn layer is warranted, a change in the coating process to ensure uniformity, or sampling of the coating should occur to ensure its ample life-time expectations. The microstructure of a typical galvanized steel depicts easily the corroded thickness of the Zn layer and the uncorroded thickness adjacent to the Fe substrate. For a typical specimen subjected to wet-dry cycles, the thickness of zinc layer approximated 112 µm with the corroded Zn amounting to 33 µm, which is the porous ZnO, as shown in Figure 6.33. A typical microstructure from a specimen acquired from an always-wetted soil showed a similar corroded region in the Zn layer (Figure 6.34).

The measured thicknesses of Zn corrosion were greater than the thicknesses predicted from the model, as shown in Figure 6.32. Measured corroded thicknesses were greater for quarries A and B but considerably less for thicknesses measured for quarries E and F. The range of the range predicted thicknesses was less than the range of thickness for the measured Zn layer, which indicates the non-uniformity of the attack. The porous ZnO does not form uniformily across the Zn layer as viewed from the oxygen distribution (or dot map) in Figure 6.10 and 6.11, as well as the corroded thickness varying beyond 33 μm in Figure 6.33.

Analysis of Corrosion of the Galvanized Steel

The geochemistry of the soil, structural properties of the MSE strand and corrosive behavior of the solution contacting the galvanized steel may affect the integrity of the wall reinforcement system. The mineral and salt dissolution from the soil forms the leach-liquor, or electrolyte, needed to connect the anodic and cathodic half-cell reactions for corrosion of the galvanized steel of MSEs. To characterize the corrosivity of the leach-liquor, the present research used sensors to measure only the conductivity of the solution and the passive current transient generated between two zinc surfaces. The intent of the sensors was to study monitoring techniques for assessing the corrosion of MSE strands.

Though the leach-liquor contained low concentrations of cations (i.e., Ca^{2+}, Na^{2+}, $Mg^{2+}$and K^{+}) and anions (i.e., Cl^{-}, SO_4^{2-} and NO_3^{-}), the sensor measured conductivity sufficiently to predict the corroded thickness of the zinc layer by simply considering the chloride ion. The chloride ion was selected, because it attacks the metallic surfaces more aggressively than sulfate and nitrate ions, as reviewed by Jones (1992) and Szklarska-Smialowska (1986). The corroded thickness of the galvanized steel embedded in soil was predicted from a relationship acquired from measured electrochemical parameters of galvanized steel immersed in NaCl solutions with their conductivities.

The dissolved oxygen integral to the cathodic reaction (i.e., reaction 2.4) for the corrosion of galvanized steel would be characterized by the electrochemical cell configured for a thin-film electrolyte, as designed and reported by Yadav et al. (2004). Yadav et al. (2005) also confirmed the Suzuki (1985) study that the reduction of dissolved oxygen to hydroxide may include the reduction of the ZnO, hydroxide and the basic hydroxide-chloride of Zn. Water permeating via the soil porosity will have dissolved oxygen, which changes upon the wetting and drying patterns of the atmosphere and road conditions. The experimental approach was to design an electrochemical cell with a thin-film electrolyte for use ultimately in field measurements. The electrochemical cell would monitor passive current coupled with conductivity measurements at low-cost with the ultimate connectivity to corrosion measurements aided by sophisticated electrochemical instrumentation. The low-conductive solution contributes an ohmic-potential, which must be considered carefully in the interpretation of electrochemical measurements.

The microstructures acquired from the scanning electron microscope coupled with an energy dispersive x-ray analysis of cross-sections of corroded samples indicated the formation of corrosion products, as depicted in Figures 6.10 to 6.13. The leach-liquor corrodes the Zn to form a layer of porous ZnO allowing the dissolved oxygen to diffuse to the Zn/ZnO interface and Zn ions diffuse outward into solution. Chloride ions also permeate through the pores of the ZnO and segregate toward the region of the Zn/ZnO interface. Sulfur was detected within the porous

ZnO layer though at a lesser extent. The oxygen and chlorine distribution (or dot mapping) along the Zn layer also confirms the research findings that the corrosion involves complicated anodic/cathodic reactions, ion (e.g., H^+ and Cl^-) diffusion and dissolved oxygen, as reported by Yadav et al. (2004 and 2005), Walter (2000), and El-Feki and Walter (2000).

Chapter 7 - Field Instrumentation

To connect more accurately the laboratory test results with on-site corrosion behavior under "real-world" conditions, three MSE walls under construction were instrumented during the course of this project so that the changes in the geochemistry and the rate of corrosion could be monitored and compared with the laboratory processes. Three MSE walls, constructed with Materials A, C and E, were selected for instrumentation. Unfortunately, the site with Material A was destroyed by flood in June 2010 before any data can be acquired.

Instrumentation

Several instruments were installed at each MSE wall to monitor several parameters affecting the corrosion rate of the metallic earth reinforcement. Figure 7.1 shows examples of the instruments that were used. The following items were installed at each site:

- Lysimeter
- Moisture Probes
- Temperature Probes
- Resistivity Probes
- Metallic Coupons

Lysimeter

A lysimeter is a metal canister that has a portion that is porous by design. This allows water from its surroundings to enter when a vacuum is applied. Lysimeters were installed to sample the water penetrating the backfill. Samples of the effluent were collected remotely using a vacuum pump. The conductivity, ion concentrations, and total organic carbon contents of the extracted effluent were measured in the laboratory.

Moisture Probe

Moisture probes were also buried in the backfill to measure the moisture content, conductivity, temperature and dielectric constants of the backfill. A Stevens Hydra-Probe II (see Figure 7.1) was used to measure these parameters. This probe simultaneously measured the different soil parameters mentioned and stored the readings in a data-logger. The data from the data-logger was manually downloaded to a computer every 2 to 3 months. These sensors were calibrated in the laboratory using the site specific backfill to ensure the accuracy of readings.

Temperature Probes

The temperature within the backfill was also monitored on a regular basis. The Stevens Hydra-probe described earlier also has the capacity to measure temperature along with moisture content, conductivity and dielectric constant.

Resistivity Probes

A set of soil resistivity probes was also installed at the site and extended to the instrumentation box so that the backfill resistivity can be measured for comparison to lab results. The probes

were copper tubes (0.25 in. in both diameter and length) soldered to electrical terminal wires. The resistivity setup consists of four probes with a spacing of 3 in.

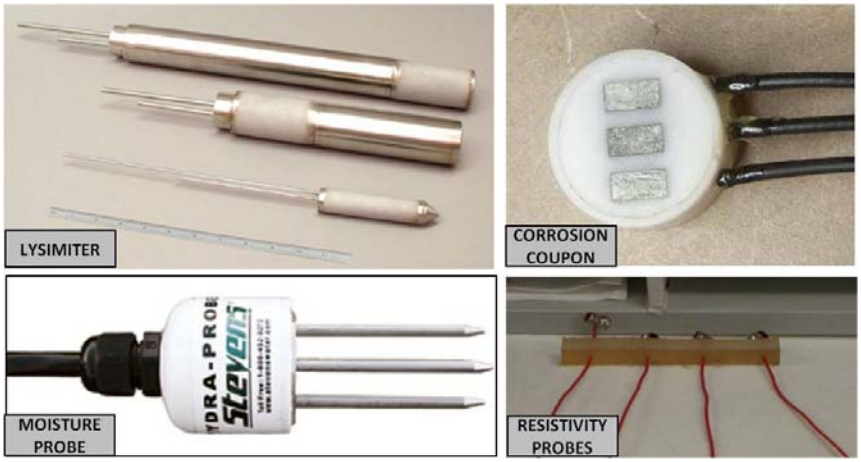

Figure 7.1 – Instruments Used at each MSE Wall to Monitor Corrosion Parameters.

Metallic Coupons

Metallic coupons as shown in Figure 7.1 were placed within the backfill in order to monitor the corrosion behavior of the earth reinforcement over time. These coupons were similar to those used within the laboratory specimens and data collected in the same manner as discussed for the laboratory specimens.

Instrument Installation

Figure 7.2 shows a side and a top view of the instrumentation setup. Depending on the height of the MSE walls, the instrumentation was placed at one or two levels.

A 2-ft square, 1 ft deep hole was dug approximately 5 ft from the face of the wall after the appropriate backfill layer was compacted to accommodate the lysimeter. The hole, which was placed between two adjacent metallic earth reinforcements, was covered with a plastic sheet and was filled with pea gravel, after the lysimeter was placed in the hole. A piece of geotextile was then placed on top of the hole to minimize the intrusion of backfill material. Two water lines per lysimeter were extended to the connection box to extract the collected the accumulated effluent by applying vacuum.

The moisture probe was then installed close to the lysimeter in the backfill. To install the probe, a 3 in.-diameter, 8-in. deep hole was dug. The probe was pushed in the backfill at the bottom of the hole. The hole was then filled with the removed fill material close to the density of the surrounding materials.

The resistivity probes were installed close to the lysimeter in the backfill. The installation simply consisted of smoothing a small area on the backfill and burying the copper heads within the backfill. A PVC spacer was used to maintain a 3-in. separation between the copper probes during their positioning.

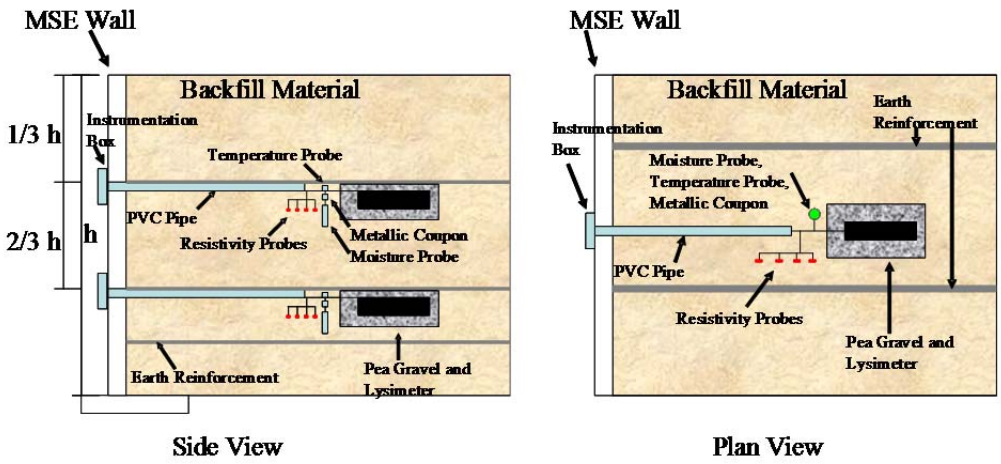

Figure 7.2 – Side and Top View of Instrumentation Placement.

The installation of the metallic coupons was very similar to the installation of the resistivity probes. Care was taken to place the coupon with the metallic samples facing upward so that moisture could be collected on the machined lip of the coupon.

Figure 7.3 shows all the sensors in place, ready to be covered by backfill material and a picture of the wall upon completion of the installation of the instrumentation. For the site using Material C, a 3-in. hole was cut to allow the PVC pipe through the wall and was later covered by an instrumentation box. For the site with Material E, PVC pipes were installed under the footing of the MSE wall so that the instrumentation box can be placed flush with the side walk.

Figure 7.4 shows the data collected with the moisture probes. The variations in temperature with time follow one another closely as one would expect, and reflect the seasonal changes in temperature. The moisture contents and dielectric constants appear to follow expected patterns as well: The higher the moisture content of the backfill is, the higher the dielectric constant would become. The conductivity on the other hand, did not follow the previous pattern, particularly for Material E (Top). While the sensor recorded a small amount of moisture in the Material E (Top) location, the Hydra-probe recorded no conductivity during the entire time.

Figure 7.3 – Sensor Placement and Metallic Enclosure from Completed Site.

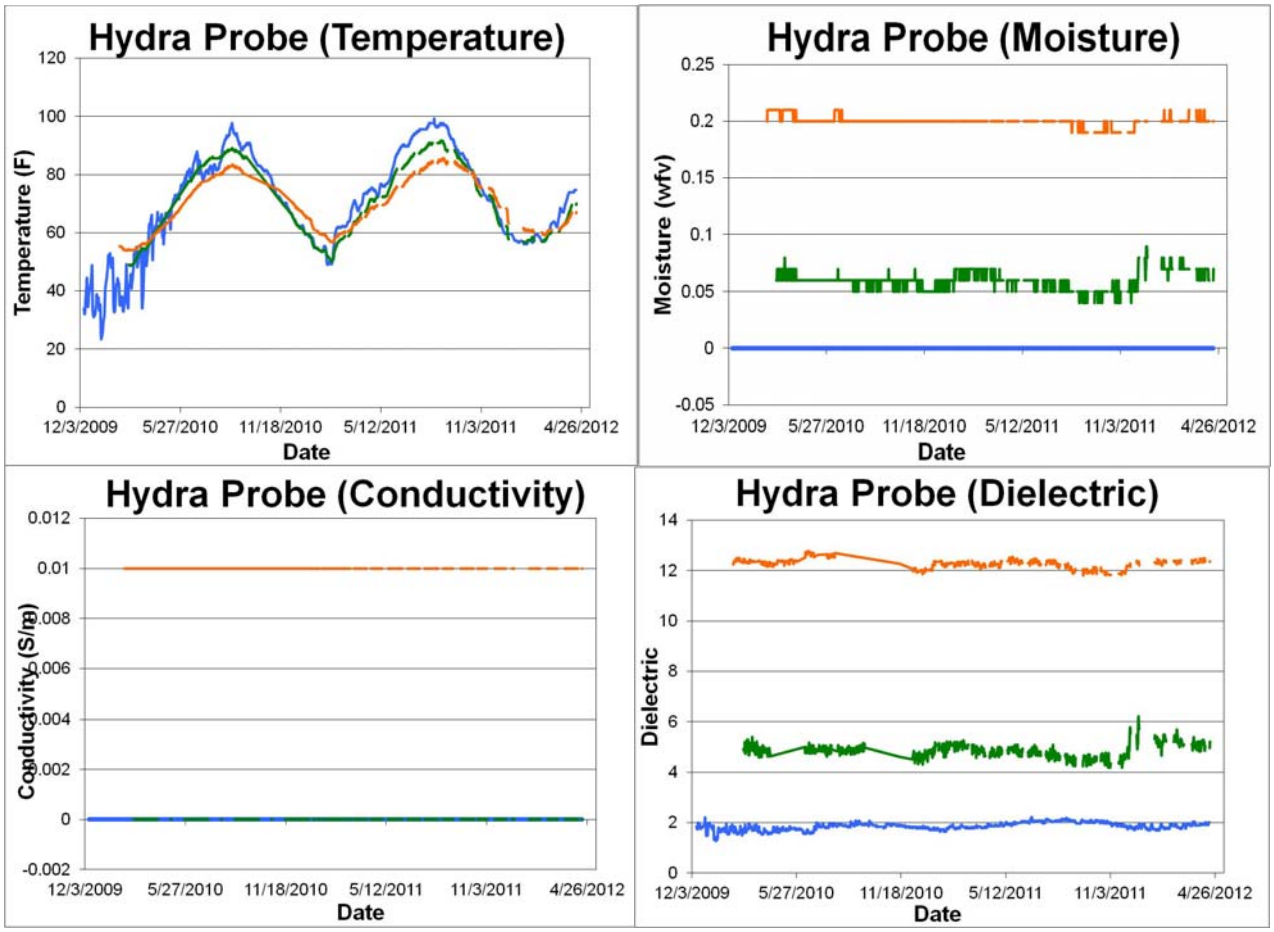

Figure 7.4 – Field Data Collected with Hydra-Probe.

Figure 7.5 shows the data collected from the corrosion coupons installed at the sites. Despite acquiring high quality hermetically sealed instrumentation boxes, water intruded the metal enclosure during two episodes of very intense rain in Material E site. To minimize this problem, the data-logger was further enclosed in a plastic box to protect it against moisture and avoid further failures. The data-logger at the material C site worked without interruption throughout the course of the project. In general, the graphs show very small changes in voltage and current. When they do happen, both voltage and current follow one another.

Figure 7.6 displays the resistivity measurements from the instrumented sites. The resistivity values from Material C are always greater than those from Material E; this pattern is confirmed by the lab results which show a similar trend. For Material E site, the resistivity values at the upper and lower levels start at similar levels, diverge and then appear to go back to a common value depending on the precipitation pattern.

The variations in the sulfate and chloride concentrations with time are presented in Figures 7.7 and 7.8. The values measured from the laboratory specimens are also superimposed on the figures. For the most part, the values from field measurements lie within the two extreme cases studied in the laboratory, always wet and wet/dry cycles.

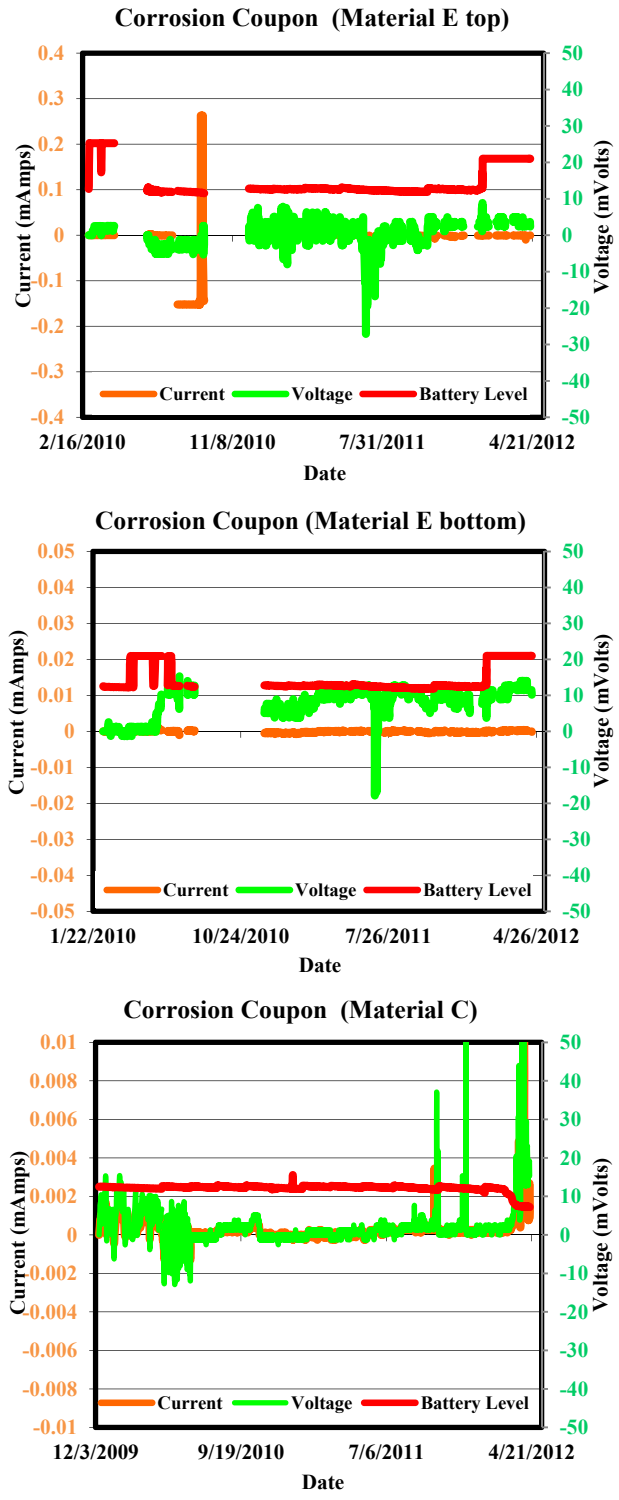

Figure 7.5 –Corrosion Coupon Data Collected from Instrumented Sites.

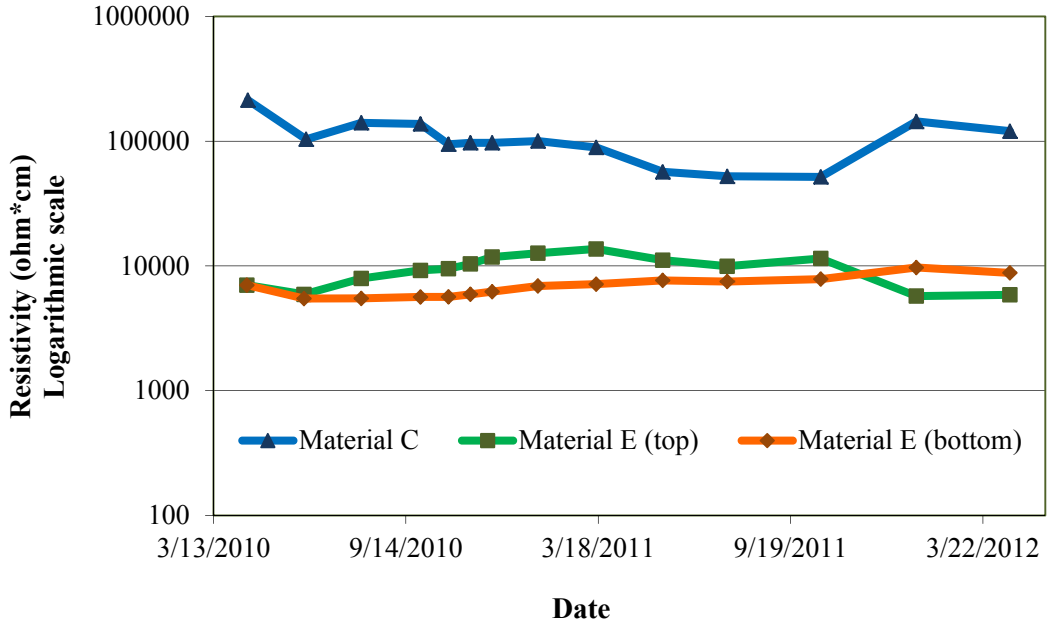

Figure 7.6 – Resistivity data collected from Waco and Dallas sites.

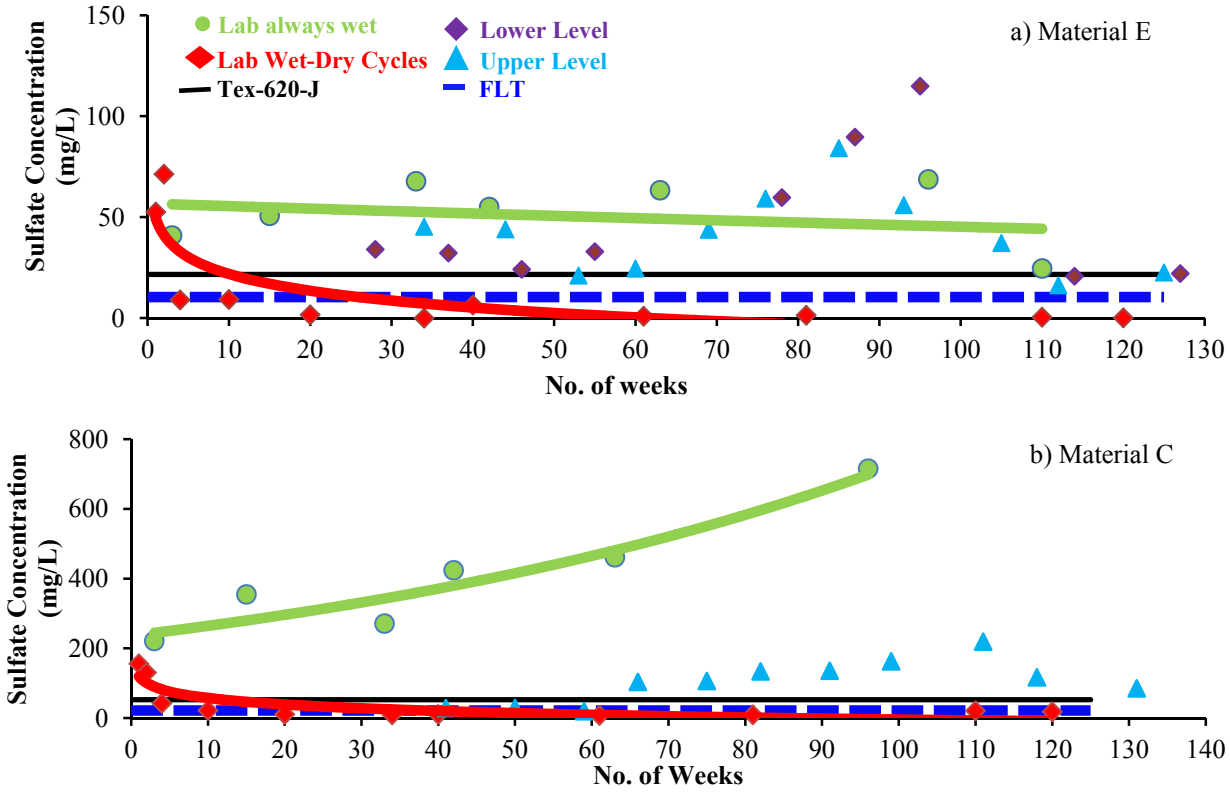

Figure 7.7 – Variations of Sulfate Concentrations with Time at Instrumented Sites

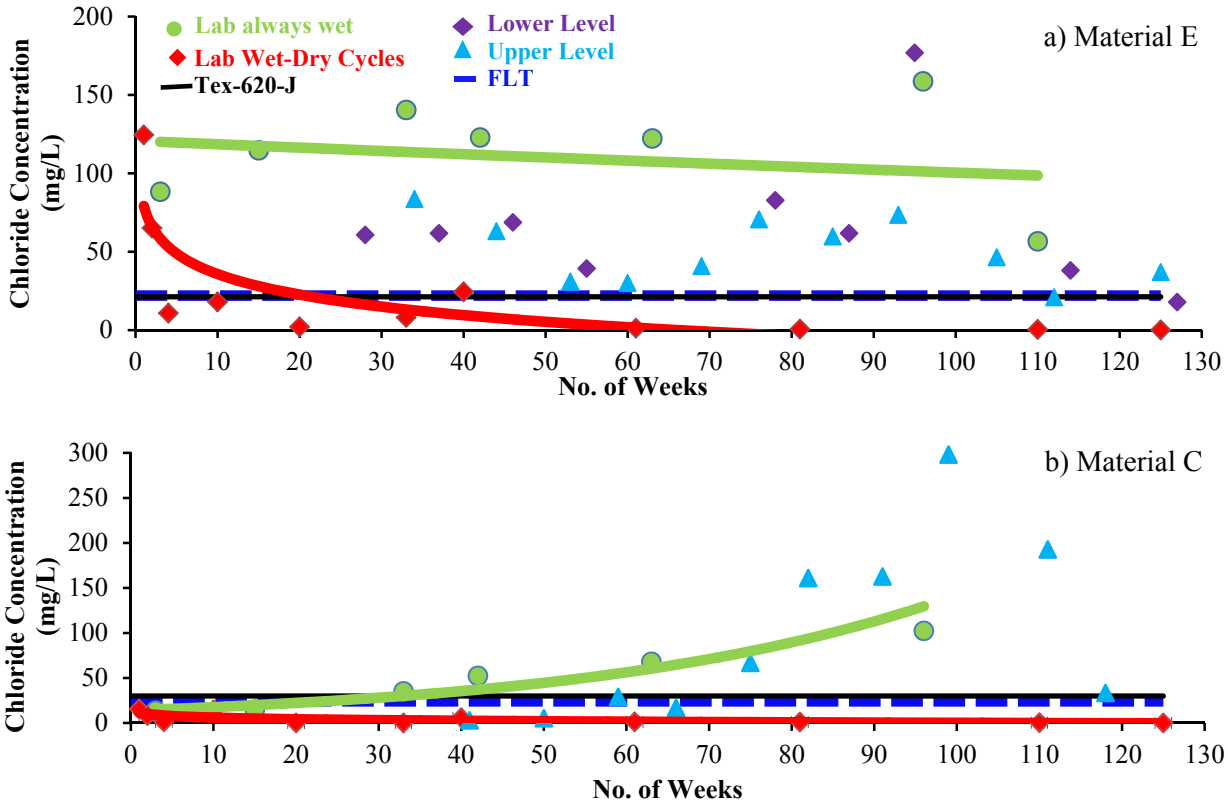

Figure 7.8 – Variations of Chloride Concentrations with Time at Instrumented Sites

Chapter 8 - Closure

This report contains the results of a coordinated effort to provide recommendations for specifying coarse (Type A and Type D) backfills used for mechanically stabilized earth (MSE) walls in Texas. The geotechnical, geochemical and corrosive aspects of coarse backfills were assessed through laboratory and field studies. The recommendations from this study can be summarized in the following items:

Geotechnical Engineering Aspects

The geotechnical aspects of the aggregates used for backfills were determined in terms of their hardness, gradation, compaction parameters and permeability. The practical recommendations are as follows:

- The geotechnical aspects of Item 324, such as gradation and index properties and compaction requirements, are for the most part appropriate for the specification and construction of coarse-backfilled MSE walls. Waiving these requirements should be discouraged.
- Hardness of aggregates should be considered as a primary factor in specifying coarse backfills and the Districts should be discouraged from waiving that requirement.
- Item 423 should be strengthened by incorporating simpler tests that assess the hardness of the aggregates (e.g., Los Angeles Abrasion or Wet Ball Mill).
- One of our practical observations was that the materials that readily lend themselves to well-defined moisture-density curves and yield a maximum dry density greater than 105 pcf are typically too soft to meet the hardness specifications for coarse (Type A and Type D) backfills.

Geochemical Aspects

The geochemical characteristics of the materials that were considered included the conductivity, pH, ionic contents (i.e., SO_4^{--}, Cl^-, NO_3^-, F^- and HCO_3^-) of the leach-liquor, and the resistivity of the soil-fluid mixture. The practical recommendations are as follows:

- Current TxDOT specifications for coarser backfills may be conservative.
- The lack of fine aggregates required for traditional tests (i.e., Resistivity as per Tex-129-E, pH as per Tex-128-E, and Chloride and Sulfate concentration as per Tex-620 J) may impact the representativeness of those values for performance of coarse-backfilled MSE walls.
- The USGS Field Leach Test is offered as a reasonable and feasible alternative to current methods. Appendix D contains the proposed test procedure that TxDOT may consider for the incorporation of that test procedure in their operation.
- Based on instrumentation of two MSE walls in Texas, the results from the proposed test procedure are reasonable and representative of field conditions.

Corrosion Aspects

To ensure that the proposed tests are representative of the common corrosion models used in the design of MSE walls, about 80 laboratory specimens were prepared and monitored for up to 27 months. These specimens were subjected to the following three different environmental conditions:

- Always dry where the backfill materials were always maintained dry
- Always wet where the backfill materials were maintained saturated for the duration of study, and
- Wet/Dry where the backfill specimens were weekly saturated for two days and then allowed to dry for 5 days (subjected over 120 cycles of fluctuation of water table).

Geochemical parameters of the leach-liquors from the always wet and wet/dry specimens were measured periodically. The rates of corrosion of the metallic reinforcements were predicted from the measured conductivities of the leach-liquors for two years. By using metallurgical cross-sections, the rates of corrosion of the galvanized steel samples were also measured after approximately 1 year and 2 years of exposures to those three moisture regimes. The practical recommendations from that aspect of the study are as follows:

- The corrosion of the metallic reinforcements embedded in always dry specimens was minimal.
- The rates of corrosion for the always wet and wet/dry specimens were directly related to the conductivity of the leach-liquor.
- The conductivity of the leach-liquor appears promising to monitor the corrosion rate even though the predicted corroded thickness was slightly less than the measured corroded thicknesses.
- For wet/dry specimens, the rate of corrosion decreased with time. This seems to occur because the sulfate and chloride concentrations were negligible after several cycles of wetting and drying, resulting in a substantial reduction in the conductivity of the leach-liquor with time.
- With the measured Zn layer in a region sometimes slightly less than 86 μm or near it, an increased Zn layer is warranted, a change in the coating process to ensure uniformity, or sampling of the coating should occur to ensure its ample life-time expectations.
- The following two-stage model that relates the amount of corrosion, δ, to time, t, is proposed:

  $\delta = A\, t_1^{B_1 - B_2} t_2^{B_2}$ with B_1=1.1 and B_2=0.74.

  The amounts of corrosion measured from the embedded specimens were in good agreement with the results obtained from that model.

References

- Ahn, S., Kwon, H. and Macdonald, D. D. (2005) "Role of Chloride Ion in Passivity Breakdown in Iron and Nickel," J. Electrochemical Society, 152 (11), pp. B482-B490.
- Aiken G. R. (1991), "Humic Substances in Soil, Sediment, and Water," Geochemistry, Isolation, and Characterization (Hardcover) Krieger Publishing Company.
- Akpofure, R.R. and Kehinde, A. J. (2006), "Investigation of Soil Corrosivity in the Corrosion of Low Carbon Steel Pipe in Soil Environment", Journal of Applied Sciences research, 2(8), pp. 466-469, INSInet Publications
- Al-Rousan, T.M. (2005), "Characterization of Aggregate Shape Properties Using a Computer Automated System," Doctoral Dissertation, Texas A&M University. Texas A&M University
- Al-Mazeedi, H. A. A. and Cottis R. A. (2004), "A practical evaluation of electrochemical noise parameters as indicators of corrosion type," Electrochemical Acta, Vol. 49, pp. 2787-2793.
- ANSI/AWWA (1999), "American National Standard for Polyethylene Encasement for Ductile-Iron Pipe Systems," American Water Works Association, Denver, CO, C105/A21.5-99:
- Arroyo J. C., Bronson A., and Varma S. K. (1990), "The Surface Morphology and Transient Current Response of Fe-16w/oCr-16w/oNi in a Scratch Test," Journal of Materials Science Letters, 1990, Vol. 10, 94-95.
- Beech I. B. (2004), "Corrosion of Technical Materials in the Presence of Biofilms–Current Understanding and State-of-the art Methods of Study," International Biodeterioration and Biodegradation 53, 177-183.
- Bertocci U., Gabrielli, Huet F., Keddam M. and Rousseau P. (1997) "Noise Resistance Applied to Corrosion Measurements," J. Electrochemical Society, Vol. 144, pp. 37-43.
- Bertocci U., J. Freydman, C. Gabrielli, F. Huet and M. Keddam (1998), "Analysis of Electrochemical Noise by Power Spectral Density Applied to Corrosion Studies," J. Electrochemical Society, Vol. 145, pp. 2780-2786.
- Bertolini L., Elsener B., Pedeferri P. and Polder R. (2004), "Corrosion of Steel in Concrete–Prevention, Diagnosis," Repair. Weinheim, Germany: Wiley-VCH Verlag GmbH & Co. KGaA.
- Broomfield, J. P. (1997), "Corrosion of Steel in Concrete," London: E&FN Spon.
- Buchholz B.A. and Landsberger S. (1995), "Leaching Dynamics Studies of Municipal Solid Waste Incinerator Ash," J. Air and Waste Management Association, vol. 45, pp. 579-590.
- Chechirlian S., Eichner P., Keddam M., Takenouti H., Mazille H. (1990), "A Specific aspect of Impedance Measurements in Low Conductivity Media. Artifacts and Their Interpretations," Electrochimica Acta, Vol. 35, pp. 1125-1131.
- Chen J.-S., Bronson A. and Knittel D (1985), "Pitting Corrosion of Zr Immersed in Cl--SO42- Solutions," Corrosion, Vol. 41, pp. 438-445.
- R. A. Cottis (2001), Interpretation of Electrochemical Noise," Corrosion, Vol. 57, pp. 265-285.
- Cui, F., Presuel-Moreno, F. J., Kelly, R. (2005), "Computational Modeling of Cathodic Limitation on Localized Corrosion of Wetted SS 316L at Room Temperature," Corrosion Science, Vol. 44, pp. 2987-3005.

- Davis, J. R. (Ed.) (2000), "Understanding the Basics," Corrosion, ASTM International, Materials Park, Ohio.
- Darbin, M., J. M. Jaillaux, and J. Montuelle, (1986), "La Perennite des Ovages en Terre Armee," Bulletin de Laison Laboratory Central des Ponts et Chaussees, Paris, France.
- Doyle G., Seica M. V. and Grabinsky M. W. F. (2003), "The Role of Soil in the External Corrosion of Cast Iron Water Mains in Toronto, Canada," Can Geotech. 40, 225-236.
- Elias, V. (2000), "Corrosion/Degradation of Soil Reinforcements for Mechanically Stabilized Earth Walls and Reinforced Soil Slopes," FHWA-NHI-00-044, National Highway Institute, Federal Highway Administration, Washington, D.C.
- El-Mahdy, G. A., Nishikata, A. Tsuru, T. (2000), "Electrochemical Corrosion Monitoring of Galvanized Steel Under cyclic Wet-Dry Conditions," Corrosion Science, Vol. 42, pp. 183-194.
- El-Feki, A. A., Walter, G. W. (2000), "Corrosion rate measurements under conditions of mixed charge transfer plus diffusion control including the cathodic metal ion deposition partial reaction," Corrosion Science, Vol. 42, pp. 1055-1070.
- Eriksson, P., and Johansson, L.-G. (1986), "The Role of NO2 in the Atmospheric Corrosion of Different Materials," Proc. 10th Scandinavian Corrosion Congress, p. 43, Stockholm,
- EPA SW-846 (1992), "Test Method 1311 on Toxicity Characteristics Leaching Procedure," (TCLP), pp. 1-35.
- EPA SW-846 (1992), "Test method 1312 on Synthetic Precipitation Leaching Procedure," (SPLP), pp. 1-35.
- Fontana, M. and Greene, N. D., (1986), "Corrosion Engineering," McGraw-Hill, p. 96-97, New York.
- Giriga, S., Mudali, U. K., Raju, V. R., Raj, B. (2005), "Electrochemical Noise Technique for Corrosion Assessment – a Review," Corrosion Reviews, Vol. 23, pp. 107-170.
- Gladstone, R. A., Anderson, P. L., Fishman, K. L., and Withiam, J. L. (2006), "Durability of Galvanized Soil Reinforcement: 30+ Years of Experience with MSE," The 85th TRB Annual Meeting, on CD-ROM.
- Hage J. L.T. and Mulder E. (2004), "Preliminary Assessment of Three New European Leaching Tests," Waste Management 24, 165-172.
- Hageman P. L. (2007), "U.S. Geological Survey Field Leach Test for Assessing Water Reactivity and Leaching Potential of Mine Wastes, Soils, and Other Geologic and Environmental Materials," U.S. Geological Survey Techniques and Methods.
- Halmen, C., Trejo, D., Folliard, K. J. (2008), "Materials in Civil Engineering," Vol. 20, pp. 366-374.
- Haruna, T., Morikawa, Y., Fujimoto, S., Shibata, T. (2003), "Electrochemical Noise Analysis for Estimation of Corrosion Rate of Carbon Steel in Bicarbonate Solution," Corrosion, Vol. 45, pp. 2093-2104.
- Johnson C. A., Kersten K., Ziegler F. and Moor H. C. (1996), "Leaching Behavior and Solubility- Controlling Solid Phase of Heavy Metals in Municipal Solid Waste Incinerator Ash," Waste Management, Vol. 16, no 1-3, 129-134.
- Jones, D.A. (1992), "Principles and Prevention of Corrosion," pp. 402-404, Macmillan Publishing Co., New York.
- Kaesche, H. (1985), "Metallic Corrosion: Principles of Physical Chemistry and Current Problems," 2nd Ed., National Association of Corrosion Engineers, Houston.

- Kappler A., Benz M., Schink B. and Brune A. (2004), "Electron Shuttling Via Humic Acids in Microbial Iron (III) Reduction in a Freshwater Sediment," FEMS Microbiol. Ecol. 47, 85–92.
- Knittel D. and Bronson A. (1984), "Review of Zirconium Pitting Corrosion," Corrosion, Vol. 40, pp. 9-14.
- Kosson D. S., Van der Sloot H. A. and Eighmy T. T. (1996), "An Approach for Estimation of Contaminant Release During Utilization and Disposal of Municipal Waste Combustion Residues," Journal of Hazardous Materials 47, 43-75.
- Lambe T. W. (1951), "Soil Testing for Engineers," John Wiley & Sons, Inc., pp 1-165.
- Lambe T. W. and Whitman R. V. (1969), "Soil Mechanics," John Wiley & Sons, Inc., pp 1-548.
- Little B. J. and Lee J. S. (2007), "Microbially Influenced Corrosion," Wiley-Interscience A John Wiley & Sons, Inc., pp. 1- 261.
- Macdonald, D. D. (1991), "Application of Electrochemical Impedance Spectroscopy in Electrochemistry and Corrosion Science," in Techniques for Characterization of Electrodes and Electrochemical Processes, Electrochemical Society, Pennington, NJ.
- Mansfeld, F., and Lorenz, W. (1991), "Techniques for Characterization of Electrodes and Electrochemical Processes," John Wiley & Sons, Inc.
- Mansfeld, F., Lin, S., Chen, Y. C. and Shih, H. (1998), Minimization of High-Frequency Phase Shifts in Impedance Measurements, J. Electrochemical Society, Vol. 135, pp. 906-907.
- Marder, A. R., The Metallurgy of Zinc-Coated Steel," Progress in Materials Science, 2000, Vol. 45, pp. 191-271.
- Margui E., Salvado V., Queralt I. and Hidalgo M. (2004), "Comparison of Three-Stage Sequential Extraction and Toxicity Characteristic Leaching Test to Evaluate Metal Mobility in Mining Wastes," Analytica Chimica Acta 524, 151-159.
- Medford, W. M. (1999), "Monitoring the Corrosion of Galvanized Earth Wall Reinforcement", North Carolina Department of Transportation Field Investigation, the 78th TRB annual meeting, on CD-ROM.
- Misawa, T., Kyuno, T., Suetaka, W., Shimodaira, S. "The Mechanism of Atmospheric Rusting and the Effect of Cu and P on the Rust Formation of Low Alloy Steel," Corrosion Science, 1971, Vol. 11, pp. 35-48.
- Morris, D. V., and Delphia, J. G. (1999). "Specifications for Backfill of Reinforced-Earth Retaining Walls." Texas Transportation Institute, FHWA/TX-99/1431-S, 189 pp.
- Nelson P. O., Huber W. C., Eldin N. N., Williamson K. J., Azizian M. F,. Thayumanavan P., Hesse E.T., Lundy J. R. and Leahy R. B. (2000), "Environmental Impact of Construction and Repair Materials on Surface and Ground Waters," Final Report Volume II, Oregon State University. Prepared for: National Cooperative Highway Research Program Transportation Research Board national research Council, pp. 1-395.
- Nishikata, A., Ichihara, Y., Tsuru, T. (1995) "An Application of Electrochemical Impedance Spectroscopy to Atmospheric Corrosion Study," Corrosion Science, 37 (6), pp. 897-911.
- Nishikata, A., Ichihara, Y., Tsuru (1996), "Electrochemical Impedance Spectroscopy of Metals Covered With A Thin Electrolyte Layer," Electrochimica Acta, Vol. 41 (7/8), pp. 1057-1062.
- Nishimura, T., Katayama, H., Noda, K., Kodama, T. (2000), "Electrochemical Behavior of Rust Formed on Carbon Steel in a Wet/Dry Environment Containing Chloride Ions," Corrosion, 56 (9), pp. 935-941.

- Nordstrom D. K. and Southam G. (1997) Geomicrobiology of Sulfide Mineral Oxidation. Geomicrobiology: Interactions Between Microbes and Minerals, Reviews in Mineralogy, Mineralogical Society of America, Washington, DC, vol. 35, pp. 361–390.
- Odegard C. and Bronson A. (1997), "The Transient Current Response of Fe-Ni-Cr Alloy Rotating Cylindrical Electrodes Scribed with a Dropped Stylus," Corrosion, Vol. 53, pp. 800-807.
- Orazem M. E., Pébère N., Tribollet B. (2006), "Enhanced Graphical Representation of Electrochemical Impedance Data," J. Electrochemical Society, Vol. 153 (4), pp. B129-B136.
- Orazem M. E. and B. Tribollet (2008), "Electrochemical Impedance Spectroscopy," John Wiley and Sons, Inc., Hoboken, New Jersey.
- Prentice, G. (1991) "Electrochemical Engineering," Prentice-Hall, Englewood Cliffs, New Jersey, pp. 114-115.
- Rimstidt, J.D. and Vaughan, D.J., (2003), "Pyrite Oxidation: a State-of-the-art Assessment of the Reaction Mechanism," Geochimica et Cosmochimica Acta, 67(5): 873-880.
- Sagües, A. A., Rossi, J., Scott, R. J., Peña, J. A., and Simmons, T. (1998) "Influence of Corrosive Inundation on the Corrosion Rates of Galvanized Tie Strips in Mechanically Stabilized Earth Walls, Final Report, Florida Department of Transportation.
- Song, F. M. and Sridhar, N. (2008) "Modeling Pipeline Crevice Corrosion Under a Disbonded Coating With and Without Cathodic Protection Under Transient and Steady State Conditions," Corrosion Science, 2008, Vol. 50, pp. 70-83.
- Suzuki, I., (1985), "The Behavior of Corrosion Products on Zinc in Sodium Chloride Solutions," Corrosion Science, Vol. 25, pp. 1029-1034.
- Szklarska-Smialowska, Z. (1986), "Pitting Corrosion of Metals," National Association of Corrosion Engineers, Houston, Texas, pp. 70-84.
- Van der Sloot and Dijkstra, H.A. Van der Sloot and J.J. Dijkstra (2004), "Development of Horizontally Standardized Leaching Tests for Construction Materials: A Material Based or Released Based Approach? ECN-C-04-060," Energy Research Centre of the Netherlands (ECN), Petten, The Netherlands.
- Van der Sloot H.A., Heasman L. and Qwevauviller P. (1997) "Harmonization of Leaching/Extraction Tests," Elsevier, Amsterdam.
- Wang, J.H., Wei, F.I., and Shih, H.C., (1996) "Modeling of Atmospheric Corrosion Behavior of Weathering Steel in Sulfur Dioxide-Polluted Atmospheres," Corrosion, Vol. 52, pp. 900-909.
- Walter, G. W. (1976) "Corrosion Rates of Zinc, Zinc Coatings and Steel in Aerated Slightly Acidic Chloride Solutions Calculated from Low Polarization Data," Corrosion Science, Vol. 16, pp. 573-586.
- Yadav, A. P., Nishikata, A., Tsuru, T. (2004), "Degradation Mechanism of Galvanized Steel in Wet-Dry Cyclic Environments Containing Chlorides," Corrosion Science, 2004, Vol. 46, pp. 361-376.
- Yadav, A. P., Nishikata, A, Tsuru T. (2005), "Oxygen Reduction Mechanism on Corroded Zinc," Journal of Electroanalytical Chemistry, Vol. 585, pp. 142-149.

Appendix A

Survey Submitted to Districts

Questionnaire for TxDOT Research Project 0-6359
Characterization of Backfill Materials for Prevention of Corrosion of Mechanically Stabilized Earth (MSE) Metallic Wall Reinforcement

UTEP has been granted a research project to evaluate the corrosion behavior of galvanized carbon steel embedded in coarse grained (Type A or D) backfill material. The research team is working towards more realistic and easy-to-use electrochemical and geochemical tests to characterize the corrosion potential of earth reinforcements in these coarser backfills. This questionnaire is the first step toward documenting the current practices of TxDOT in using MSE walls. Your response to this questionnaire will help the research team to focus their efforts to provide a more practical and useful final product.

Questionnaire for TxDOT Research Project 0-6359

District: _____ Contact Person(s): _____

Telephone numbers and e-mails of contact persons:

_____

(1) As per Item 423, what are the major types of the backfill materials used in your district? Please fill out the table below (assign a 1 for the ones you most use, a 2 for the ones you sometime use, and a 3 for those that you rarely use). Please provide the best estimates of the percentages of each backfill type used.

Type	A	B	D
Ranking (1, 2 or 3)			
Percentage Use			

(2) What typical aggregate sources does your district use on MSE wall projects? Please fill out the table below (assign a 1 for the ones you most use, a 2 for the ones you sometime use, and a 3 for those that you rarely use). Please provide the best estimates of the percentages of each backfill type used.

Type	Limestone	Sandstone	Granite	Sand & Gravel	Other (specify) _____	Other (specify) _____
Ranking (1, 2 or 3)						
Percentage Use						

(3) Do you add recycled materials to your backfill materials used in MSE walls?

RAP Crushed Concrete Others (specify) _____

(4) Do you add chemical additives to your backfill material used in MSE walls?

Cement Others (specify) _____

(5) Which ones of the following tests do you routinely perform on your backfill materials?

Test Method	Backfill Type			Remark on concerns you have with these tests
	A	B	D	
Plasticity Index (Tex-106-E)				
Organics (Tex-110-E)				
Mg Sulfate Soundness (Tex-411-A)				
pH (Tex-128-E)				
Resistivity (Tex-129-E)				
Sulfate Content (Tex-620-J)				
Chloride Content (Tex-620-J)				
Gradation (Tex-110-E)				

(6) In addition to the test specified in question 5, are there any other tests that you run on your backfill materials?

No Yes (specify)

_____

(7) What types of problems, if any,-have been encountered during the construction of MSE walls?

_____

_____

_____

(8) Could we contact you for more information?

Yes No

(9) Do you have any candidate Type A or D backfill materials that you would like us to include as part of this research study?

Yes No

If yes, please provide the following information:

Type A Type D

Material Type (limestone, sandstone, etc.) _____

Source Pit _____

Appendix B

Results from Survey

Questionnaire

Introduction

A survey was conducted to identify the types of backfill to be used, and to suggest projects that can be incorporated in this study. The questionnaire, which was distributed statewide to ensure that the inference space of the materials within Texas is covered, is included in the appendix at the end of this report.

Survey responses were received from the following twelve districts: Abilene, Austin, Brownwood, Bryan, Dallas, El Paso, Fort Worth, Houston, Pharr, San Angelo, San Antonio, and Waco. The responses so far are summarized in this section.

Question 1
As per Item 423, what are the major types of the backfill materials used in your district?

Figure 1 shows the percentages of material types used by the districts. Out of the responses obtained, 50% of the MSE walls have a Type B backfill and 44% Type A or Type D backfills.

Question 2
What typical aggregate sources does your district use on MSE wall projects? Please provide the best estimates of the percentages of each backfill type used.

As shown in Figure 2, about 73% of the districts use limestone as aggregate in MSE walls.

Question 3
Do you add recycled materials to your backfill materials used in MSE walls?

Only three districts use recycles materials. Fort Worth and San Antonio use RAP in their MSE walls.

Question 4
Do you add chemical additives to your backfill material used in MSE walls?

El Paso and San Angelo are the only districts that use chemical stabilizers. El Paso uses cement while San Angelo does not specify the type of chemical stabilizer they use.

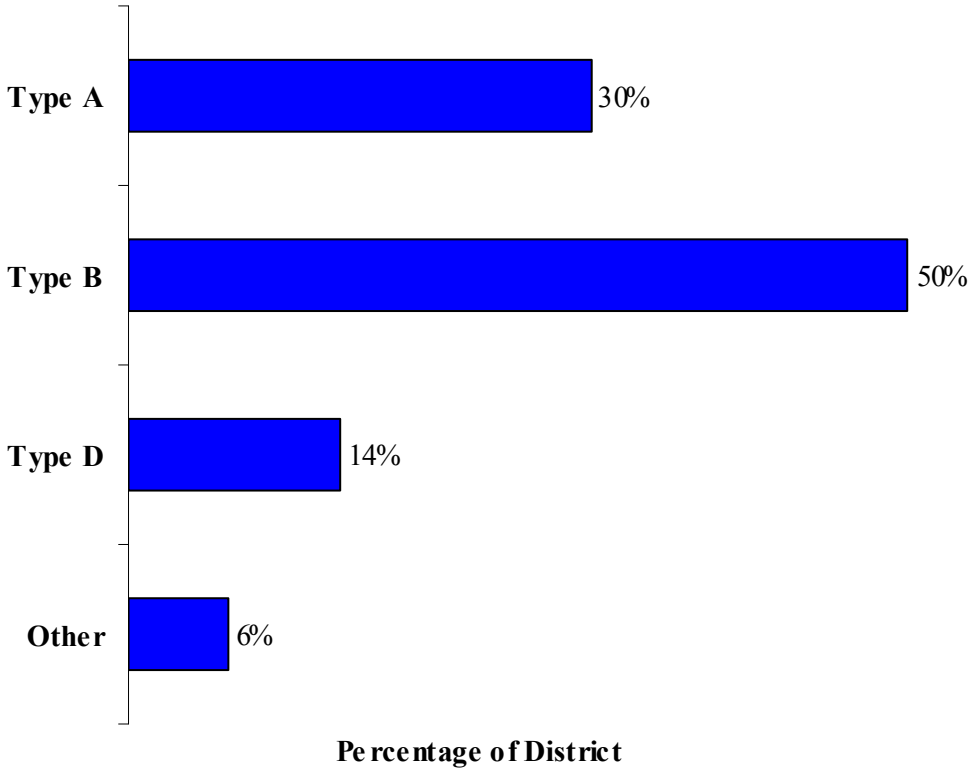

Figure B.1 - Percentages of Material Type Used

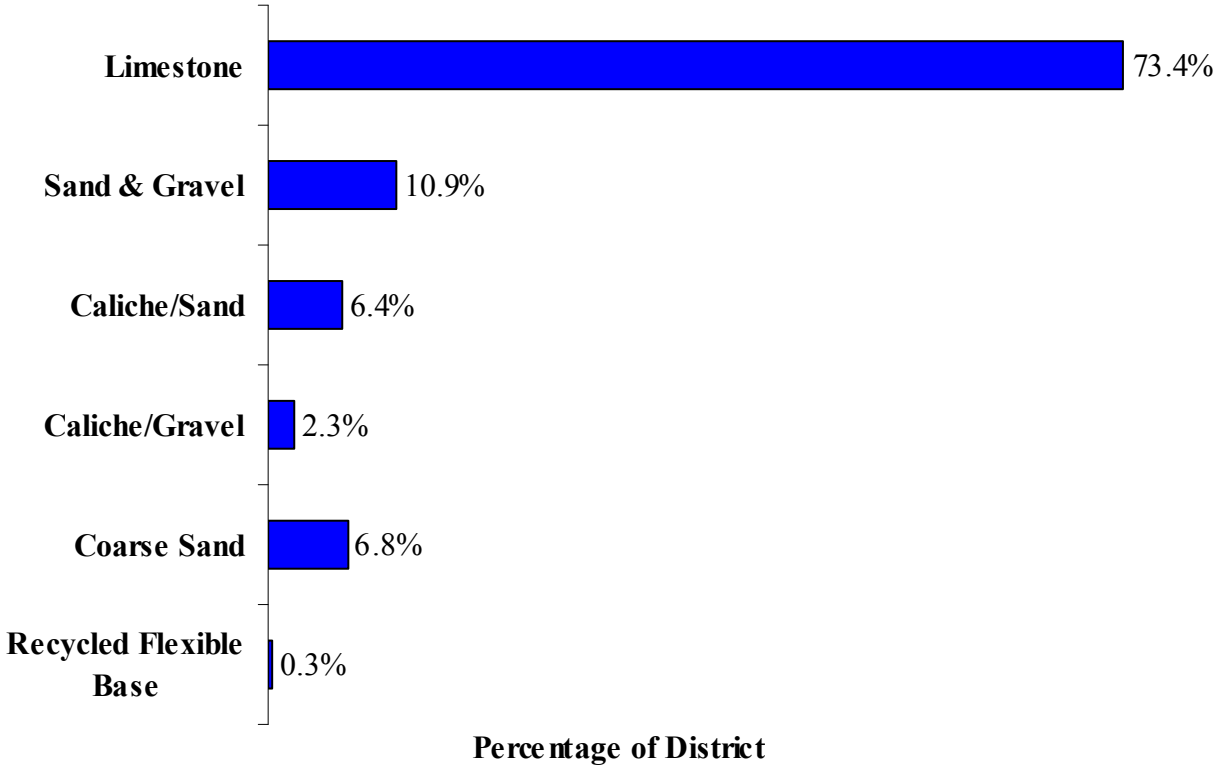

Figure B.2 – Types of Aggregates Used in MSE Walls

Question 5

Which ones of the following tests do you routinely perform on your backfill materials?

Figure 3 shows the frequency of each test used by the districts that responded to the questionnaire. The tests that are more frequently used are the pH (Tex-128-E), Resistivity (Tex-129-E) and Gradation (Tex-110-E). Some of the districts had a concern with the implementation of coarser gradations, the amount of finer material required for resistivity, sulfate and chloride testing requires crushing and in some cases that artificially elevates the sulfate concentration.

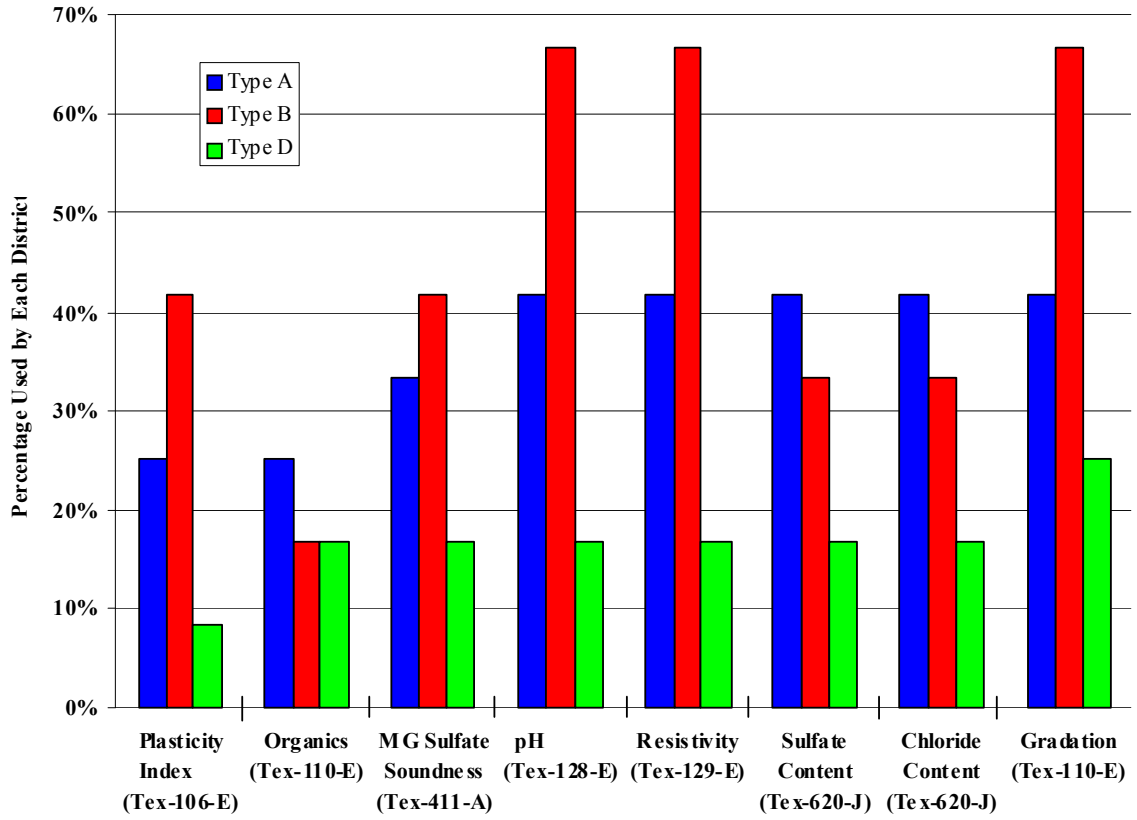

Figure B.3 - Factors for selection of ATB in projects

Question 6

In addition to the test specified in Question 5, are there any other tests that you run on your backfill materials?

The additional tests performed by Brownwood, Houston, Pharr and San Angelo districts include Tex-113-E and 114-E. Austin District occasionally tests the water used in the field for compaction, as some of the compaction water used on projects contains high levels of soluble salts, including sulfates and chloride.

Question 7

What types of problems, if any, have been encountered during the construction of MSE walls?

Based on the responses to the questionnaire, the majority of the districts have compaction and settlement problems. Table 1 shows the specified problems for each district.

Table B.1 - Problems Encountered During the Construction of MSE Walls

District	Specified Problems
Abilene	Movement of steel reinforcements in backfill material, when sand is used for backfill.
Austin	Compaction issues on coarsely graded Type D backfill.
Brownwood	None
Bryan	Mainly quality control type issues with the contractor, such as making sure the interface between the regular embankment and the select backfill was well compacted without a distinct vertical joint. The embankment and the select fill were placed by two different contractors bringing up their lifts at different depths and it was challenging to make sure that the interface was properly rolled. It was difficult to get the contractor to compact the backfill to an even surface all the way up to the strap anchors, especially near the face of the wall. Often they would place the straps and they would not be level or there would be gaps underneath where the backfill surface was uneven.
Dallas	None
El Paso	None, the contractors in the District are experienced with the materials and construction processes and wall system.
Pharr	Wall settlement due to being placed on poorly compacted soil. Wall layout not being followed as per shop drawings. Some improper reinforcement to drill shafts at abutment.
	Wall layout not being followed as per shop drawings.
	Some improper reinforcement to drill shafts at abutment.
San Angelo	We had a project in which Type A backfill material was required for the backfilling operations of the MSE walls. The contractor did not provide for the proper drainage away from the backfilling operations, the wall collapsed, and the contractor had to redo the wall at his own expense
San Antonio	Fills with fines such as flexible base, there have been issues with undesirable settlement and lateral movement of a wall that does not have adequate drainage provided in the interim before the wall has reached full height
Waco	Most problem we have experienced have to do with construction technique in the form of compaction (generally lack thereof). Have no knowledge of corrosion issues.

Question 8
Could we contact you for more information?

All of the districts would like to be contacted for more information.

Question 9
Do you have any candidate Type A or D backfill materials that you would like us to include as part of this research study?

Most of the districts use Type B backfill material in constructing their MSE walls. Only three of the districts have a candidate Type A or Type D backfill material, among them are Austin, Dallas and Waco. Based on the responses to the questionnaire, most of the districts use limestone as aggregate for MSE wall construction.

Appendix C

Corrosion Related Results for Galvanized Steel

The Bode plots acquired for electrochemical impedance spectroscopic measurements for 0.001, 0.01 and 0.1 M NaCl solutions are given in the Figures C.1 to C.4, respectively. Current transients of specimens 1 and 2 (indicated as sp1 and sp2, respectively) acquired for the materials are given in Figures C.5 to C.6. The power spectral densities determined via fast Fourier transform (FFT) and maximum entropy method (MEM) for specimens 2 and 4 are summarized in Figures C.7 and C.8.

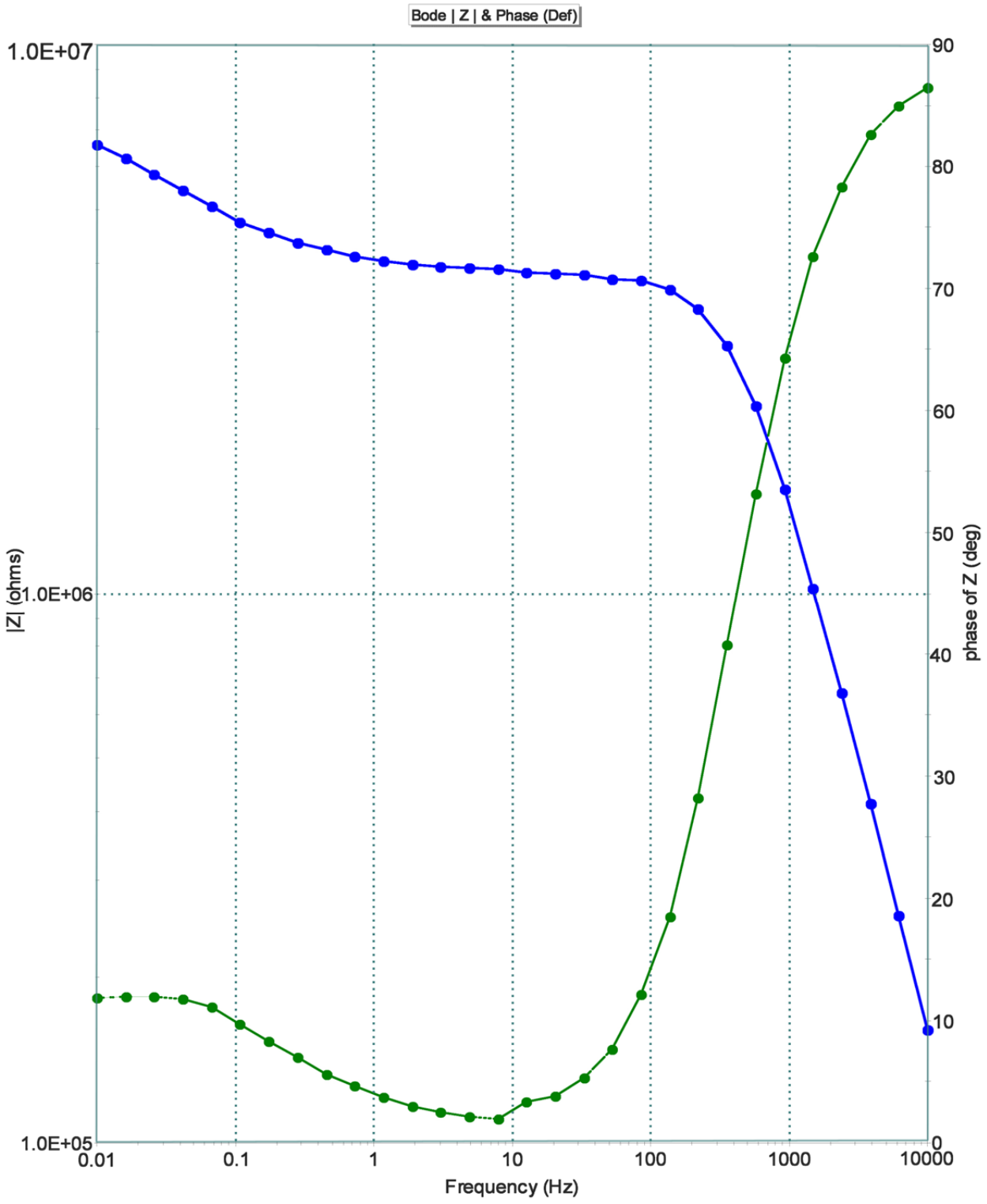

Figure C.1. Bode and phase angle plots for galvanized steel immersed in a 0.0001 M NaCl solution.

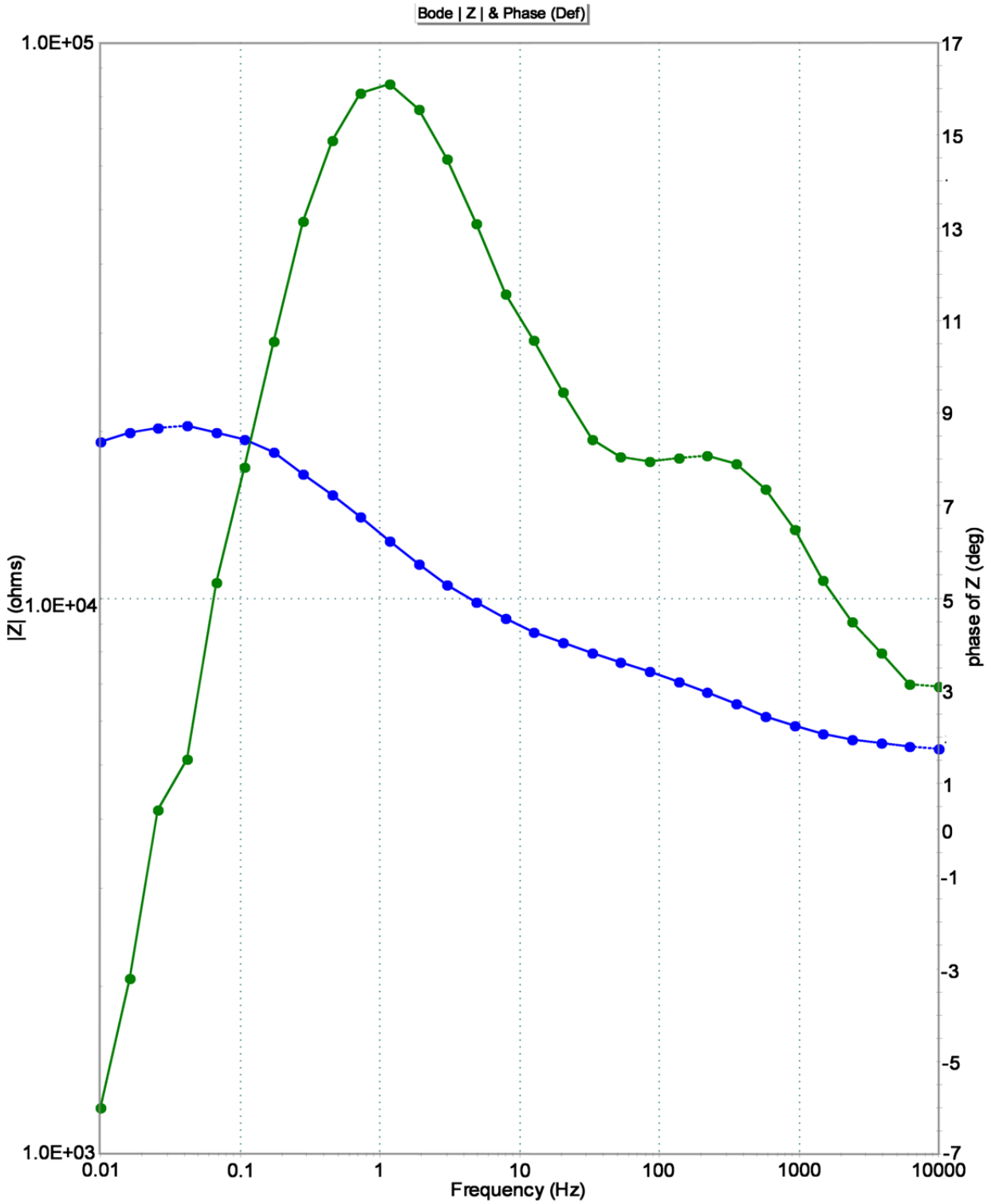

Figure C.2. - Bode and phase angle plots for galvanized steel immersed in a 0.001 M NaCl solution.

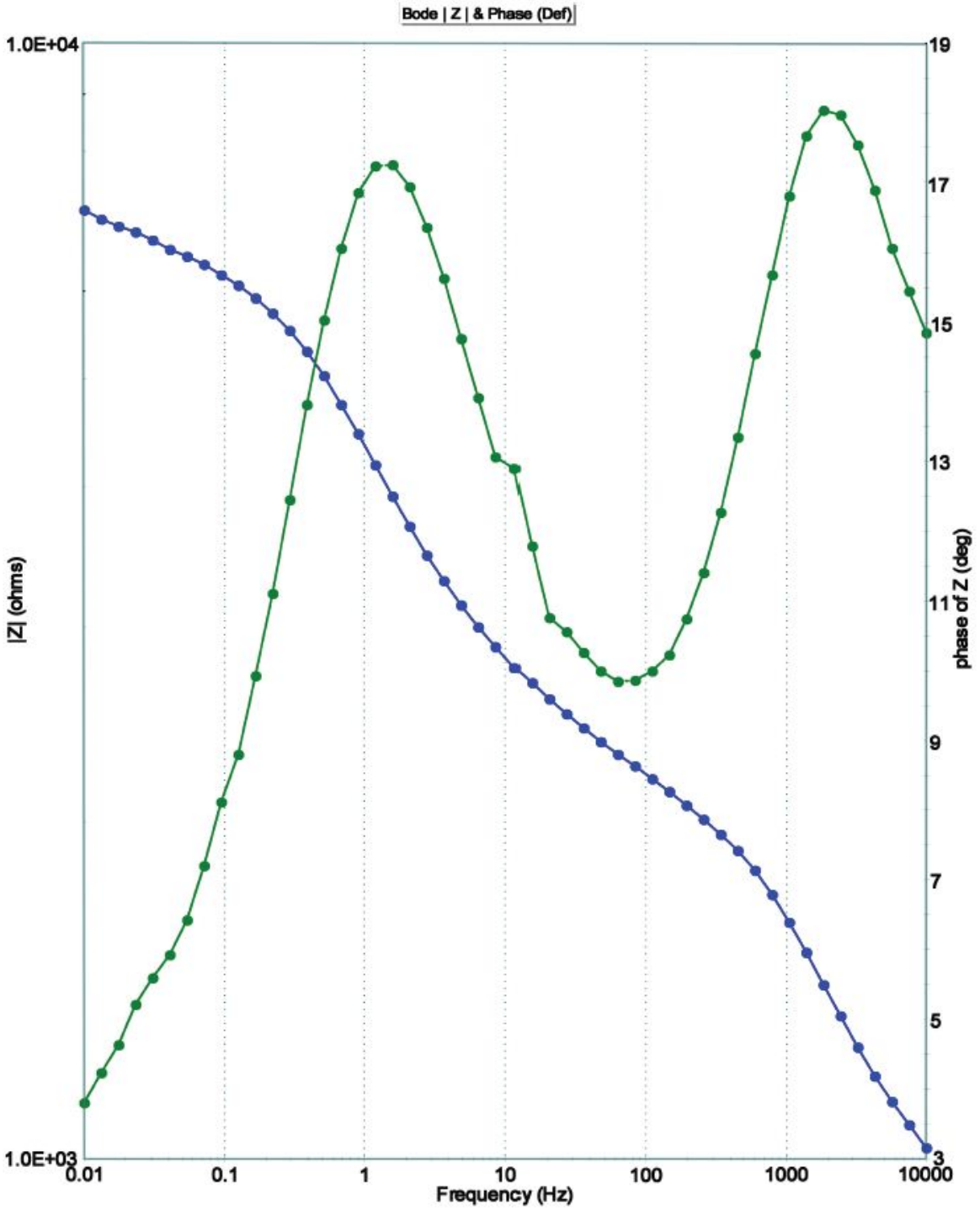

Figure C. 3 – Bode and phase angle plots for galvanized steel immersed in a 0.01 M NaCl solution.

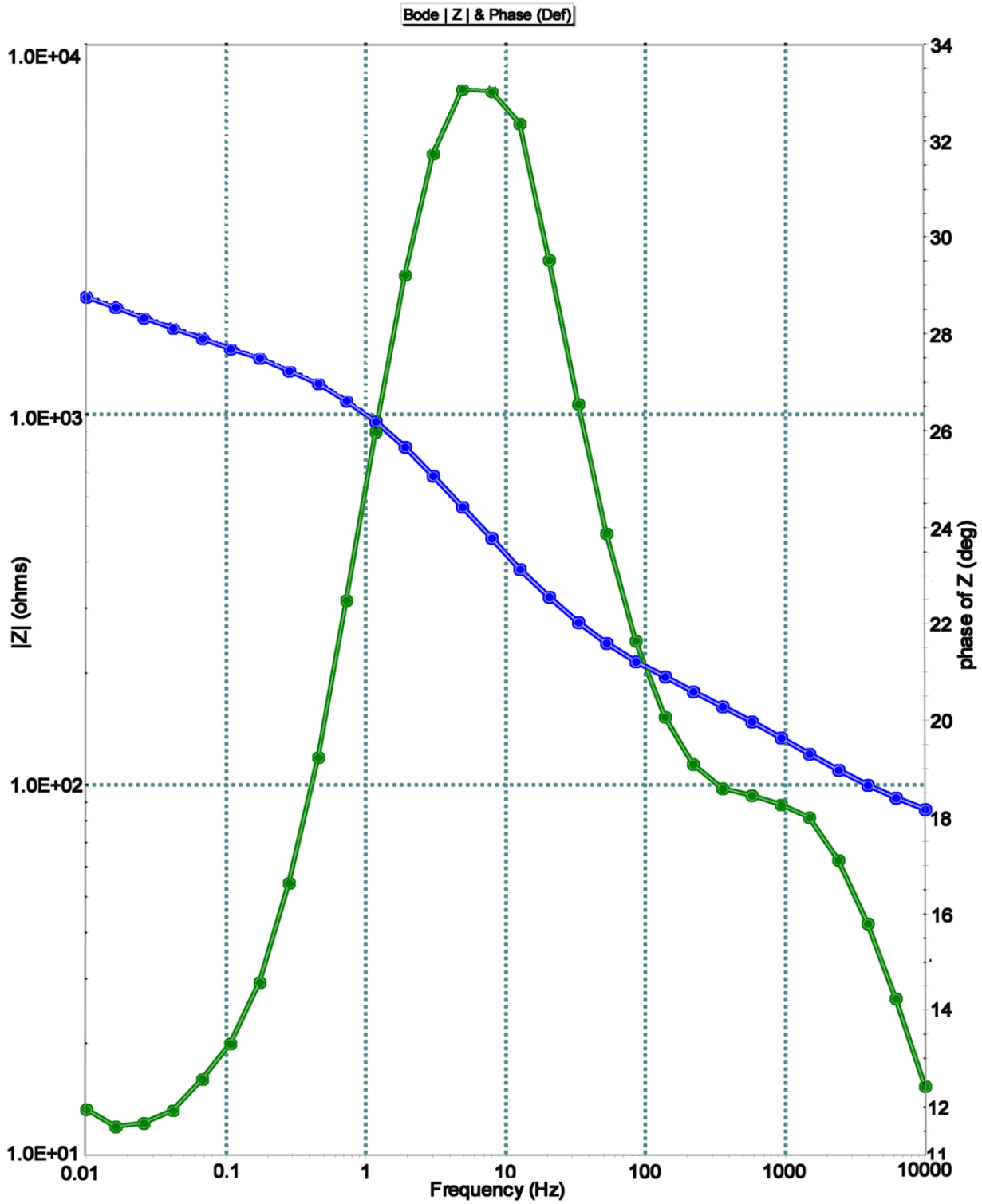

Figure C.4 – Bode and phase angle plots for galvanized steel immersed in 0.1 M NaCl solution.

Current Transients

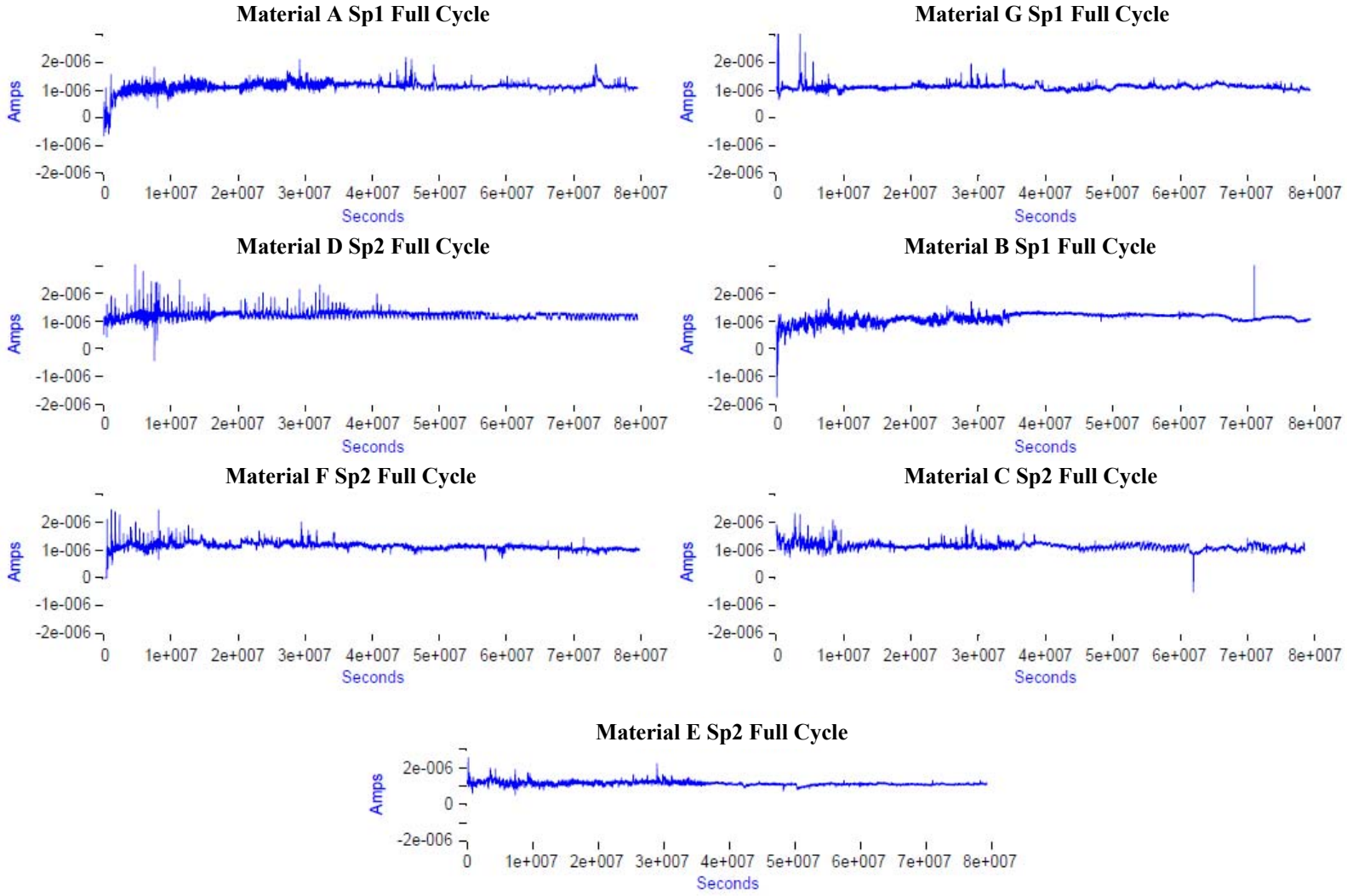

Figure C.5 – Current transients acquired for materials specimens 1 and 2.

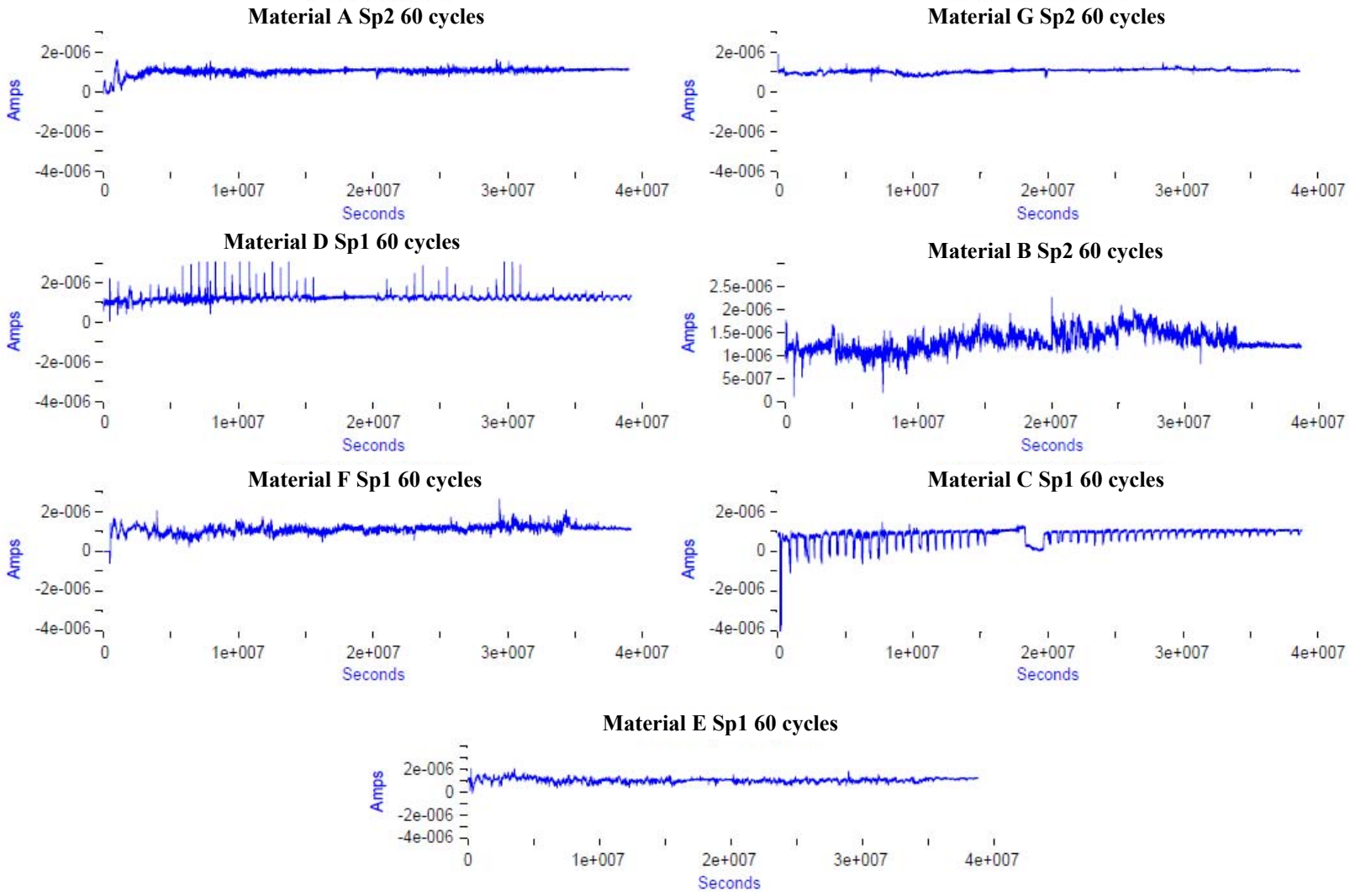

Figure C.6– Current transients acquired for materials specimens 1 and 2.

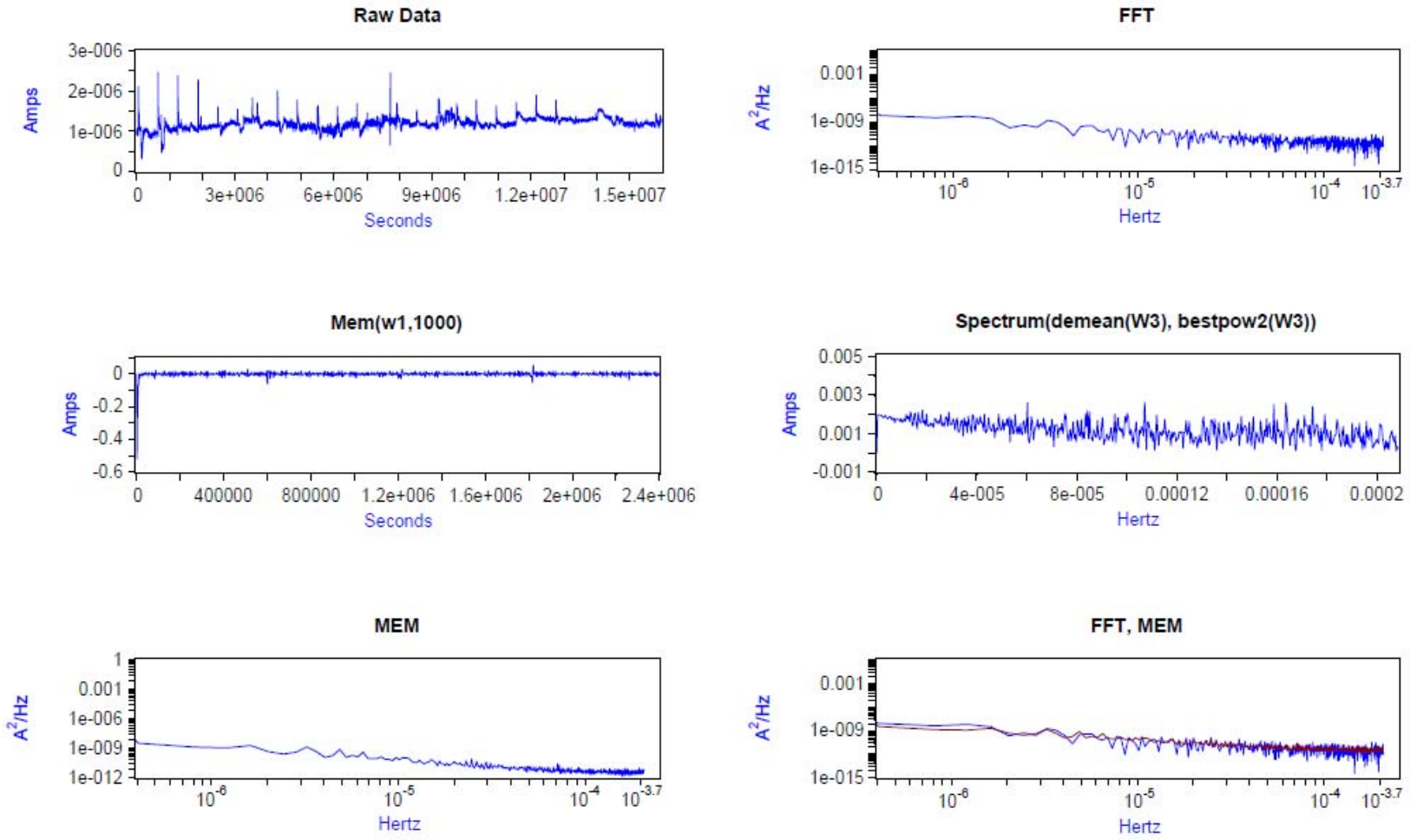

Figure C.7 - Power spectral densities acquired by using the FFT and MEM for Material F wet/dry cycles Sp2 with DADISP

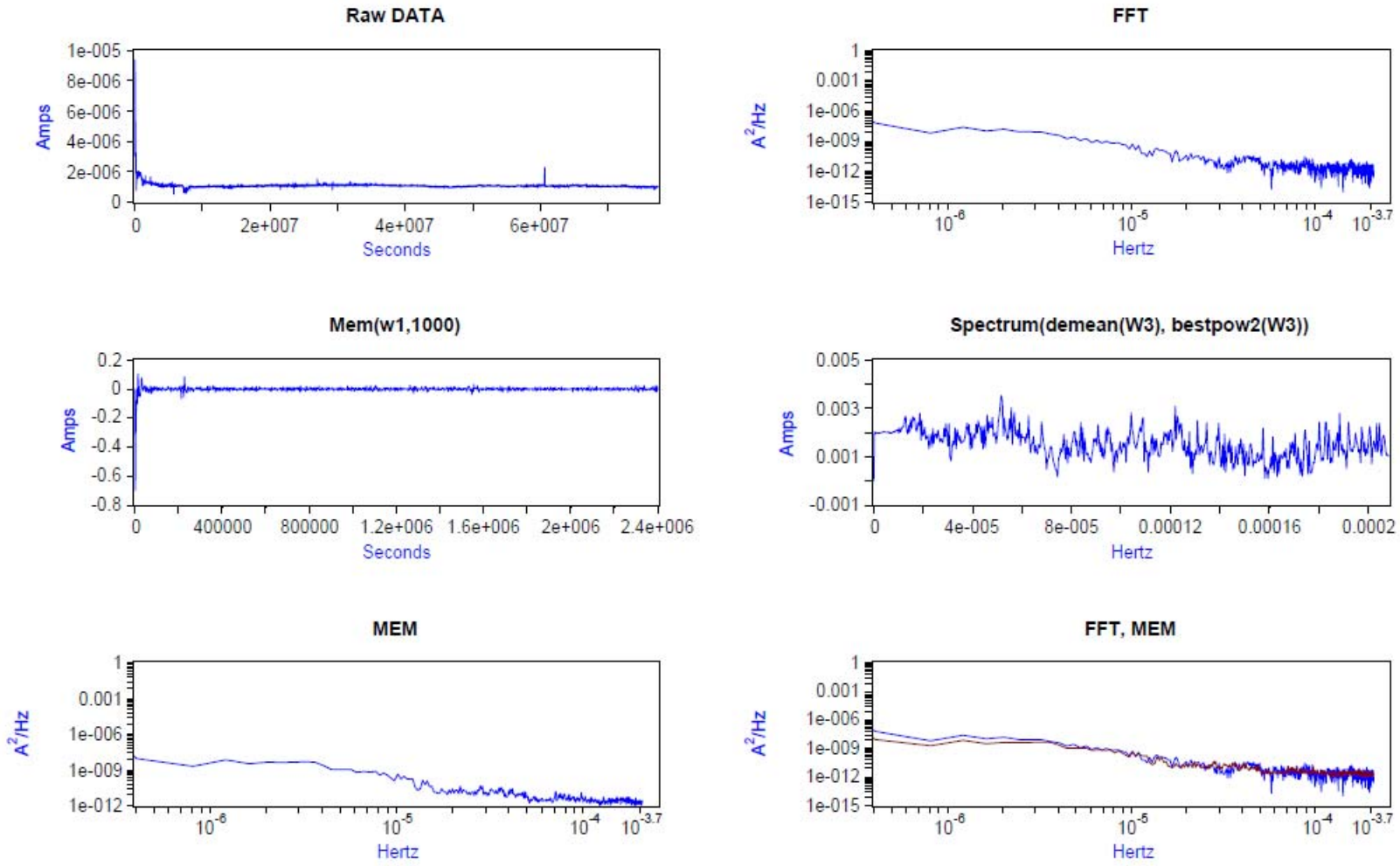

Figure C.8 - Power spectral densities acquired by using the FFT and MEM for Material F wet/dry cycles Sp4 with DADISP

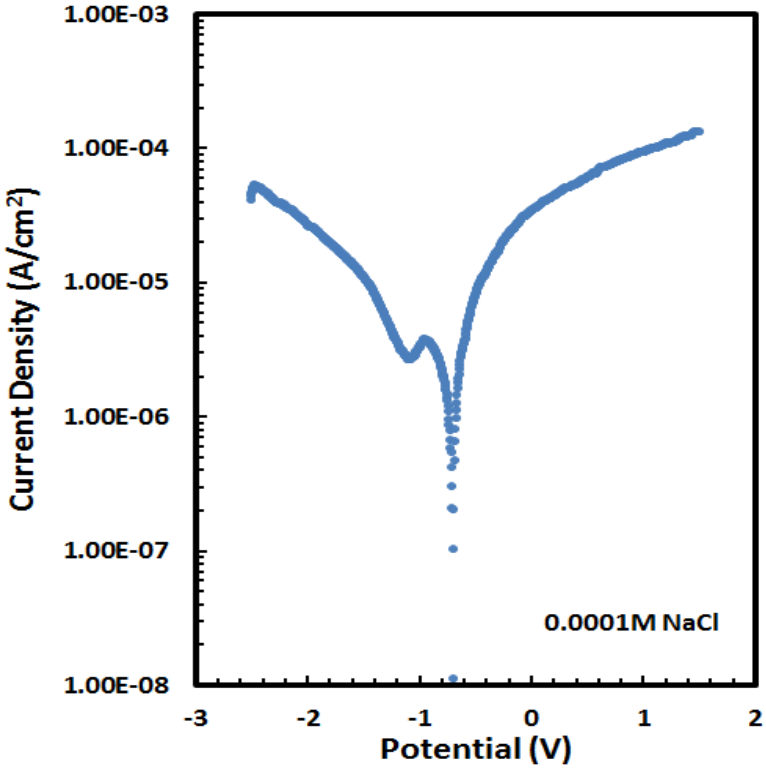

Figure C9 - Polarization scan for galvanized steel immersed in a 0.0001 M NaCl solution

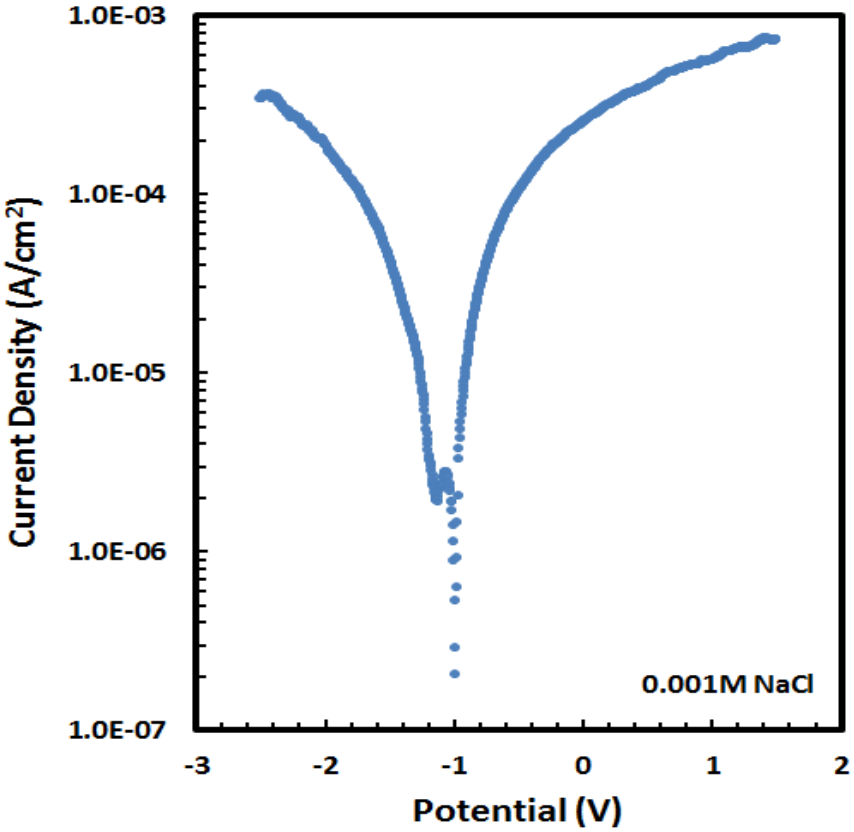

Figure C10 - Polarization scan of galvanized steel in a 0.0001 M NaCl solution.

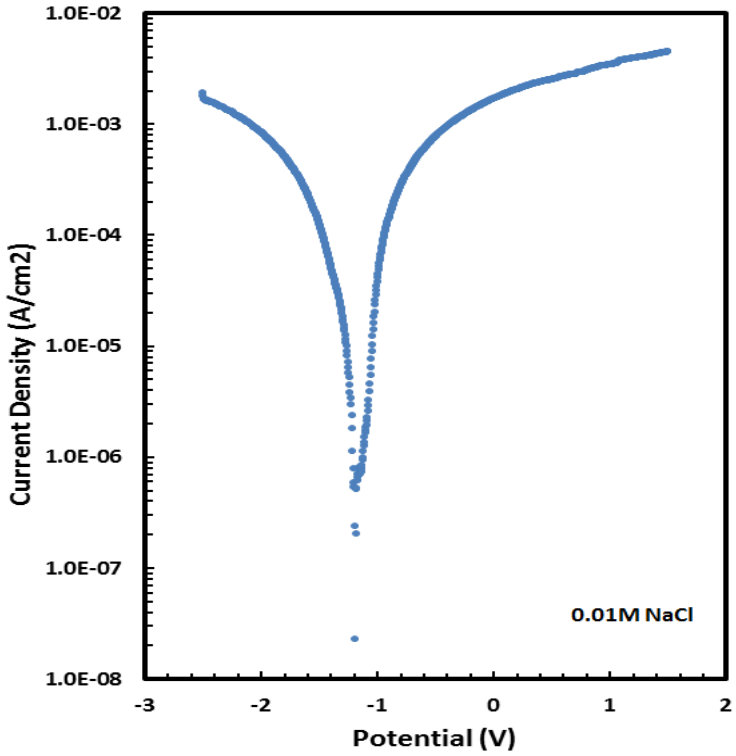

Figure C11 - Polarization scan for galvanized steel immersed in a 0.01 M NaCl solution.

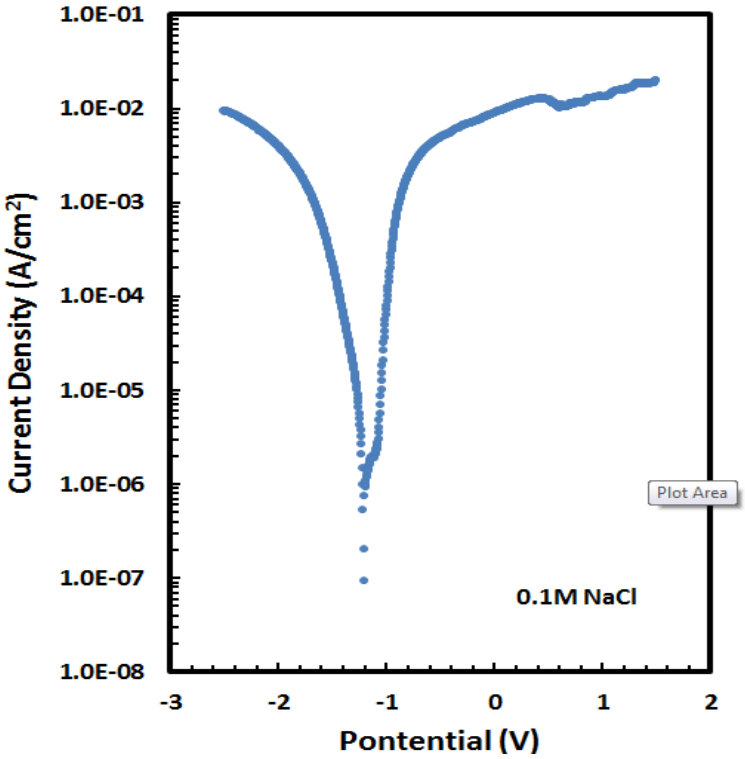

Figure C12 - Polarization scan of galvanized immersed in a 0.1 M NaCl solution.

Appendix D

Tex-620-M

Tex-620-M: Determining pH and Chloride and Sulfate Content in Soils

Contents:

Section 1

Overview

This method describes how to determine the pH and chloride and sulfate content in soil.

Units of Measurement

The values given in parentheses (if provided) are not standard and may not be exact mathematical conversions. Use each system of units separately. Combining values from the two systems may result in nonconformance with the standard.

Section 2

Apparatus

The following apparatus is required:

- balance, calibrated to weigh to nearest 0.1 g
- plastic bottle – 1 L (larger plastic bottles must be used to accommodate larger sample sizes – see section 3)
- oven, capable of maintaining a temperature of 60 ± 5°C
- shaker table or similar shaking apparatus
- 0.45 µm nylon membrane syringe filter
- 10 mL disposable plastic syringe
- volumetric flask – 1 L
- pipette
- 30 mL plastic sample storage bottles (or similar)
- **pH meter, *with glass electrode, pH range 0 - 14 ±0.1.***
- *Buffer solutions*, such as pH 4.0, 7.0, and 9.0

Section 3

Materials

- Distilled or de-ionized water
- Certified anion standard reference solution, containing 100 mg/L (100 ppm) chloride and sulfate.

Section 4

Preparing Sample

The following describes preparing the sample.

Preparing Sample	
Step	**Action**
1	Collect a representative grab sample of the material from the field. The mass of the sample should be approximately 100 g, but must be increased as necessary to accurately represent the average size and character of the material.
2	Dry the sample in a 60 ± 5 °C (140 ± 9 °F) oven and cool to 25 ± 3 °C (77 ± 5 °F) in a desiccator to constant weight.
3	Weigh to the nearest 0.1 g.

Section 5

Procedure

The following describes the steps required to determine chloride and sulfate content.

Chloride and Sulfate Content	
Step	**Action**
1	Before using them, thoroughly clean the sample storage bottle, syringe filter, and syringe with distilled or de-ionized water and air dry. Water must be passed through the filter during the cleaning step.
2	Based on the mass of the representative sample, transfer the entire sample into the appropriate sized plastic bottle. The appropriate size is based on a sample to liquid ratio of 1g to 10 mL (for example, a 100g sample would require, at minimum, a 1L bottle. A 300g sample would require, at minimum, a 3L bottle).
3	Add deionized water to the bottle to achieve a sample to liquid ratio of 1g to 10 mL
4	Cap the bottle and place on a shaker table (or similar shaking apparatus) and allow to vigorously shake for 30 minutes.
5	At the end of the 30 minute period remove the bottle from the shaker table and let stand for 1 hour.
6	While the bottle is left standing, standardize the pH meter (buffer solution of pH 7.0) according to the manufacturer's recommendations.
7	Clean electrode with water.
8	After 1 hour of standing time, remove the cap and measure pH using the calibrated meter. Place the tip of the electrode approximately 5 cm into the mixture. Allow reading to stabilize.
9	Read and record the pH value to the nearest tenth of a whole number.
10	Remove and clean the electrode with water.
11	If the pH of sample is below 5 or above 9, standardize meter with appropriate buffer and repeat items 6-9.
12	Place the tip of the syringe filter in the liquid and draw in 10mL of sample.
13	Immediately screw the 0.45 µm filter onto the end of the syringe and filter the liquid into the sample storage bottle.
14	Store the sample in a refrigerator prior to analyses.

Section 6

Analyses of Chloride and Sulfate Content using an ion chromatograph

The following describes the steps required to measure chloride and sulfate content using an ion chromatograph.

Chloride and Sulfate Content	
Step	**Action**
1	Prepare 5 standards using the anion standard solution that cover the concentration range from 0.1 to 100 mg/L. The same distilled or de-ionized water used in the experiments should be used for preparing the samples.
2	If very high concentrations (>100 mg/L) are suspected, dilute the sample by a factor of 10 using standard procedures prior to analysis. Note that dilutions can be made in separate pre-washed bottles or test tubes. Dilutions should use the same distilled or de-ionized water used in the experiments.
3	Follow the manufacturer's instructions to start the ion chromatograph's pump and electronic systems. Pump eluent through the column and detector until the ion chromatograph obtains a stable baseline.
4	Pour samples into properly labeled sample vials. Run one prepared standard and one deionized water blank after every four to five samples to check the accuracy of the chromatograph.
5	Run the samples through the ion chromatograph to determine the concentration of the chloride and sulfate ions.
6	Obtain chloride and sulfate contents in mg/L as determined by the ion chromatograph. Multiply this concentration by the dilution factor to achieve the true concentration.
7	The true concentration (in mg/L) is then multiplied by the volume of water used (in liters; section 5 - step 3) and divided by the mass of the sample (in kilograms) to obtain the concentration of sulfate and chloride in units of mg/Kg (ppm)